



Social behavior in a network of UAVs with collision avoidance

Master's Thesis
DC 2020.093

Author

W. de Jonge

Supervisor

prof. dr. H. Nijmeijer

Coach

dr. ir. A. A. J. Lefeber

Eindhoven University of Technology
Department of Mechanical Engineering
Dynamics and Control Group

September 14, 2020

Summary

As the interest in applications involving multiple cooperating agents continuously increases, so does the need for a sophisticated collision avoidance strategy. Where collision avoidance is already present abundantly in literature, it generally lacks proof that collisions will indeed be avoided in the system. Most often, it only gives optimal reference trajectories as an indication that collisions are avoided. Therefore, introducing a theoretical framework to prove absence of collision opens up a promising direction for progression in multi-agent systems. Based on recent stabilizing results for a network of quadrotor UAVs on $SO(3)$ that apply almost globally, a notion for collision avoidance is introduced. By introducing such a collision avoidance strategy, cost and robustness benefits are expected, as the absence of collisions in the system will result in less failures, increased robustness, and a reduced number of crashes of, most often, expensive UAVs. To develop such a theoretical framework to prove absence of collisions in a network of quadcopter UAVs, a network of single integrators in 1D is considered first. To prove absence of collisions in the network, a control Lyapunov function is composed with which simultaneously a control law is designed. With the resulting combination of control Lyapunov function and control input, local exponential stability of both equilibria is proven, while also proving absence of collisions in a network of two single integrators in 1D. This theoretical framework proves to be suitable for expansion to a network of double integrators in arbitrary dimension and the resulting equilibria are proven asymptotically stable with the designed control law, while proving the absence of collisions in the network. As the dynamic model of a UAV can be considered as a cascade of two double integrator systems, the obtained knowledge of the double integrator system is eventually applied to a network of quadcopter UAVs. Next, a projection is used, in which both equilibria of the position tracking subsystem are projected on the origin of the projected system. This allows to prove global asymptotic stability and local exponential stability of the origin of the projected system by following the constructed theoretical framework, while also proving absence of collisions in the network, under certain assumptions on the reference trajectories. Subsequently, the attitude tracking subsystem is proven uniformly locally exponentially stable and uniformly almost globally asymptotically stable, under the same assumptions on the reference trajectories, and additional assumptions on the initial conditions to compensate for the lack of saturation in the control law. The total cascaded system of the quadcopter UAVs is proven almost globally asymptotically stable, and locally exponentially stable, based on cascaded theory, under the aforementioned assumptions. The obtained result is then expanded to a network with an arbitrary number of drones, in which almost global asymptotic stability, and local exponential stability, of the resulting cascaded system is also obtained. The effectiveness of the introduced theoretical framework and the corresponding results is emphasized by execution of a series of experiments with a network of two quadcopter UAVs, and a comparison of the obtained results with the corresponding simulated situations.

Acknowledgements

First of all, I would like to express my gratitude to prof. dr. H. Nijmeijer, for the motivating feedback and support during the course of this project. Thank you for the inspiration, for providing me the opportunity to work on this project, and your guidance and support throughout my entire Master's degree.

Furthermore, I would like to thank dr. ir. A. A. J. Lefeber. Thank you for triggering me to get the most out of it, and your patience in the process. Thank you for all the meetings that we had, where you never failed to give inspirational and motivational ideas. And thank you especially for your continuous support and your effort to have these meetings, even when the COVID-19 pandemic reared its head.

A special thanks goes out to all fellow students in the DCT lab for the necessary distractions, the endless games of table soccer and the online Padéén meetings we had when the pandemic hit. Although nothing beats the DCT lab, I would also like to thank the people in the Robotics lab for including me in their group when I was finally allowed to go to the university again for the execution of experiments.

Lastly, I would like to thank my parents, brother, girlfriend, the friends that I made during my time in Eindhoven, and the ones that I had from before. Thanks for your support and for all the times you made me forget about my studies and simply enjoy my leisure time.

Willem de Jonge
Eindhoven, September 14, 2020

Contents

1	Introduction	1
1.1	Cooperation with collision avoidance	2
1.1.1	Motivation	2
1.1.2	Collision avoidance strategies	2
1.2	Problem definition	3
1.3	Thesis outline	4
2	Preliminaries	5
2.1	Attitude representation	5
2.1.1	Rotation matrices and Euler angles	5
2.1.2	Quaternions	6
2.2	Stability results	8
3	Stability analysis	11
3.1	Single integrators in 1D	11
3.1.1	Instability of collision point	12
3.1.2	Stability analysis	13
3.2	Double integrators in 1D	15
3.2.1	Converse Lyapunov theorem	16
3.3	Stability with control Lyapunov function	18
3.3.1	Single integrators in 1D with constant reference	18
3.3.2	Double integrators in arbitrary dimension with constant reference	20
3.4	Stability of quadcopters in 3D with constant reference	23
3.4.1	Position tracking control with collision avoidance	25
3.4.2	Attitude control	28
3.4.3	Cascaded system analysis	31
3.5	Expansion to network of arbitrary number of UAVs	32
3.6	Concluding remarks	35
4	Numerical and experimental validation	37
4.1	Experimental setup	37
4.2	Towards experimental validation	38
4.2.1	Conversion of controller to quaternions	38
4.2.2	Performance of a single drone	40
4.2.3	Setting up the communication channel	44
4.3	Results	49
4.4	Concluding remarks	51
5	Conclusions and recommendations	53
5.1	Conclusions	53
5.2	Recommendations	55

A	Local stability analysis in a kinematic model	57
B	Local stability analysis in projected dynamics	59
C	Modification of Simulink Support Package	63

Nomenclature

Reference frames

\mathcal{B}_i	Right-handed orthonormal body-fixed coordinate frame of agent i
\mathcal{D}_i	Right-handed orthonormal frame that describes the desired attitude of agent i
\mathcal{F}	Right-handed orthonormal virtual center of formation frame
\mathcal{I}	Right-handed orthonormal inertial frame in North-East-Down (NED) configuration
\mathcal{R}_i	Right-handed orthonormal reference frame of agent i

Number sets

\mathbb{H}	Quaternion space
\mathbb{N}	The set of natural numbers
\mathbb{R}^n	The n -dimensional Euclidian space
$\text{SE}(3)$	The n -dimensional Euclidian group
$\text{SO}(3)$	The n -dimensional Special Orthogonal group

Operators

$\text{eig}(\cdot)$	Function that provides the eigenvalues of its matrix argument
$\text{diag}(\cdot)$	Function that provides a row vector containing all diagonal elements of its argument
$\text{S}(\cdot)$	Function providing skew symmetric matrix of its vector argument
\dot{x}	Time-derivative of a system state x
A^\top	The transpose of a matrix
x^\top	The transpose of a vector
\otimes	Quaternion product
\odot	Quaternion rotation
$\ \cdot\ $	Function providing the two-norm of its argument

Acronyms

APF	Artificial Potential Function
IMU	Internal Measurement Unit
MPC	Model Predictive Control
NAP	Network Access Point
RMS	Root Mean Square
UAV	Unmanned Aerial Vehicle
UGV	Unmanned Ground Vehicle
VTOL	Virtual Take-Off and Landing

Constants and variables

θ	Pitch angle of a body
λ	Eigenvalue of considered system
ν	Linear velocity with respect to body-fixed frame
ρ	Position vector
τ	Torque generated by the rotors
ϕ	Roll angle of a body
ψ	Yaw angle of a body
ω	Angular velocity with respect to body-fixed frame
e_i	Unit vector i of a frame of reference
f	Total force generated by the motors
g	Gravitational acceleration constant
I_n	Identity matrix of size $n \times n$
J	Inertia of a body
K_i	Matrix controller gain
k_i	Scalar controller gain
m	Mass of a body
R	Rotation matrix of a body
u	Control input or virtual input
v	Velocity vector in n D or speed in 1D
q	Attitude of a body expressed in quaternions
x	State vector in n D or position in 1D

Chapter 1

Introduction

Everybody has heard of drones, and while most people know them for their applications in photography, they are becoming more common everyday in the current street scene. The interest in drones, or quadrotors, a type of Unmanned Aerial Vehicle (UAV), is maybe even further propelled by the current Covid-19 pandemic and the resulting social distancing measures. As quadcopters currently appear, for example, to deliver books for students [1] or for police warnings at crowded places [2]. The quadcopter belongs to the multirotor subclass of UAVs and is most frequently used in practical applications as the four propellers can be aligned with the body-fixed frame of a quadcopter, resulting in a more straightforward control with respect to multirotors consisting of other numbers of propellers. Another major advantage of quadcopter UAVs is their aerial agility and vertical take-off and landing (VTOL) capabilities, although this comes at the expense of battery consumption. Besides the quadcopter UAV, the fixed-wing type is most commonly used, which generally has longer battery life but is far less agile and most of the time lacks the ability to vertically takeoff. To combine the advantages of both systems, even hybrid models are being developed [3]. Other models, like flapping-wing models, exist but as their dynamics becomes quite complicated, they are generally not preferred for application [4].

With drone applications sprouting left right and centre, interest in applications that require combined effort of multiple drones also rises. Cooperating UAVs can together conduct tasks in a shorter time period, or accomplish goals that are simply impossible to achieve for a single drone. Think for example of the possibility of networks of UAVs to monitor and spray crops together to reduce uncovered areas of crops or overlapping of sprayed areas [5]. Other examples include the localization and prevention of wildfires [6] and rescue missions [7, 8], where a network of drones can cover more area and could even be used to efficiently search for victims through inter-robot communication. Similar UAV swarm technologies even receive interest for military applications, as DARPA, a military agency of the USA, recently conducted field experiments with swarms of UAVs [9]. A nice example of an application where a single drone is simply not capable of executing the task would be lifting heavy objects with a multitude of drones [10]. Such an application could be interesting to realize Amazon's Prime Air [11]. A last, well known, example of the usage of swarms of drones is in light shows, as Intel broke the Guinness World Record of having the "most unmanned aerial vehicles airborne simultaneously" by lighting up the sky with 1218 drones [12]. Cooperation of quadrotors might even be used to balance the main disadvantage of quadrotors with respect to fixed wing aircrafts, which is battery consumption, by enabling faster execution of tasks and thus reducing necessary battery capacity.

The common factor in these applications is that certain tasks or processes, previously executed by humans or some kind of machines, are automated. Therefore, autonomous flight is aspired, which is most often formulated as a trajectory tracking problem in which the drones are to move along a predefined path without any external interference. Recently, a controller is presented that

achieves uniform almost global stability (UaGAS) of the error tracking dynamics for a quadrotor UAV on $SE(3)$ [13]. Subsequently, the controller is adjusted in order to achieve uniform almost global asymptotic stability of the formation tracking error dynamics for multiple UAVs on $SO(3)$ [14]. Moreover, the designed controller in [14] allows to select whether the UAVs emphasize on individual error tracking, or formation forming. By representing the UAV attitude on $SO(3)$ the ambiguities that arise by using quaternions or singularities that are induced by usage of Euler angles are avoided and as a consequence, large angular maneuvers are allowed. As the theoretical and numerical results of [14] look promising, it is desired to invigorate the results with an experimental validation. However, where in numerical simulations the occurrence of collisions is a mere inconvenience, collisions can actually damage or destroy an experimental setup in practice. Therefore, to eventually execute experiments with the designed controller in [14], this research aims to implement a collision avoidance strategy in the control law and prove the absence of collisions in the resulting system.

1.1 Cooperation with collision avoidance

Research considering collision avoidance strategies is present abundantly and a motivation for all this interest in the topic is presented. Subsequently, the state of the art of collision avoidance strategies is illustrated by introducing some existing collision avoidance strategies and discussing their effectiveness.

1.1.1 Motivation

Compared to a single, probably more complex, agent, a bevy of more simple agents can provide cost and robustness benefits [15], as the system may still be able to operate when a single agent fails. Moreover, one could state that usage of multiple drones is more efficient, as the number of drones used could be scaled to the task's requirements. An additional advantage of using multi-agent systems is that they introduce parallelism [15] and therefore, smart charging or smart maintenance protocols could be introduced to allow for continuous operation. Therefore, a system of cooperating agents can be considered super-additive, as the cooperating agents' performance surpasses that of the sum of the capabilities of individuals. This super-additivity attribute originates from the fact that cooperating agents can together perform tasks that a single agent simply cannot [16], like multiple people are required to lift heavy objects. Also, by enabling mutual communication, the sensor data of the agents can be accessed by all agents in the pack, allowing for more efficient behavior [17]. As cooperation is getting more important, so is the capability of the network to avoid collisions. While in networks of unmanned ground vehicles (UGV), a collision would result in mere a bump, colliding agents in a network of UAVs will suffer mostly from the impact with the ground upon crashing. As stated before, an abundant amount of research has been conducted investigating collision avoidance strategies, but previous research generally lacks proof that collisions are indeed avoided, or only gives optimal collision avoidance strategies, if it gives some substantiation at all. This stimulates the desire to extend the approach of [14] to also incorporate a collision avoidance strategy and serve as a basis for experimental implementation.

1.1.2 Collision avoidance strategies

Roughly three main types of collision avoidance strategies are distinguished; using model predictive control (MPC) to continuously recompute reference trajectories, defining the system as a switched system, and introduction of an artificial potential field (APF).

The MPC approach models obstacles as three dimensional ellipsoids and uses these as constraints in an optimization problem to compute new reference trajectories [18], or can additionally be used to address reference and attitude tracking [19]. An interesting feature of this method is

that it allows to model ellipsoids tightly or loosely around an obstacle, depending on how well the obstacle is observed. However, since MPC only gives an optimal solution, no guarantee that collisions are indeed avoided can be given. Additionally, continuously recomputing reference trajectories becomes computationally expensive, which is undesirable as the aim is autonomous operation of agents which most often only provide limited processor capacity.

Another approach to incorporate collision avoidance is through defining the dynamics such that the behavior of the agents switches from reference tracking to collision avoidance. In [20] the behavior of the agents switches from reference tracking to collision avoidance when another agent comes within a predefined range of the considered agent, and when a collision is avoided the behavior of the systems switches back to reference tracking. While stability can be proven using a common Lyapunov function for both systems, this approach becomes rather cumbersome and complex, especially when it is additionally required to prove that collisions are avoided.

The collision avoidance strategy that seems to be most in line with [13, 14], is the introduction of an artificial potential field (APF). While an APF can have multiple names like repelling vector field [10, 21, 22] or bump function [23], the underlying method is equal. To implement an APF, the control action is split up in multiple parts; a reference tracking part and a collision avoidance part. In [22], this collision avoidance part is split up even further in a dedicated avoidance strategy for obstacles, and one for other agents. The collision avoidance part then consists of a potential placed at the other agents' positions, i.e., at the collision points, and thus driving the agents away from this collision point. This could be compared with artificially placing the collision point on a hill and the reference position in a nadir, where the considered system is an arbitrarily placed ball subject to gravity. But again, existing research lacks any proof of the absence of collisions.

1.2 Problem definition

Previous research conducted at the Eindhoven University of Technology presents a control strategy on $SE(3)$ for a single quadcopter allowing large angular maneuvers [13, 24], and extended this strategy to control a network of quadcopters [14, 25]. Since only [24] presents an experimental validation, it is desired to also implement the results of [14] in an experimental setup. As a first step towards the goal of autonomously flying a network of quadcopters, [26] extends the standard state estimator to include also external influences and achieves omission of external position data coming, for example, from an external camera system as OptiTrack [27]. According to [26], the newly designed state estimator is supposed to be sufficiently accurate when reference trajectories in the horizontal plane are considered, in vertical direction a small mismatch between simulation and experiment remains. Therefore, this research aims to provide a basis for conduction of experiments with a network of quadcopters. A first step towards conducting experiments with a network of quadcopters is to extend the current experimental setup to support simultaneous flight of multiple quadcopters, as the software support package of the experimental setup initially only supports control of a single drone. Before conducting experiments with multiple live quadcopters, a collision avoidance strategy is to be implemented in the dynamic framework of [14] to avoid unnecessary damage to the setup. When a theoretically substantiated collision avoidance strategy is developed with promising results, the designed control law is to be implemented in the adjusted experimental setup in order to evaluate its performance. For successful execution of this research, the following objectives are to be achieved;

- Consider a one-dimensional kinematic model with multiple agents and design a control law with which both reference tracking and collision avoidance can be simultaneously proven. To stress the relevance of considering this situation, such a model can be crudely compared with a platooning problem on a single lane.
- Extend the obtained result of a one-dimensional kinematic model to a network of double

integrators in arbitrary dimension. This is considered a relevant intermediate step as the dynamic framework in [13, 14] is based on the assumption that the quadcopters are a cascade of double integrators as in [28].

- Follow the analysis and dynamical framework of [13, 14] in order to find control laws with which both reference tracking and collision avoidance can be proven.
- Validate the theoretical findings by combining a simulated environment with experimental validation. This also includes preparing the experimental setup in order to support simultaneous flight of multiple quadcopters.

1.3 Thesis outline

The remainder of this report kicks off by introducing some preliminary mathematical notions which are used throughout the report. Chapter 3 presents the theoretical analyses of the different considered systems and the corresponding proofs. To invigorate the theoretical analysis, the findings are validated by comparison with simulations and experiments in Chapter 4. Finally, the obtained results are contemplated in Chapter 5 in the form of conclusions and recommendations.

Chapter 2

Preliminaries

For notational and comprehensive efficiency later on in the report, some theorems, notations, and definitions that are used extensively throughout this report, are presented here. The used attitude representations are introduced and some theorems and proofs regarding stability are given.

2.1 Attitude representation

As quadcopter UAVs are underactuated systems, the attitude of an agent plays a key role in the dynamics. Since the attitude representation is this important, a significant amount of research has been conducted in the different representations, each representation satisfying different needs and requirements. When it is desired to represent attitude mathematically efficient, for example when data (rate) or computational power is limited, quaternions can be used [29]. However, attitude representation using quaternions introduces sign ambiguity, while it actually is quite important to have the attitude uniquely defined. Therefore, it is chosen to represent the attitude using rotation matrices of the special orthogonal group $SO(3)$ of order 3. As one is entirely free to convert the designed controller to quaternions for implementation, it is possible in to exploit the advantages of both representations, being; unambiguous attitude representation and computational and communication efficiency. Both representations are presented in this section, some mathematical notions are stated and some complementary information on the motivation of the chosen attitude representation is given.

2.1.1 Rotation matrices and Euler angles

First, a right-handed orthonormal world-fixed inertial frame \mathcal{I} is introduced. Now the rotation matrix $R_i \in SO(3)$ is defined as the attitude of the right handed orthonormal body-fixed frame \mathcal{B}_i of agent i , with respect to the inertial frame \mathcal{I} , where $SO(3) = \{\mathbb{R}_i^{3 \times 3} \mid \det(R_i) = 1, R_i^\top R_i = I\}$ represents the 3-dimensional Special Orthogonal group. For any rotation matrix $R_i \in SO(3)$ the following should hold [30];

- The orthogonality property of the rotation matrix implies that $R_i R_i^\top = I_3$, where I_3 is the 3×3 identity matrix, implying $R_i^\top = R_i^{-1}$.
- Since R_i defines a pure rotation, i.e., no elongations are incorporated, $\det(R_i) = 1$.
- Each column of R_i and R_i^\top is mutually orthogonal since they are both rotation matrices.
- Each column of R_i and R_i^\top is of unit length since they are both rotation matrices.

To describe a rotation from \mathcal{I} to \mathcal{B}_i in the three dimensional space, rotation matrices $R_i \in SO(3)$ are considered. Now, the rotation from \mathcal{I} to \mathcal{B}_i can be defined using different sequences of

rotations. One could define a rotation by using the axis-angle convention, which defines a rotation between two frames as an axis with a rotation angle around the defined axis. Yet, a commonly used method in (aero)nautical applications to represent a rotation is by using Euler angles [31], as

$$R = R_{z,i}(\psi_i)R_{y,i}(\theta_i)R_{x,i}(\phi_i), \quad (2.1a)$$

$$= \begin{bmatrix} \cos \psi_i & -\sin \psi_i & 0 \\ \sin \psi_i & \cos \psi_i & 0 \\ 0 & 0 & 1 \end{bmatrix} \begin{bmatrix} \cos \theta_i & 0 & \sin \theta_i \\ 0 & 1 & 0 \\ -\sin \theta_i & 0 & \cos \theta_i \end{bmatrix} \begin{bmatrix} 1 & 0 & 0 \\ 0 & \cos \phi_i & -\sin \phi_i \\ 0 & \sin \phi_i & \cos \phi_i \end{bmatrix}, \quad (2.1b)$$

which is the so called Roll-Pitch-Yaw angles (RPY) variant, as they correspond to the roll, pitch, and yaw motion of the body i when aligned with the axes of the body fixed frame \mathcal{B}_i . Note that the same rotations in the reversed order generally not result in the same attitude [32]. The Euler angles attitude representation is widely used for its ease of use and tangibility. Note however, that (2.1) emphasizes the occurrence of singularities when two axes are aligned. The inertial frame is considered in North-East-Down (NED) configuration along the lines of [14, 26], as it has proven useful for the modeling and control of aerial vehicles [33]. Since a dynamic system is to be considered, the time-derivative of the attitude representation also deserves elaboration, especially since the time-derivatives of rotation matrices in $\text{SO}(n)$ come with some convenient properties.

Definition 2.1.1. (cf. [30]) *Consider a rotation matrix $R \in \text{SO}(3)$ and define three generators for $\text{SO}(3)$ that correspond to the derivatives of rotation around each of the standard axes [34]*

$$G_x = \begin{bmatrix} 0 & 0 & 0 \\ 0 & 0 & -1 \\ 0 & 1 & 0 \end{bmatrix}, \quad G_y = \begin{bmatrix} 0 & 0 & 1 \\ 0 & 0 & 0 \\ -1 & 0 & 0 \end{bmatrix}, \quad G_z = \begin{bmatrix} 0 & -1 & 0 \\ 1 & 0 & 0 \\ 0 & 0 & 0 \end{bmatrix}, \quad (2.2)$$

consider also the body-fixed angular velocity of the rotated frame $\omega \in \mathbb{R}^3$ with which

$$S(\omega) := \omega_x G_x + \omega_y G_y + \omega_z G_z = \begin{bmatrix} 0 & -\omega_z & \omega_y \\ \omega_z & 0 & -\omega_x \\ -\omega_y & \omega_x & 0 \end{bmatrix} \in \text{SO}(3), \quad (2.3)$$

is defined.

2.1.2 Quaternions

As an alternative to rotation matrices, quaternions can be used for attitude representation. Both rotation matrices and quaternions are well suited for integrating angular velocities of bodies over time, nonetheless, a benefit of using quaternions is that no singularities occur in the involved functions. Though this comes at the cost of ambiguity, implying that an equal positive and negative quaternion describe the same rotation [35]. When designing the controller using rotation matrices and converting to quaternions before implementation, this disadvantage can be effectively bypassed. Moreover, a quaternion has the feature that it can describe a rotation using only four parameters,

$$q = q_w + q_x i + q_y j + q_z k, \quad (2.4)$$

making it a preferred choice over rotation matrices when computational effort, storage capacity or data rates are limited [29], for example when implementing in an experimental setup or when communication channels are used. Consider a quaternion $q \in \mathbb{H}$, with \mathbb{H} the quaternion space, which can be considered as a number system that extends the complex numbers [36]. Besides (2.4), quaternions can be represented as

$$q = (q_w, \tilde{q}), \quad q = [q_w \ q_x \ q_y \ q_z]^\top, \quad (2.5)$$

which includes a vector notation consisting of a scalar and an imaginary vector. The imaginary units i , j , and k satisfy

$$i^2 = j^2 = k^2 = ijk = -1. \quad (2.6)$$

Additionally, the norm $\|q\|$ and conjugate \bar{q} of a quaternion are computed as

$$\|q\| = \sqrt{q_w^2 + q_x^2 + q_y^2 + q_z^2}, \quad (2.7)$$

$$\bar{q} = [q_w \quad -q_x \quad -q_y \quad -q_z]^\top = (q_w, -\tilde{q}). \quad (2.8)$$

Now using (2.6), a quaternion multiplication is denoted by the \otimes operator, and is defined as

$$p \otimes q = \begin{bmatrix} p_w q_w - p_x q_x - p_y q_y - p_z q_z \\ p_w q_x + p_x q_w + p_y q_z - p_z q_y \\ p_w q_y - p_x q_z + p_y q_w + p_z q_x \\ p_w q_z + p_x q_y - p_y q_x + p_z q_w \end{bmatrix}, \quad (2.9)$$

which alternatively can be written as the inner product of a skew-symmetric matrix $Q(p)$ and a quaternion q as

$$p \otimes q = Q(p)q = \begin{bmatrix} p_w & -\tilde{p}^\top \\ \tilde{p} & p_w I_3 + S(\tilde{p}) \end{bmatrix} q = \begin{bmatrix} p_w & -p_x & -p_y & -p_z \\ p_x & p_w & -p_z & p_y \\ p_y & p_z & p_w & -p_x \\ p_z & -p_y & p_x & p_w \end{bmatrix} \begin{bmatrix} q_w \\ q_x \\ q_y \\ q_z \end{bmatrix}, \quad (2.10a)$$

$$= \bar{Q}(q)p = \begin{bmatrix} q_w & -\tilde{q}^\top \\ \tilde{q} & q_w I_3 + S(\tilde{q}) \end{bmatrix} p = \begin{bmatrix} q_w & -q_x & -q_y & -q_z \\ q_x & q_w & -q_z & q_y \\ q_y & q_z & q_w & -q_x \\ q_z & -q_y & q_x & q_w \end{bmatrix} \begin{bmatrix} p_w \\ p_x \\ p_y \\ p_z \end{bmatrix}. \quad (2.10b)$$

Using the axis-angle method [35], every rotation can be described by defining an axis and a clockwise rotation around the defined axis. This clearly holds for a sequence of multiple rotations as well, and consequently, a sequence of rotations can be expressed using a single quaternion [37] as

$$q_w = \cos\left(\frac{\theta}{2}\right), \quad \tilde{q} = \sin\left(\frac{\theta}{2}\right) \bar{e}, \quad (2.11)$$

with $\bar{e} \in \mathbb{R}^3$ a unit vector representing the rotation axis and $\theta \in \mathbb{R}$ denoting the clockwise rotation angle. Thus, a quaternion, actually a unit quaternion, i.e., $\{q \mid \|q\| = 1\}$, can be used to describe a rotation. To express a rotation in quaternions, the vector ρ to be rotated is first converted to a quaternion q_ρ by setting $q_\rho = (q_{\rho,w}, \tilde{q}_\rho)$ with $q_{\rho,w} = 0$ and $\tilde{q}_\rho = \rho$. The resulting quaternion is called a pure quaternion since $q_{\rho,w} = 0$. Next, the rotated vector ρ' is obtained by pre- and post-multiplying ρ with the rotation quaternion $q = (q_w, \tilde{q})$ and its conjugate $\bar{q} = (q_w, -\tilde{q})$, respectively, as

$$\begin{bmatrix} 0 \\ \rho' \end{bmatrix} = q \otimes \begin{bmatrix} 0 \\ \rho \end{bmatrix} \otimes \bar{q}, \quad (2.12)$$

which can be computed more efficiently [29] as

$$\rho' = \rho + 2\tilde{q} \times (\tilde{q} \times \rho + q_w \rho), \quad (2.13)$$

which for simplicity is denoted compactly as $\rho' = q \odot \rho$, where it is noted that the inverse rotation is given by $\rho = \bar{q} \odot \rho'$. Now, a quaternion describing a rotation describes a full Euler rotation [38] as

$$q = \begin{bmatrix} \cos(\phi/2)\cos(\theta/2)\cos(\psi/2) + \sin(\phi/2)\sin(\theta/2)\sin(\psi/2) \\ \sin(\phi/2)\cos(\theta/2)\cos(\psi/2) - \cos(\phi/2)\sin(\theta/2)\sin(\psi/2) \\ \cos(\phi/2)\sin(\theta/2)\cos(\psi/2) + \sin(\phi/2)\cos(\theta/2)\sin(\psi/2) \\ \cos(\phi/2)\cos(\theta/2)\sin(\psi/2) - \sin(\phi/2)\sin(\theta/2)\cos(\psi/2) \end{bmatrix}, \quad (2.14)$$

of which the inverse conversion is given as

$$\begin{bmatrix} \phi \\ \theta \\ \psi \end{bmatrix} = \begin{bmatrix} \arctan 2(2(q_w q_x + q_y q_z), 1 - 2(q_x^2 + q_y^2)) \\ \arcsin(2(q_w q_y - q_z q_x)) \\ \arctan 2(2(q_w q_z + q_x q_y), (1 - 2(q_y^2 + q_z^2))) \end{bmatrix}, \quad (2.15)$$

with ϕ , θ , and ψ representing again the roll, pitch, and yaw angle, respectively. Finally, the derivative of a quaternion is computed using

$$\dot{q} = \frac{1}{2}q \otimes \begin{bmatrix} 0 \\ \omega \end{bmatrix} = \frac{1}{2}Q(q) \begin{bmatrix} 0 \\ \omega \end{bmatrix}. \quad (2.16)$$

2.2 Stability results

Stability of dynamic systems is a widely studied subject, and some results regarding stability are recalled here for notation efficiency further in the report.

Proposition 2.2.1. (cf. [39], Theorem 4.3) *Let $x_{\text{eq}} = 0$ be an equilibrium point of*

$$\dot{x} = f(x). \quad (2.17)$$

Let $V : D \rightarrow \mathbb{R}$ be a continuously differentiable function such that $V(0) = 0$ and $V(x_0) > 0$ for some x_0 with arbitrary small $\|x_0\|$. Define a set $U = \{x \in B_r \mid V(x) > 0\}$ with $B_r = \{x \in \mathbb{R}^n \mid \|x\| \leq r\}$ a ball contained in D , with $r > 0$ and suppose that $\dot{V}(x) > 0$ in U . Then, $x = 0$ is unstable.

Proposition 2.2.2. (cf. [39], Theorem 4.14) *Let $x = 0$ be an equilibrium point for the nonlinear system*

$$\dot{x} = f(t, x), \quad (2.18)$$

where $f : [0, \infty) \times D \rightarrow \mathbb{R}^n$ is continuously differentiable, $D = \{x \in \mathbb{R}^n \mid \|x\| < r\}$, and the Jacobian matrix $[\partial f / \partial x]$ is bounded on D , uniformly in t . Let k , λ , and r_0 be positive constants with $r_0 < r/k$. Let $D_0 = \{x \in \mathbb{R}^n \mid \|x\| < r_0\}$. Assume that the trajectories of the system satisfy

$$\|x(t)\| \leq k\|x(t_0)\|e^{-\lambda(t-t_0)}, \quad \forall x(t_0) \in D_0, \quad \forall t \geq t_0 \geq 0, \quad (2.19)$$

then, there is a function $V : [0, \infty) \times D_0 \rightarrow \mathbb{R}$ that satisfies the inequalities

$$c_1\|x\|^2 \leq V(t, x) \leq c_2\|x\|^2, \quad (2.20a)$$

$$\frac{\partial V}{\partial t} + \frac{\partial V}{\partial x} f(t, x) \leq -c_3\|x\|^2, \quad (2.20b)$$

$$\left\| \frac{\partial V}{\partial x} \right\| \leq c_4\|x\|, \quad (2.20c)$$

for some positive constants c_1 , c_2 , c_3 , and c_4 . Moreover, if $r = \infty$ and the origin is globally exponentially stable, then $V(t, x)$ is defined and satisfies the aforementioned inequalities on \mathbb{R}^n . Furthermore, if the system (2.18) is autonomous, V can be chosen independent of t .

Proposition 2.2.3. (cf. [39], Theorem 4.15) *Let $x = 0$ be an equilibrium point for the nonlinear system (2.18) where $f : [0, \infty) \times D \rightarrow \mathbb{R}^n$ is continuously differentiable, $D = \{x \in \mathbb{R}^n \mid \|x\|_2 < r\}$, and the Jacobian matrix $[\partial f / \partial x]$ is bounded and Lipschitz on D , uniformly in t . Let*

$$A(t) = \left. \frac{\partial f}{\partial x}(t, x) \right|_{x=0}, \quad (2.21)$$

then, $x = 0$ is an exponentially stable equilibrium point for the nonlinear system if and only if it is an exponentially stable equilibrium point for the linear system

$$\dot{x} = A(t)x. \quad (2.22)$$

Proposition 2.2.4. (cf. [39], Theorem 4.1) *Consider the autonomous system*

$$\dot{x} = f(x), \quad (2.23)$$

where $f : D \rightarrow \mathbb{R}^n$ is a locally Lipschitz map from a domain $D \subset \mathbb{R}^n$ into \mathbb{R}^n . Let $x = 0$ be an equilibrium point for (2.23) and $D \subset \mathbb{R}^n$ be a domain containing $x = 0$. Let $V : D \rightarrow \mathbb{R}$ be a continuously differentiable function such that

$$V(0) = 0, \quad V(x) > 0 \text{ in } D \setminus \{0\}, \quad \dot{V}(x) \leq 0 \text{ in } D, \quad (2.24)$$

then, $x = 0$ is stable. Moreover, if

$$\dot{V}(x) < 0 \text{ in } D \setminus \{0\}, \quad (2.25)$$

then, $x = 0$ is asymptotically stable.

Theorem 2.1. (adopted from [39], Theorem 4.1, see Proposition 2.2.4) *Consider the autonomous system (2.23), let $x = 0$ be an equilibrium point of (2.23) on a domain $D \subset \mathbb{R}^n$, and $x = \gamma$ be an arbitrary point satisfying $\gamma \in D \setminus \{0\}$. Let $V : D \rightarrow \mathbb{R}$ be a continuously differentiable function such that*

$$V(0) = 0, \quad V(x) > 0 \text{ in } D \setminus \{0\}, \quad \dot{V}(x) \leq 0 \text{ in } D, \quad (2.26)$$

now, if additionally

$$V(\gamma) \rightarrow \infty \text{ for } x \rightarrow \gamma, \quad x_0 \neq \gamma, \text{ and } \dot{V} < 0 \text{ in } B_\gamma \quad (2.27)$$

with $B_\gamma = \{x \in \mathbb{R}^n \mid \|x - \gamma\| < r\}$ a ball of radius $r > 0$ around γ , contained in D , then, for every solution x to (2.23) with initial conditions satisfying $x(t_0) \neq \gamma$, there exists $\epsilon > 0$ such that $\|x(t) - \gamma\| \geq \epsilon \forall t$.

Proposition 2.2.5. (cf. [25, 40]) *Consider the system*

$$\dot{\tilde{R}} = \tilde{R}S(\tilde{\omega}), \quad J\dot{\tilde{\omega}} = -K_\omega\tilde{\omega} + K_R \sum_{i=1}^3 k_i(e_i \times \tilde{R}^\top e_i), \quad (2.28)$$

with $\tilde{R} \in \text{SO}(3) = \{\tilde{R} \in \mathbb{R}_i^{3 \times 3} \mid \det(\tilde{R}) = 1, \tilde{R}^\top \tilde{R} = 0\}$, $\tilde{\omega} \in \mathbb{R}^3$, $J = J^\top > 0$ and $S(\tilde{\omega})$ the operator defined in (2.3). If $K_\omega = K_\omega^\top > 0$, $K_R = K_R^\top > 0$, and $k_i > 0$ distinct, i.e., $k_1 \neq k_2 \neq k_3 \neq k_1$, it can be concluded that the resulting equilibrium point $(\tilde{R}, \tilde{\omega}) = (I, 0)$ is ULES and UaGAS, i.e., let $E_c = \{I, \text{diag}(1, -1, -1), \text{diag}(-1, 1, -1), \text{diag}(-1, -1, 1)\}$, then \tilde{R} converges to E_c and $\tilde{\omega}$ converges to zero. The equilibria $(\tilde{R}, 0)$ where $\tilde{R} \in E_c \setminus \{I\}$ are unstable and the set of all initial conditions converging to the equilibrium $(\tilde{R}, 0)$, where $\tilde{R} \in E_c \setminus \{I\}$ form a lower dimensional manifold.

Theorem 2.2. (cf. [14, 41]) *Consider the cascaded system $\dot{x} = f(t, x)$, with $f(t, 0) = 0$, that can be written as*

$$\dot{x}_1 = f_1(t, x) + g(t, x_1, x_2)x_2, \quad (2.29a)$$

$$\dot{x}_2 = f_2(t, x_2), \quad (2.29b)$$

where $x_1 \in \mathbb{R}^n$, $x_2 \in \mathbb{R}^m$, $f_1(t, x_1)$ is continuously differentiable in (t, x_1) and $f_2(t, x_2)$, $g(t, x_1, x_2)$ are continuous in their arguments, and locally Lipschitz in x_2 and (x_1, x_2) , respectively. This system is a cascade of the system

$$\dot{x}_1 = f_1(t, x_1), \quad (2.30)$$

and (2.29b). If the origins of the systems (2.30) and (2.29b) are uniform globally asymptotically stable (UGAS) and solutions of (2.29) remain bounded, then the origin of the system (2.29) is UGAS. In addition, if the systems (2.30) and (2.29b) are uniformly locally exponentially stable (ULES), then the system (2.29) is ULES.

Chapter 3

Stability analysis

This chapter aims to give a theoretical framework to be used when a collision avoidance strategy is required and it is desired to actually prove the absence of collisions in the network. The complexity of the considered dynamics is gradually increased from a system of single integrators in 1D, to a system of double integrators in arbitrary dimension and finally, quadcopter dynamics are considered to implement a collision avoidance strategy. This increasing complexity helps in understanding the functioning of the introduced framework, while considering some interesting situations. A system of single integrators in the one dimensional space could for example represent a simplified model of a platoon of autonomously driving cars on a single lane highway, for which one would like to guarantee that no collisions occur when overtaking is not allowed. Considering a system of double integrators in arbitrary dimension proves to be useful as the analysis uses vectors instead of scalars. Moreover, it gives some valuable insights already for the analysis of a network of quadcopter UAVs, as these systems can be considered a cascade of two double integrator systems.

3.1 Single integrators in 1D

As a first step towards stability in a network of UAVs with obstacle avoidance, a system of two single integrators in 1D is considered. The considered system in 1D can give valuable insights for the final analysis of a system of UAVs, but is also a relevant system as it can represent a model of autonomously driving cars on a single lane. For the considered system it is desired to show stability of the tracking behavior while proving also that no collisions occur in the system. A first challenge is therefore to design a controller which achieves reference tracking and collision avoidance simultaneously. Additionally, an interesting situation is analyzed which occurs when the two agents are initialized in such a way that the agents will have to collide before reaching their respective references.

The considered system of a single integrator is given as

$$\dot{x}_i = u_i, \tag{3.1}$$

where $i \in \{1, 2\}$, and $x_i \in \mathbb{R}$, and $u_i \in \mathbb{R}$ denote, respectively, the position and input of agent i . Next, the reference trajectory $x_{i,r}$ is introduced which is also subject to (3.1), implying $\dot{x}_{i,r} = u_{i,r}$. Now, the tracking error for node i is defined as $\tilde{x}_i = x_i - x_{i,r}$, the position of node i with respect to node j is denoted by $d_{ij} = -d_{ji} = x_i - x_j$, and the referenced relative position of node i with respect to node j is defined as $d_{ij,r} = -d_{ji,r} = x_{i,r} - x_{j,r}$, which are scalars as a one-dimensional system is considered. Note that it is assumed that $x_{i,r}(t) \neq x_{j,r}(t)$, i.e., $d_{ij,r}(t) \neq 0 \forall t$, since $x_{i,r}(t) = x_{j,r}(t)$ implies a collision for the reference trajectory. The reference tracking dynamics is now given as

$$\dot{\tilde{x}}_i = \dot{x}_i - \dot{x}_{i,r} = u_i - u_{i,r}, \tag{3.2}$$

and the relative position dynamics is given as

$$\dot{d}_{ij} = \dot{x}_i - \dot{x}_j = u_i - u_j. \quad (3.3)$$

With the system properly defined, the control objectives can be stated as the following problem.

Problem 3.1. *Consider the reference tracking dynamics (3.2) with $i \in \{1, 2\}$. Find an appropriate control law*

$$u_i = u_i(t, \tilde{x}_1, \tilde{x}_2), \quad (3.4)$$

such that the resulting closed-loop system yields

$$\lim_{t \rightarrow \infty} \tilde{x}_1 = 0, \quad \lim_{t \rightarrow \infty} \tilde{x}_2 = 0, \quad d_{12}(t) \neq 0 \quad \forall t. \quad (3.5)$$

As a possible solution to the stated objectives, a controller is designed which combines the tracking controller used in [28] and a collision avoidance strategy based on [42], resulting in the combined control input

$$u_i = u_{i,r} - k_1 \tilde{x}_i + k_2 \left(\frac{1}{d_{ij}} - \frac{1}{d_{ij,r}} \right) = u_{i,r} - k_1 \tilde{x}_i + (-1)^i k_2 \frac{\tilde{x}_1 - \tilde{x}_2}{(\tilde{x}_1 - \tilde{x}_2 + d_{12,r})d_{12,r}}, \quad (3.6)$$

where the gains k_1 and k_2 are to be chosen freely, and the term $k_2 \left(\frac{1}{d_{ij}} - \frac{1}{d_{ij,r}} \right)$ represents the collision avoidance strategy and results from usage of an artificial potential field (APF) in [42]. The reference tracking subsystem (3.2) is considered in closed-loop with control law (3.6), yielding

$$\dot{\tilde{x}}_i = u_i - u_{i,r} = -k_1 \tilde{x}_i + k_2 \left(\frac{1}{d_{ij}} - \frac{1}{d_{ij,r}} \right), \quad (3.7)$$

with $k_1, k_2 > 0$, which can be rewritten as

$$\dot{\tilde{x}}_1 = -k_1 \tilde{x}_1 - k_2 \frac{\tilde{x}_1 - \tilde{x}_2}{(\tilde{x}_1 - \tilde{x}_2 + d_{12,r})d_{12,r}}, \quad (3.8a)$$

$$\dot{\tilde{x}}_2 = -k_1 \tilde{x}_2 + k_2 \frac{\tilde{x}_1 - \tilde{x}_2}{(\tilde{x}_1 - \tilde{x}_2 + d_{12,r})d_{12,r}}. \quad (3.8b)$$

3.1.1 Instability of collision point

Before analyzing stability of the reference tracking subsystem (3.8), it is desired to show that no collisions occur in the system, i.e., $d_{12}(t) \neq 0 \quad \forall t$. Therefore, consider the following proposition.

Proposition 3.1.1. *Consider the dynamics (3.3) in closed-loop with input (3.6) where $k_1, k_2 > 0$. If the reference signals $|d_{12,r}|$, $|d_{12,r}^{-1}|$, and $|u_{1,r} - u_{2,r}|$ are bounded, then for every solution to (3.3) in closed loop with (3.6), with initial conditions satisfying $d_{12}(t_0) \neq 0$, there exists $\epsilon > 0$ such that $|d_{12}(t)| \geq \epsilon \quad \forall t$.*

Proof. Differentiating the candidate Lyapunov function

$$V(d_{12}) = \frac{1}{2} d_{12}^2, \quad (3.9)$$

along solutions of the system (3.3) in closed-loop with (3.6) yields

$$\dot{V}(d_{12}) = 2k_2 - k_1 d_{12}^2 + \left(k_1 d_{12,r} - \frac{2k_2}{d_{12,r}} + u_{1,r} - u_{2,r} \right) d_{12}, \quad (3.10)$$

with $d_{12} = x_1 - x_2 = \tilde{x}_1 - \tilde{x}_2 + d_{12,r}$, and $d_{12}(t_0) \neq 0$, as \dot{d}_{12} is undefined for $d_{12} = 0$. Since it is assumed that $|d_{12,r}|$, $|d_{12,r}^{-1}|$, and $|u_{1,r} - u_{2,r}|$ are bounded;

$$|d_{12,r}(t)| \leq M_1, \quad |d_{12,r}^{-1}(t)| \leq M_2, \quad |u_{1,r}(t) - u_{2,r}(t)| \leq M_3, \quad (3.11)$$

where it can be assumed that $d_{12,r} > 0$, without loss of generality, as $d_{12,r}(t) \neq 0 \forall t$, resulting in

$$\dot{V}(d_{12}) \geq 2k_2 - k_1 d_{12}^2 - (k_1 M_1 + 2k_2 M_2 + M_3) d_{12}, \quad (3.12)$$

which is used to give some bounds on the domain for which $\dot{V}(d_{12}) > 0$ by computing the roots of the right hand side as

$$0 < \epsilon_1 < \frac{-(k_1 M_1 + 2k_2 M_2 + M_3) + \sqrt{(k_1 M_1 + 2k_2 M_2 + M_3)^2 + 8k_1 k_2}}{2k_1}, \quad (3.13)$$

and

$$0 > \epsilon_2 > \frac{-(k_1 M_1 + 2k_2 M_2 + M_3) - \sqrt{(k_1 M_1 + 2k_2 M_2 + M_3)^2 + 8k_1 k_2}}{2k_1}. \quad (3.14)$$

Thus, there always exists a domain $\delta = \{d_{12} \mid \epsilon_2 < d_{12} < \epsilon_1\} = \{\tilde{x} \mid \epsilon_2 < \tilde{x}_1 - \tilde{x}_2 + d_{12,r}(t) < \epsilon_1\}$ where $\dot{V}(d_{12}) \geq f(d_{12}) > 0 \forall d_{12} \in \delta$, see Figure 3.1 for a visual indication of the situation. From Figure 3.1 it can be seen that $\dot{V}(d_{12}) > 0 \forall d_{12} \in \delta$, and there always exists such a domain δ as $2k_2 > 0$. Applying Chetaev's theorem, as in Proposition 2.2.1, indicates that the collision point

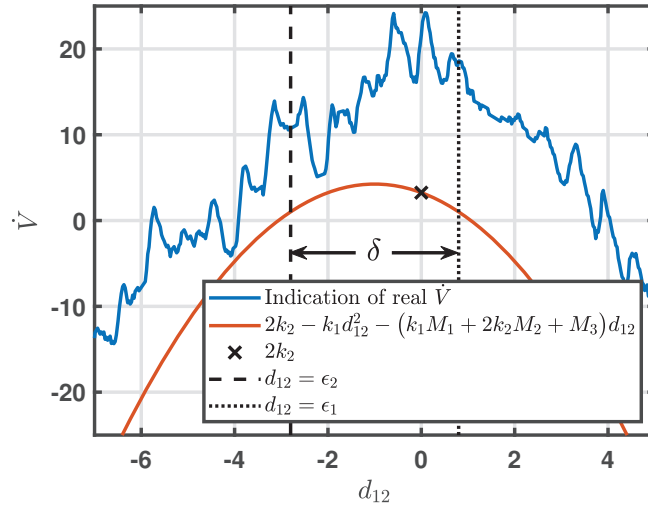


Figure 3.1: Visual indication of $\dot{V}(d_{12})$ and its lower bound given by $2k_2 - k_1 d_{12}^2 - (k_1 M_1 + 2k_2 M_2 + M_3) d_{12}$.

is unstable, and thus for every solution to the closed-loop system (3.8), with initial conditions satisfying $d_{12}(t_0) \neq 0$, there exists $\epsilon > 0$ such that $|d_{12}(t)| \geq \epsilon \forall t$. \square

3.1.2 Stability analysis

As Proposition 3.1.1 provides a solution to the part of Problem 3.1 requiring $d_{12}(t) \neq 0 \forall t$, the remaining two requirements still need to be proven. In order to provide a solution to the remaining requirements, it is desired to prove stability of the origin of the closed-loop system (3.8). Note that it can be assumed that $d_{12,r}(t) > 0$ without loss of generality (w.l.o.g.), since $d_{12}(t) = \tilde{x}_1(t) - \tilde{x}_2(t) + d_{12,r}(t) \neq 0 \forall t$ according to Proposition 3.1.1. To this end, consider the following proposition.

Proposition 3.1.2. *Consider the closed-loop reference tracking dynamics (3.8). If the controller gains satisfy $k_1, k_2 > 0$, the origin of the closed-loop system (3.8) is uniformly globally asymptotically stable (UGAS) on an invariant domain $D_1(t) = \{\tilde{x}(t) \mid d_{12}(t) > 0\}$, i.e., $\tilde{x}(t) \rightarrow 0$ for $t \rightarrow \infty$ with $\tilde{x}(t) \in D_1$.*

Proof. Define domain $D_1(t) = \{\tilde{x}(t) \mid d_{12}(t) > 0\}$ and note that this domain is invariant according to Proposition 3.1.1. Next, w.l.o.g. it is assumed that $d_{12,r}(t) > 0$, with which it is apparent that $\tilde{x} = [0, 0]^\top \in D_1$, when using $d_{12} = \tilde{x}_1 - \tilde{x}_2 + d_{12,r}$. Now consider the Lyapunov function V given by

$$V = \frac{1}{2}\tilde{x}_1^2 + \frac{1}{2}\tilde{x}_2^2, \quad (3.15)$$

differentiating along solutions of (3.8) yields

$$\dot{V} = -k_1\tilde{x}_1^2 - k_1\tilde{x}_2^2 - \frac{k_2(\tilde{x}_1 - \tilde{x}_2)^2}{(\tilde{x}_1 - \tilde{x}_2 + d_{12,r})d_{12,r}} \leq 0 \quad \text{for } \tilde{x} \in D_1. \quad (3.16)$$

Now, by using the definition of the domain D_1 and the assumption that $d_{12,r}(t) > 0$, it can be concluded that for $\tilde{x} \in D_1$ it holds that $V > 0 \forall \tilde{x} \neq 0$ and $\dot{V} < 0 \forall \tilde{x} \neq 0$. Applying Proposition 2.2.4 renders the equilibrium point $\tilde{x}_{\text{eq}} = [0, 0]^\top$ uniformly globally asymptotically stable (UGAS) on D_1 , completing the proof. \square

Additionally, in order to analyse stability for $\tilde{x}_1 - \tilde{x}_2 + d_{12,r} = d_{12} < 0$, i.e., when $d_{12} \notin D_1$, consider the following proposition.

Proposition 3.1.3. *Consider a projection of the closed-loop reference tracking dynamics (3.8) defined by*

$$z_1 = \tilde{x}_1 + \tilde{x}_2, \quad (3.17)$$

differentiating yields the projected dynamics

$$\dot{z}_1 = \dot{\tilde{x}}_1 + \dot{\tilde{x}}_2 = -k_1 z_1. \quad (3.18)$$

If the controller gains are chosen as $k_1, k_2 > 0$, the origin of (3.18) is uniformly globally asymptotically stable (UGAS), i.e., $z_1(t) \rightarrow 0$ for $t \rightarrow \infty$, and $\tilde{x}_1 - \tilde{x}_2$ stays bounded.

Proof. Consider candidate Lyapunov function

$$V(z_1) = \frac{1}{2}k_1 z_1^2, \quad (3.19)$$

differentiating along solutions (3.18) yields

$$\dot{V}(z_1) = -k_1 z_1^2 \leq 0, \quad (3.20)$$

and it can be seen that $V > 0 \forall z_1 \neq 0$ and $\dot{V} < 0 \forall z_1 \neq 0$. Applying Proposition 2.2.4 renders the origin of (3.18) UGAS. To additionally show that $\lim_{t \rightarrow \infty} \tilde{x}_1(t) - \tilde{x}_2(t)$ is bounded, consider the additional projected variable

$$z_2 = \tilde{x}_1 - \tilde{x}_2, \quad (3.21)$$

differentiating yields the projected dynamics

$$\dot{z}_2 = \dot{\tilde{x}}_1 - \dot{\tilde{x}}_2 = -k_1 z_2 - 2k_2 \frac{z_2}{(z_2 + d_{12,r})d_{12,r}}. \quad (3.22)$$

Now consider candidate Lyapunov function

$$V(z_2) = \frac{1}{2}k_1 z_2^2, \quad (3.23)$$

differentiating along solutions (3.22) yields

$$\dot{V}(z_2) = - \left(k_1 + \frac{2k_2}{(z_2 + d_{12,r})d_{12,r}} \right) z_2^2, \quad (3.24)$$

and note that when $z_2 + d_{12,r} = d_{12} > 0$, it can be seen that $\dot{V} \leq 0$ and the result of Proposition 3.1.2 is obtained. From (3.24) it can be seen that $\dot{V} \leq 0$ for $z_2 \leq -d_{12,r} - \frac{2k_2}{k_1 d_{12,r}}$ when $z_2 + d_{12,r} = d_{12} < 0$, and thus z_2 is bounded as long as $d_{12,r}$ is bounded. This completes the proof. \square

Note that Proposition 3.1.3 can be used to obtain the result of Proposition 3.1.2, but it also proves $\lim_{t \rightarrow \infty} (\tilde{x}_1(t) + \tilde{x}_2(t)) = 0$ for $\tilde{x} \in D_2 = \{\tilde{x} \mid d_{12} < 0\}$, while showing that $\tilde{x}_1(t) - \tilde{x}_2(t)$ remains bounded.

Collision before reaching reference

When $\tilde{x} \in D_2 = \{\tilde{x} \mid \tilde{x}_1 - \tilde{x}_2 + d_{12,r} < 0\}$ it might be interesting to require $d_{12}(t) = -d_{12,r}(t)$ for $t \rightarrow \infty$, since the resulting formation shape would be the desired formation shape. To achieve this, (3.24) is set equal to zero and consider $z_2 + d_{12,r} = d_{12} < 0$ to obtain

$$z_2 + d_{12,r} = d_{12} = -\frac{2k_2}{k_1 d_{12,r}}, \quad (3.25)$$

from which it can be seen that $\lim_{t \rightarrow \infty} d_{12}(t) = -\lim_{t \rightarrow \infty} d_{12,r}(t)$ for controller gains k_1 and k_2 chosen according to

$$\lim_{t \rightarrow \infty} d_{12,r} = \sqrt{\frac{2k_2}{k_1}}, \quad (3.26)$$

as only time-independent controller gains are considered. This indicates that when $\lim_{t \rightarrow \infty} d_{12,r}$ is a constant, the formation shape in steady-state will always be the desired formation shape, irrespective of initial conditions, albeit that agent one might be at the position of agent two.

Concluding remarks

Combining Propositions 3.1.1 and 3.1.2 provides a solution to Problem 3.1, proving stability of the reference tracking subsystem, while simultaneously proving the absence of collisions in the entire system. Additionally, Proposition 3.1.3 shows that $\lim_{t \rightarrow \infty} \tilde{x}_1(t) + \tilde{x}_2(t) = 0$ is UGAS for solutions with $d_{12}(t_0) < 0$, which will never reach $d_{12} = d_{12,r}$, while showing that $\tilde{x}_1(t) - \tilde{x}_2(t)$ is bounded. Finally, a special situation is considered where $\lim_{t \rightarrow \infty} d_{12}(t) = -\lim_{t \rightarrow \infty} d_{12,r}(t)$ is required when $d_{12} \in D_2$, and the corresponding controller gains are given.

3.2 Double integrators in 1D

Now that the system of single integrators in 1D is fully analyzed with respect to tracking behavior and instability of the collision point, the system dynamics (3.1) is extended from a kinematic model to a dynamic model as

$$\dot{x}_i = v_i, \quad (3.27a)$$

$$\dot{v}_i = u_i, \quad (3.27b)$$

where $i \in \{1, 2\}$, and $x_i \in \mathbb{R}$, $v_i \in \mathbb{R}$ and $u_i \in \mathbb{R}$ denote, respectively, the position, velocity and input of agent i . Again, the reference trajectory $x_{i,r}$ is introduced which is also subject to (3.27), implicating $\dot{x}_{i,r} = v_{i,r}$, $\dot{v}_{i,r} = u_{i,r}$. The tracking and velocity error for node i are, respectively, defined as $\tilde{x}_i = x_i - x_{i,r}$ and $\tilde{v}_i = v_i - v_{i,r}$, the position of node i with respect to node j is denoted by $d_{ij} = -d_{ji} = x_i - x_j$, the referenced relative position of node i with respect to node j is defined as $d_{ij,r} = -d_{ji,r} = x_{i,r} - x_{j,r}$, the relative velocity of node i with respect to node j is denoted as $v_{ij} = v_i - v_j$, and the reference relative velocity is given as $v_{ij,r} = v_{i,r} - v_{j,r}$, which are all scalars as a one-dimensional system is considered. Note that it is assumed that $x_{i,r}(t) \neq x_{j,r}(t)$, i.e., $d_{ij,r}(t) \neq 0 \forall t \neq 0$, since $x_{i,r}(t) = x_{j,r}(t)$ would result in a collision. The reference tracking dynamics is now given as

$$\dot{\tilde{x}}_i = \dot{x}_i - \dot{x}_{i,r} = v_i - v_{i,r} = \tilde{v}_i, \quad (3.28a)$$

$$\dot{\tilde{v}}_i = \dot{v}_i - \dot{v}_{i,r} = u_i - u_{i,r}, \quad (3.28b)$$

and the relative position dynamics is given as

$$\dot{d}_{ij} = \dot{x}_i - \dot{x}_j = v_i - v_j = v_{ij}, \quad (3.29a)$$

$$\dot{v}_{ij} = \dot{v}_i - \dot{v}_j = u_i - u_j. \quad (3.29b)$$

Problem 3.2. Consider the reference tracking dynamics (3.28) with $i \in \{1, 2\}$. Find an appropriate control law

$$u_i = u_i(t, \tilde{x}_1, \tilde{x}_2, \tilde{v}_1, \tilde{v}_2), \quad (3.30)$$

such that the resulting closed-loop system yields

$$\lim_{t \rightarrow \infty} \tilde{x}_1 = 0, \quad \lim_{t \rightarrow \infty} \tilde{x}_2 = 0, \quad \lim_{t \rightarrow \infty} \tilde{v}_1 = 0, \quad \lim_{t \rightarrow \infty} \tilde{v}_2 = 0, \quad d_{12}(t) \neq 0 \quad \forall t. \quad (3.31)$$

3.2.1 Converse Lyapunov theorem

Since a double, rather than a single integrator system is considered, composition of a Lyapunov function as a function of d_{12} , similar to (3.9), becomes quite cumbersome. To get an idea of what a suitable Lyapunov function would look like, a numerical Lyapunov function is composed using converse Lyapunov theory. To compose a numerical Lyapunov function of a nonlinear system of which the origin is exponentially stable, Proposition 2.2.2 and Proposition 2.2.3 are combined. First, in order to apply this theorem, a coordinate transformation is applied to (3.29) as

$$\begin{bmatrix} z_1 \\ z_2 \end{bmatrix} = \begin{bmatrix} \frac{1}{d_{12}} - \frac{1}{2} \\ \frac{v_{12}}{d_{12}} \end{bmatrix}, \quad \begin{bmatrix} d_{12} \\ v_{12} \end{bmatrix} = \begin{bmatrix} \frac{1}{z_1 + \frac{1}{2}} \\ \frac{z_2}{z_1 + \frac{1}{2}} \end{bmatrix}, \quad (3.32)$$

and the dynamics (3.27) is considered in closed-loop with the control input

$$u_i = u_{i,r} - k_1 \tilde{x}_i - k_2 \tilde{v}_i - k_3 (v_{ij} - v_{ij,r}) + k_4 \left(\frac{1}{d_{ij}} - \frac{1}{d_{ij,r}} \right). \quad (3.33)$$

An extension of (3.6) with controller gains k_1 , k_2 , k_3 , and k_4 to be chosen freely. The resulting closed-loop dynamics is given as

$$\dot{z}_1 = - \left(z_1 + \frac{1}{2} \right) z_2, \quad (3.34a)$$

$$\begin{aligned} \dot{z}_2 = & (u_{1,r} - u_{2,r}) \left(z_1 + \frac{1}{2} \right) - k_1 + k_1 d_{12,r} \left(z_1 + \frac{1}{2} \right) \\ & - (k_2 + 2k_3) \left(z_2 - v_{12,r} \left(z_1 + \frac{1}{2} \right) \right) + 2k_4 \left(z_1 + \frac{1}{2} \right)^2 - \frac{2k_4}{d_{12,r}} \left(z_1 + \frac{1}{2} \right) - z_2^2. \end{aligned} \quad (3.34b)$$

With the stated transformation the aim is to show stability of a certain domain in the (z_1, z_2) -space and with that, prove both stability of the two equilibria in the defined region, and absence of collisions in solutions starting in the considered domain. It should be noted that with the coordinate transformation (3.32), the collision point is conveniently shifted to $\pm\infty$ and $d_{12} = \pm\infty$ is shifted to the $z_1 = -0.5$ axis. Next, the system (3.34) is to be linearized around the equilibria in order to investigate local stability and eventually apply the converse Lyapunov theorem along the lines of Proposition 2.2.2 and Proposition 2.2.3. Before this can be done, certain parameters need to be explicitly defined, and in this case $d_{12,r}(t) = 2$, $v_{12,r}(t) = 0$ and $u_{1,r}(t) = u_{2,r}(t) = 0$ are considered, with which (3.34) reduces to

$$\dot{z}_1 = - \left(z_1 + \frac{1}{2} \right) z_2, \quad (3.35a)$$

$$\dot{z}_2 = 2k_4 z_1^2 - z_2^2 + (2k_1 + k_4) z_1 - (k_2 + 2k_3) z_2, \quad (3.35b)$$

of which the equilibria are computed as $z_{\text{eq}} = [0, 0]$ and $z_{\text{eq}} = [-\frac{2k_1+k_4}{2k_4}, 0]$, where the equilibria at $z_1 = -\frac{1}{2}$ are deemed irrelevant as they represent the situation for which $d_{12} = \pm\infty$. Now the Jacobian of (3.35) is computed to be

$$J(z_1, z_2) = \begin{bmatrix} -z_2 & -(z_1 + \frac{1}{2}) \\ 4k_4z_1 + 2k_1 + k_4 & -2z_2 - k_2 - 2k_3 \end{bmatrix}, \quad (3.36)$$

and evaluating at the equilibrium points gives

$$J(0, 0) = \begin{bmatrix} 0 & -\frac{1}{2} \\ 2k_1 + k_4 & -k_2 - 2k_3 \end{bmatrix} = A_1. \quad (3.37)$$

and

$$J\left(-\frac{2k_1+k_4}{2k_4}, 0\right) = \begin{bmatrix} 0 & \frac{2k_1+k_4}{2k_4} - \frac{1}{2} \\ -2(2k_1+k_4) + 2k_1+k_4 & -k_2 - 2k_3 \end{bmatrix} = A_2, \quad (3.38)$$

from which it can be seen that $\text{Re}(\text{eig}(A_i)) < 0 \forall k_1, k_2, k_3, k_4 > 0$ with $i \in \{1, 2\}$ and thus both equilibria of both linearizations are locally exponentially stable (LES), and according to Proposition 2.2.3 they are LES equilibrium points for the nonlinear system (3.35). Lyapunov functions for both equilibria in the linearized dynamics can now be composed using controller gains $k_1 = 2k_2 = 2k_3 = 2k_4 = 2$ according to

$$V_{\text{lin},i} = w_i^\top P_i w_i, \quad \dot{V}_{\text{lin},i} = -w_i^\top Q w_i, \quad P_i A_i + A_i^\top P_i = -Q, \quad (3.39)$$

with $w_1 = z = [z_1, z_2]^\top$ and $w_2 = z + [2.5, 0]^\top$. Simply using $Q = I_2$ yields P_1 and P_2 according to

$$P_1 = \begin{bmatrix} \frac{73}{30} & \frac{-1}{10} \\ \frac{-1}{10} & \frac{11}{60} \end{bmatrix}, \quad P_2 = \begin{bmatrix} \frac{11}{15} & \frac{-1}{7} \\ \frac{-1}{7} & \frac{11}{30} \end{bmatrix}. \quad (3.40)$$

The proof of Proposition 2.2.2, see [39], uses a Lyapunov function as

$$V_{\text{conv}}(z) = \int_0^\infty \phi^\top(\tau) \phi(\tau) d\tau, \quad (3.41)$$

where $\phi(\tau)$ denotes the solution of the nonlinear system on time τ , as the system (3.34) is autonomous. Now, since solutions converge to the equilibria, and thus only reach the equilibria for $t \rightarrow \infty$, computing the integral (3.41) can become cumbersome and time consuming. Therefore, the total numeric Lyapunov function is computed by assuming that close to the equilibria, the behavior can be approached by using the linearized dynamics of the respective equilibrium, i.e., it is assumed that the system is linear for $w_i = \{w_i \mid V_{\text{lin},i} \leq 0.01\}$. Finally, the total converse numeric Lyapunov function is composed as

$$V_i(z) = \begin{cases} V_{\text{lin},i} & \text{for } w_i = \{w_i \mid V_{\text{lin},i} \leq 0.01\}, \\ \int_0^{t_e} \phi^\top(w_i(t_0), \tau) \phi(w_i(t_0), \tau) d\tau & \text{else,} \end{cases} \quad (3.42)$$

where t_0 is the time corresponding to the chosen initial conditions $w_i(t_0)$, t_e the time corresponding to $V_{\text{lin},i} = 0.01$, and $\phi(w_i(t_0), \tau)$ denotes the solution starting at initial conditions $w_i(t_0)$. In Figure 3.2, V_i is plotted with $i = 1 \forall z_1 > -0.5$ and $i = 2 \forall z_1 < -0.5$, note that V_i is undefined at $z_1 = -0.5$ since this would be $d_{12} = \pm\infty$. From this figure it can be seen that $V = 0$ only at the two equilibrium points and $V > 0$ elsewhere in the considered domain, similarly, \dot{V} is also computed to be $\dot{V} = 0$ at the equilibrium points and $\dot{V} < 0$ elsewhere in the considered domain. Since the resulting numeric converse Lyapunov function only holds for a very specific situation, i.e., $d_{12,r}, v_{12,r}, u_{1,r}, u_{2,r}$ and all the controller gains are to be specifically chosen, the converse Lyapunov method is deemed not suitable to provide a solution to Problem 3.2. However, the shape of the resulting numeric Lyapunov function inspires a different approach which proves to be more fruitful.

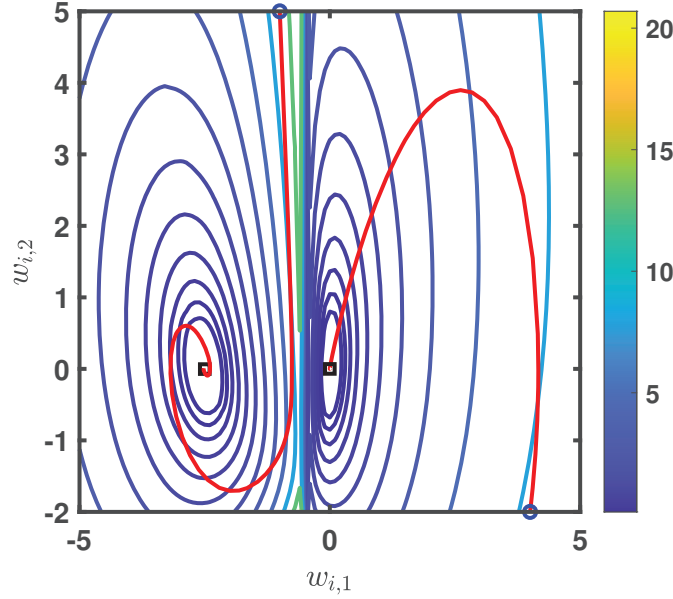


Figure 3.2: Level sets of composed numeric manifold V_i with two solution paths.

3.3 Stability with control Lyapunov function

From Figure 3.2 it can be seen that $V_i \rightarrow \infty$ for $z_1 \rightarrow -\frac{1}{2}$, and since it is computed that $\dot{V}_i < 0$ for z_1 values close to $z_1 = -\frac{1}{2}$, this indicates that solutions starting close to $z_1 = -\frac{1}{2}$ will diverge from $z_1 = -\frac{1}{2}$, i.e., solutions diverge from $d_{12} = \pm\infty$. This observation is used in an approach to prove solutions diverging from the collision point $d_{12} = 0$. A first analysis using a control Lyapunov function to prove stability of a system of single integrators in 1D, while achieving collision avoidance, is executed to compare with the previously obtained results. Next, the considered system is gradually expanded to a system of double integrators in arbitrary dimension, and finally a system of UAVs in 3D is analyzed.

3.3.1 Single integrators in 1D with constant reference

To verify whether usage of a control Lyapunov function satisfying $V \rightarrow \infty$ for $d_{12} \rightarrow 0$ can indeed give the contemplated results, a system of two single integrators in 1D is considered again. Therefore, the kinematics (3.1) is considered again with $i \in \{1, 2\}$ in 1D, of which the tracking behavior is given according to (3.2), and Problem 3.1 is slightly adjusted to the following control problem.

Problem 3.3. Consider the reference tracking dynamics (3.2) with $i \in \{1, 2\}$ and a constant reference trajectory, i.e., $\dot{x}_{i,r} = 0$, implying $\dot{d}_{12,r}(t) = 0$. Find an appropriate control law

$$u_i = u_i(\tilde{x}_1, \tilde{x}_2), \quad (3.43)$$

such that the resulting closed-loop system yields

$$\lim_{t \rightarrow \infty} \tilde{x}_1 = 0, \quad \lim_{t \rightarrow \infty} \tilde{x}_2 = 0, \quad d_{12}(t) \neq 0 \quad \forall t. \quad (3.44)$$

In order to provide a solution to Problem 3.3 using a control Lyapunov function, consider the following proposition.

Proposition 3.3.1. *Consider the kinematic system (3.2) in 1D with $i \in \{1, 2\}$ and a constant reference signal, i.e., $\dot{x}_{i,r}(t) = 0$. Choosing the control law*

$$u_i = -k_i \tilde{x}_i - (-1)^i k_3 \left(\frac{1}{d_{12}} - \frac{1}{d_{12,r}} \right) \left(\frac{1}{d_{12}^2} \right), \quad (3.45)$$

with $k_1, k_2, k_3 > 0$ control parameters, yields the time-invariant closed-loop system

$$\dot{\tilde{x}}_1 = -k_1 \tilde{x}_1 + k_3 \left(\frac{1}{d_{12}} - \frac{1}{d_{12,r}} \right) \left(\frac{1}{d_{12}^2} \right) = -k_1 \tilde{x}_1 + k_3 \frac{\tilde{x}_2 - \tilde{x}_1}{d_{12,r}(\tilde{x}_1 - \tilde{x}_2 + d_{12,r})^3}, \quad (3.46a)$$

$$\dot{\tilde{x}}_2 = -k_2 \tilde{x}_2 - k_3 \left(\frac{1}{d_{12}} - \frac{1}{d_{12,r}} \right) \left(\frac{1}{d_{12}^2} \right) = -k_2 \tilde{x}_2 - k_3 \frac{\tilde{x}_2 - \tilde{x}_1}{d_{12,r}(\tilde{x}_1 - \tilde{x}_2 + d_{12,r})^3}, \quad (3.46b)$$

of which the equilibria are asymptotically stable and locally exponentially stable (LES). Moreover, no collisions between agents occur in the system, i.e., for every solution to (3.46) with initial conditions satisfying $d_{12}(t_0) \neq 0$, there exists $\epsilon > 0$ such that $|d_{12}(t)| \geq \epsilon \forall t$.

Proof. Consider the kinematic system (3.2) in 1D and define $\tilde{x} = [\tilde{x}_1 \ \tilde{x}_2]^\top$. Subsequently, consider the candidate control Lyapunov function

$$V(\tilde{x}) = \frac{k_1}{2} \tilde{x}_1^2 + \frac{k_2}{2} \tilde{x}_2^2 + \frac{k_3}{2} \left(\frac{1}{d_{12}} - \frac{1}{d_{12,r}} \right)^2, \quad (3.47)$$

where $k_1, k_2, k_3 > 0$ are gains which are free to choose, and an artificial potential field is introduced by the term $\frac{k_3}{2} \left(\frac{1}{d_{12}} - \frac{1}{d_{12,r}} \right)^2$. Next, since the reference signal is restricted to a constant reference signal, i.e., $\dot{x}_{i,r} = u_{i,r} = 0$, the derivative of the control Lyapunov function (3.47) along solutions of (3.2) is given as

$$\begin{aligned} \dot{V}(\tilde{x}) &= k_1 \tilde{x}_1 u_1 + k_2 \tilde{x}_2 u_2 + k_3 \left(\frac{1}{d_{12}} - \frac{1}{d_{12,r}} \right) \left(-\frac{1}{d_{12}^2} \right) (u_1 - u_2), \\ &= \left[k_1 \tilde{x}_1 - k_3 \left(\frac{1}{d_{12}} - \frac{1}{d_{12,r}} \right) \left(\frac{1}{d_{12}^2} \right) \right] u_1 + \left[k_2 \tilde{x}_2 + k_3 \left(\frac{1}{d_{12}} - \frac{1}{d_{12,r}} \right) \left(\frac{1}{d_{12}^2} \right) \right] u_2, \end{aligned} \quad (3.48)$$

from which it can be seen that $\dot{V} \leq 0$ when the control inputs are chosen as

$$u_1 = -k_1 \tilde{x}_1 + k_3 \left(\frac{1}{d_{12}} - \frac{1}{d_{12,r}} \right) \left(\frac{1}{d_{12}^2} \right) = -k_1 \tilde{x}_1 + k_3 \frac{d_{12,r} - d_{12}}{d_{12,r} d_{12}^3}, \quad (3.49a)$$

$$u_2 = -k_2 \tilde{x}_2 - k_3 \left(\frac{1}{d_{12}} - \frac{1}{d_{12,r}} \right) \left(\frac{1}{d_{12}^2} \right) = -k_2 \tilde{x}_2 - k_3 \frac{d_{12,r} - d_{12}}{d_{12,r} d_{12}^3}, \quad (3.49b)$$

resulting in

$$\dot{V}(\tilde{x}) = - \left[k_1 \tilde{x}_1 - k_3 \left(\frac{1}{d_{12}} - \frac{1}{d_{12,r}} \right) \left(\frac{1}{d_{12}^2} \right) \right]^2 - \left[k_2 \tilde{x}_2 + k_3 \left(\frac{1}{d_{12}} - \frac{1}{d_{12,r}} \right) \left(\frac{1}{d_{12}^2} \right) \right]^2 \leq 0. \quad (3.50)$$

Since the closed-loop system (3.46) is a time-invariant system, LaSalle's invariance principle tells us that the system converges to the largest invariant subset of $\{\tilde{x} \mid \dot{V}(\tilde{x}) = 0\}$. This invariant subset is defined by

$$k_1 \tilde{x}_1 = k_3 \left(\frac{1}{d_{12}} - \frac{1}{d_{12,r}} \right) \left(\frac{1}{d_{12}^2} \right) = -k_2 \tilde{x}_2, \quad (3.51)$$

and note that this set defines the equilibria of the closed loop system (3.46). By using $d_{12} = \tilde{x}_1 - \tilde{x}_2 + d_{12,r}$ it can be seen that (3.51) has two (real) solutions; $\tilde{x}_1 = \tilde{x}_2 = 0$, and

$$\tilde{x}_1 = \left(\sqrt[3]{\frac{-k_3}{k_1 d_{12,r}} \left(1 + \frac{k_1}{k_2} \right) - d_{12,r}} \right) \left(1 + \frac{k_1}{k_2} \right)^{-1}, \quad (3.52a)$$

$$\tilde{x}_2 = -\frac{k_1}{k_2} \left(\sqrt[3]{\frac{-k_3}{k_1 d_{12,r}} \left(1 + \frac{k_1}{k_2} \right) - d_{12,r}} \right) \left(1 + \frac{k_1}{k_2} \right)^{-1}, \quad (3.52b)$$

which are the equilibrium points, \tilde{x}_{eq} , of (3.46). Following Theorem 2.1, it can now be concluded that the equilibria of (3.46) with the considered group of reference trajectories, are asymptotically stable. Moreover, according to Theorem 2.1, (3.50) indicates that $\frac{1}{d_{12}}$ is bounded, implicating that d_{12} is bounded away from zero and therefore, for each initial condition $d_{12}(t_0) \neq 0$, there exists $\epsilon > 0$ such that $|d_{12}(t)| \geq \epsilon \forall t$ and thus collisions will never occur for $d_{12}(t_0) \neq 0$. Next, to analyze local stability of the equilibria of (3.46), given by (3.51), the Jacobian of the closed-loop system is computed to be

$$J(\tilde{x}_1, \tilde{x}_2) = \begin{bmatrix} -k_1 + B(\tilde{x}_1, \tilde{x}_2) & -B(\tilde{x}_1, \tilde{x}_2) \\ -B(\tilde{x}_1, \tilde{x}_2) & -k_2 + B(\tilde{x}_1, \tilde{x}_2) \end{bmatrix}, \quad (3.53)$$

with

$$B(\tilde{x}_1, \tilde{x}_2) = k_3 \frac{2(\tilde{x}_1 - \tilde{x}_2) - d_{12,r}}{(\tilde{x}_1 - \tilde{x}_2 + d_{12,r})^4 d_{12,r}}. \quad (3.54)$$

Evaluating J at the equilibrium $(\tilde{x}_1, \tilde{x}_2) = (0, 0)$ gives $B(0, 0) = -k_3/d_{12,r}^4$ and

$$J(0, 0) = \begin{bmatrix} -k_1 - \frac{k_3}{d_{12,r}^4} & \frac{k_3}{d_{12,r}^4} \\ \frac{k_3}{d_{12,r}^4} & -k_2 - \frac{k_3}{d_{12,r}^4} \end{bmatrix}, \quad (3.55)$$

of which the eigenvalues are computed to be

$$\lambda_{J(0,0)} = \frac{-\left(2k_3 + (k_1 + k_2)d_{12,r}^4 \pm \sqrt{(k_1 - k_2)^2 d_{12,r}^8 + 4k_3^2}\right)}{2d_{12,r}^4}, \quad (3.56)$$

and by using

$$2k_3 + (k_1 + k_2)d_{12,r}^4 > \sqrt{(k_1 - k_2)^2 d_{12,r}^8 + 4k_3^2}, \quad (3.57a)$$

$$(2k_3 + (k_1 + k_2)d_{12,r}^4)^2 > (k_1 - k_2)^2 d_{12,r}^8 + 4k_3^2, \quad (3.57b)$$

$$(k_1 - k_2)^2 d_{12,r}^8 + 4k_1 k_2 d_{12,r}^8 + 4k_3(k_1 + k_2)d_{12,r}^4 + 4k_3^2 > (k_1 - k_2)^2 d_{12,r}^8 + 4k_3^2, \quad (3.57c)$$

$$4k_1 k_2 d_{12,r}^8 + 4k_3(k_1 + k_2)d_{12,r}^4 > 0, \quad (3.57d)$$

and recalling $k_1, k_2, k_3, d_{12,r} > 0$, it can be seen that both eigenvalues $\lambda_{J(0,0)}$ are strictly negative. A similar analysis of the equilibrium point given in (3.52) is given in Appendix A, also giving two strictly negative eigenvalues, and applying Proposition 2.2.3 renders both equilibria of (3.46) locally exponentially stable (LES). This completes the proof. \square

Concluding remarks

Using a control Lyapunov function and simultaneously choosing a control input u_i , both equilibria are proven LES, while also proving the absence of possible collisions, thus providing a solution to Problem 3.3. Note that this section only provides a solution to Problem 3.3, as only constant reference signals are considered, in contrast to the approach in Section 3.1. However, using a control Lyapunov function turns out to be a promising approach to now analyze a system of double integrators and to complete the analysis of Section 3.2.

3.3.2 Double integrators in arbitrary dimension with constant reference

Now that a system of two single integrators in 1D is analyzed using a control Lyapunov function in order to prove stability of equilibria and avoidance of collisions, the system is expanded to that of two double integrators in n D with $n \in \mathbb{N}^+$. Consider therefore the dynamic system

$$\dot{\rho}_i = v_i, \quad (3.58a)$$

$$\dot{v}_i = u_i, \quad (3.58b)$$

where $i \in \{1, 2\}$, and $\rho_i \in \mathbb{R}^n$, $v_i \in \mathbb{R}^n$ and $u_i \in \mathbb{R}^n$ denote, respectively, the position, velocity, and input of agent i in inertial frame \mathcal{I} . The reference trajectory $\rho_{i,r}$ is introduced which is also subject to (3.58), implicating $\dot{\rho}_{i,r} = v_{i,r}$ and $\dot{v}_{i,r} = u_{i,r}$. The tracking and velocity error for node i are now, respectively, defined as $\tilde{\rho}_i = \rho_i - \rho_{i,r}$ and $\tilde{v}_i = v_i - v_{i,r}$. The relative position of node i with respect to node j is defined as $\rho_{ij} = \rho_i - \rho_j$ and the relative distance between node i and j is defined as $d_{ij} = \|\rho_{ij}\|$, where $\|\rho_{ij}\|$ denotes the two-norm of vector ρ_{ij} , i.e., $\|\rho_{ij}\| = \|\rho_{ij}\|_2 = \sqrt{\rho_{ij}^\top \rho_{ij}}$. Similarly, the reference relative distance is defined as $d_{ij,r} = \|\rho_{ij,r}\| = \|\rho_{i,r} - \rho_{j,r}\|$, and it should be noted that $d_{ij} = d_{ji} > 0$, as well as $d_{ij,r} = d_{j,i,r} > 0$. Note that it is assumed that $\rho_{i,r}(t) \neq \rho_{j,r}(t)$, i.e., $d_{ij,r}(t) \neq 0 \forall t$, since $\rho_{i,r}(t) = \rho_{j,r}(t)$ would result in a collision. Finally, the state vector is denoted as $x_i = [\rho_i \ v_i]^\top \in \mathbb{R}^{2n}$ and accordingly $x_{i,r} = [\rho_{i,r} \ v_{i,r}]^\top$, with which $\tilde{x}_i = x_i - x_{i,r}$ is defined. The reference tracking dynamics is now given as

$$\dot{\tilde{\rho}}_i = \dot{\rho}_i - \dot{\rho}_{i,r} = v_i - v_{i,r} = \tilde{v}_i, \quad (3.59a)$$

$$\dot{\tilde{v}}_i = \dot{v}_i - \dot{v}_{i,r} = u_i - u_{i,r}, \quad (3.59b)$$

with the relative speed between node i and j expressed as

$$\dot{d}_{ij} = \frac{v_{ij}^\top \rho_{ij}}{\|\rho_{ij}\|}, \quad (3.60)$$

for $\rho_{ij} \neq 0$, where $v_{ij} = v_i - v_j$ denotes the relative velocity. Control Problem 3.2, aiming to achieve reference tracking and collision avoidance in a system of double integrators in 1D where time-varying reference signals are allowed, is now slightly adjusted and stated as follows.

Problem 3.4. Consider the reference tracking dynamics (3.59) with $i \in \{1, 2\}$ and a constant reference trajectory, i.e., $\dot{\rho}_{i,r} = 0$, $\dot{v}_{i,r} = 0$. Find an appropriate control law

$$u_i = u_i(\tilde{\rho}_1, \tilde{\rho}_2, \tilde{v}_1, \tilde{v}_2), \quad (3.61)$$

such that the resulting closed-loop system yields

$$\lim_{t \rightarrow \infty} \tilde{\rho}_1 = 0, \quad \lim_{t \rightarrow \infty} \tilde{\rho}_2 = 0, \quad \lim_{t \rightarrow \infty} \tilde{v}_1 = 0, \quad \lim_{t \rightarrow \infty} \tilde{v}_2 = 0, \quad d_{12}(t) \neq 0 \forall t. \quad (3.62)$$

In order to provide a solution to Problem 3.4 using a control Lyapunov function, let us consider the following proposition.

Proposition 3.3.2. Consider the reference tracking dynamics (3.59) in nD with $n \in \mathbb{N}^+$, $i \in \{1, 2\}$, and a constant reference signal, i.e., $\dot{\rho}_{i,r}(t) = 0$, $\dot{v}_{i,r}(t) = 0$. Choosing the control law

$$u_i = -k_{i+(i-1)}\tilde{\rho}_i - k_{2i}\tilde{v}_i - (-1)^i k_5 \frac{d_{12,r} - d_{12}}{d_{12,r}d_{12}^4}(\tilde{\rho}_1 - \tilde{\rho}_2 + \rho_{12,r}), \quad (3.63)$$

with $k_1, k_2, k_3, k_4, k_5 > 0$, yields the time-invariant closed-loop system

$$\dot{\tilde{\rho}}_1 = \tilde{v}_1, \quad (3.64a)$$

$$\dot{\tilde{v}}_1 = -k_1\tilde{\rho}_1 - k_2\tilde{v}_1 + k_5 \frac{d_{12,r} - d_{12}}{d_{12,r}d_{12}^4}(\tilde{\rho}_1 - \tilde{\rho}_2 + \rho_{12,r}), \quad (3.64b)$$

$$\dot{\tilde{\rho}}_2 = \tilde{v}_2, \quad (3.64c)$$

$$\dot{\tilde{v}}_2 = -k_3\tilde{\rho}_2 - k_4\tilde{v}_2 - k_5 \frac{d_{12,r} - d_{12}}{d_{12,r}d_{12}^4}(\tilde{\rho}_1 - \tilde{\rho}_2 + \rho_{12,r}), \quad (3.64d)$$

of which the equilibria are asymptotically stable. Moreover, no collisions between agents occur in the system, i.e., for every solution to (3.64) with initial conditions satisfying $d_{12}(t_0) \neq 0$, there exists $\epsilon > 0$ such that $|d_{12}(t)| \geq \epsilon \forall t$.

Proof. Consider the reference tracking dynamics (3.59) with $\rho_i \in \mathbb{R}^n$, $v_i \in \mathbb{R}^n$, $u_i \in \mathbb{R}^n$, and $n \in \mathbb{N}^+$. Subsequently, consider the candidate control Lyapunov function, based on (3.47), as

$$V(\tilde{x}_1, \tilde{x}_2) = \frac{k_1}{2} \tilde{\rho}_1^\top \tilde{\rho}_1 + \frac{1}{2} \tilde{v}_1^\top \tilde{v}_1 + \frac{k_3}{2} \tilde{\rho}_2^\top \tilde{\rho}_2 + \frac{1}{2} \tilde{v}_2^\top \tilde{v}_2 + \frac{k_5}{2} \left(\frac{1}{d_{12}} - \frac{1}{d_{12,r}} \right)^2, \quad (3.65)$$

with $k_1, k_3, k_5 > 0$. Differentiating along solutions yields

$$\dot{V}(\tilde{x}_1, \tilde{x}_2) = k_1 \tilde{\rho}_1^\top \dot{\tilde{v}}_1 + \tilde{v}_1^\top (u_1 - u_{1,r}) + k_3 \tilde{\rho}_2^\top \dot{\tilde{v}}_2 + \tilde{v}_2^\top (u_2 - u_{2,r}) - k_5 \left(\frac{1}{d_{12}} - \frac{1}{d_{12,r}} \right) \left(\frac{v_{12}^\top \rho_{12}}{d_{12}^3} \right), \quad (3.66)$$

where the assumption $\dot{d}_{12,r} = 0$ is used. When further restricting the reference signal to a constant reference position in the inertial frame \mathcal{I} , i.e., $\dot{\rho}_{i,r}(t) = 0$ and $\dot{v}_{i,r}(t) = 0$, (3.66) can be rewritten as

$$\dot{V}(\tilde{x}_1, \tilde{x}_2) = \tilde{v}_1^\top \left[k_1 \tilde{\rho}_1 + u_1 - k_5 \frac{d_{12,r} - d_{12}}{d_{12,r} d_{12}^4} \rho_{12} \right] + \tilde{v}_2^\top \left[k_3 \tilde{\rho}_2 + u_2 + k_5 \frac{d_{12,r} - d_{12}}{d_{12,r} d_{12}^4} \rho_{12} \right], \quad (3.67)$$

and when the inputs u_1 and u_2 are chosen as

$$u_1 = -k_1 \tilde{\rho}_1 - k_2 \tilde{v}_1 + k_5 \frac{d_{12,r} - d_{12}}{d_{12,r} d_{12}^4} (\tilde{\rho}_1 - \tilde{\rho}_2 + \rho_{12,r}), \quad (3.68a)$$

$$u_2 = -k_3 \tilde{\rho}_2 - k_4 \tilde{v}_2 - k_5 \frac{d_{12,r} - d_{12}}{d_{12,r} d_{12}^4} (\tilde{\rho}_1 - \tilde{\rho}_2 + \rho_{12,r}), \quad (3.68b)$$

where $\rho_{12} = \tilde{\rho}_1 - \tilde{\rho}_2 + \rho_{12,r}$, and $k_2, k_4 > 0$ is used and it is noted that $d_{12} = \|\rho_{12}\| = \|\tilde{\rho}_1 - \tilde{\rho}_2 + \rho_{12,r}\|$, it can be seen that

$$\dot{V}(\tilde{x}) = -k_2 \tilde{v}_1^\top \tilde{v}_1 - k_4 \tilde{v}_2^\top \tilde{v}_2 \leq 0. \quad (3.69)$$

Since the closed-loop system (3.64) is a time-invariant system, LaSalle's invariance principle tells us that the system converges to the largest invariant subset of $\{(\tilde{x}_1, \tilde{x}_2) \mid \dot{V}(\tilde{x}_1, \tilde{x}_2) = 0\}$. This invariant subset is defined by

$$\tilde{v}_1 = 0, \quad \tilde{v}_2 = 0, \quad k_1 \tilde{\rho}_1 = k_5 \frac{d_{12,r} - d_{12}}{d_{12,r} d_{12}^4} \rho_{12} = -k_3 \tilde{\rho}_2, \quad (3.70)$$

as $\dot{V} = 0$ gives $\tilde{v}_1 = \tilde{v}_2 = 0$, and substitution of $\tilde{v}_1 = \tilde{v}_2 = 0$ in (3.64) and setting $\dot{\rho}_1 = \dot{v}_1 = \dot{\rho}_2 = \dot{v}_2 = 0$ gives $k_1 \tilde{\rho}_1 = k_5 \frac{d_{12,r} - d_{12}}{d_{12,r} d_{12}^4} \rho_{12} = -k_3 \tilde{\rho}_2$. Now using $d_{12} = \|\rho_{12}\|$ and $\rho_{12} = \tilde{\rho}_1 - \tilde{\rho}_2 + \rho_{12,r}$, gives

$$\rho_{12,r} = \rho_{12} - \tilde{\rho}_1 + \tilde{\rho}_2 = \left[1 - \frac{(k_1 + k_3)k_5}{k_1 k_3} \frac{(d_{12,r} - d_{12})}{d_{12,r} d_{12}^4} \right] \rho_{12}, \quad (3.71)$$

and therefore

$$d_{12,r}^2 = \left[1 - \frac{(k_1 + k_3)k_5}{k_1 k_3} \frac{(d_{12,r} - d_{12})}{d_{12,r} d_{12}^4} \right]^2 d_{12}^2, \quad (3.72)$$

resulting in the two solutions

$$\pm \frac{d_{12,r}}{d_{12}} = 1 - \frac{(k_1 + k_3)k_5}{k_1 k_3} \frac{(d_{12,r} - d_{12})}{d_{12,r} d_{12}^4}, \quad (3.73)$$

also denoted as

$$[k_1 k_3 d_{12,r} d_{12}^3 + (k_1 + k_3)k_5] (d_{12} - d_{12,r}) = 0, \quad (3.74a)$$

$$k_1 k_3 d_{12,r} d_{12}^4 + k_1 k_3 d_{12,r}^2 d_{12}^3 + (k_1 + k_3)k_5 d_{12} - (k_1 + k_3)k_5 d_{12,r} = 0. \quad (3.74b)$$

Using $d_{12} = \sqrt{\rho_{12}^\top \rho_{12}} \geq 0$, (3.74a) gives only one feasible solution; $d_{12} = d_{12,r}$. The second equation, (3.74b), is negative for $d_{12} = 0$, while its derivative is strictly positive for $d_{12} > 0$, indicating that the function is increasing in d_{12} . Combining this with the fact (3.74b) is positive for $d_{12} = d_{12,r}$, indicates that there is also only one feasible solution for d_{12} to (3.74b), which satisfies $0 < d_{12} < d_{12,r}$ and which can be computed conveniently using, for example, bisection. Finally, (3.70) and (3.71) are combined to get

$$\tilde{\rho}_1 = \frac{k_3 k_5 (d_{12,r} - d_{12})}{k_1 k_3 d_{12,r} d_{12}^4 - (k_1 + k_3) k_5 (d_{12,r} - d_{12})} \rho_{12,r}, \quad (3.75a)$$

$$\tilde{\rho}_2 = \frac{k_1 k_5 (d_{12} - d_{12,r})}{k_1 k_3 d_{12,r} d_{12}^4 - (k_1 + k_3) k_5 (d_{12,r} - d_{12})} \rho_{12,r}, \quad (3.75b)$$

which gives $\tilde{\rho}_1 = \tilde{\rho}_2 = 0$ for $d_{12} = d_{12,r}$, and in the particular case that $\tilde{\rho}_1$ and $\tilde{\rho}_2$ are on the line through $\rho_{1,r}$ and $\rho_{2,r}$, $\tilde{\rho}_1$ and $\tilde{\rho}_2$ relate according to $k_1 \tilde{\rho}_1 = -k_3 \tilde{\rho}_2$.

Following Theorem 2.1, it can now be concluded that the equilibria of (3.64) with the considered group of reference trajectories, are asymptotically stable. Moreover, according to Theorem 2.1, (3.50) indicates that $\frac{1}{d_{12}}$ is bounded, implicating that d_{12} is bounded away from zero and therefore, for each initial condition $d_{12} \neq 0$, there exists $\epsilon > 0$ such that $|d_{12}(t)| \geq \epsilon \forall t$ and thus collisions will never occur for $d_{12}(t_0) \neq 0$. This completes the proof. \square

Concluding remarks

Using a control Lyapunov function and simultaneously designing a control input u_i , asymptotic stability of the equilibria is proven. Moreover, the absence of possible collisions in a system of two double integrators in arbitrary dimension is proven, and thus a solution to Problem 3.4 is provided. Note that this section now achieves the contemplated result of Section 3.2 for a constant reference signal and, on top of that, the proof is generalized to arbitrary dimension.

3.4 Stability of quadcopters in 3D with constant reference

After successful analysis, with respect to tracking behavior and collision avoidance, of a system of double integrators in the n -dimensional space with a constant reference signal, the step to a system of quadcopters in 3D is made. Now, let $\rho_i \in \mathbb{R}^3$ denote the position of the center of mass of a quadrotor UAV relative to a North-East-Down (NED) inertial frame \mathcal{I} , with $i \in \{1, 2\}$ and where the quadrotor is assumed to be axisymmetric, implying that the distance from the center of mass to each of the four rotors is identical. Fixed to the center of mass at ρ_i , a body-fixed, right-handed coordinate frame \mathcal{B}_i is considered with relative rotation $R_i \in \text{SO}(3) = \{R \in \mathbb{R}^{3 \times 3} | R^\top R = I, \det R = 1\}$ with respect to inertial frame \mathcal{I} . The linear velocity of quadrotor UAV i relative to its body-fixed frame \mathcal{B}_i is denoted as $\nu_i \in \mathbb{R}^3$ and angular velocities relative to the body-fixed frame \mathcal{B}_i are defined as $\omega_i \in \mathbb{R}^3$. The quadrotor is considered in \times -configuration in order to have a dedicated forward direction. The dynamical model of a quadrotor UAV is now given by following the Newton-Euler modelling approach [32] as

$$\dot{\rho}_i = R_i \nu_i, \quad (3.76a)$$

$$\dot{\nu}_i = -S(\omega_i) \nu_i + g R_i^\top e_3 - \frac{f_i}{m_i} e_3, \quad (3.76b)$$

$$\dot{R}_i = R_i S(\omega_i), \quad (3.76c)$$

$$J_i \dot{\omega}_i = S(J_i \omega_i) \omega_i + \tau_i, \quad (3.76d)$$

where m_i denotes the total mass of UAV i , $J_i = J_i^\top > 0$ the inertia matrix of UAV i with respect to its body-fixed frame, e_i for $i \in \{1, 2, 3\}$ denotes the standard unit vector, $f_i \in \mathbb{R}$ and $\tau_i \in \mathbb{R}^3$

are assumed to be the inputs which denote the total thrust magnitude and the total moment vector in the body fixed frames, and finally, the skew symmetric operator $S(\cdot)$ is defined along the lines of Definition 2.1.1, as

$$S(a) = -S(a)^\top = \begin{bmatrix} 0 & -a_3 & a_2 \\ a_3 & 0 & -a_1 \\ -a_2 & a_1 & 0 \end{bmatrix} \in \text{SO}(3). \quad (3.77)$$

Next, consider a reference trajectory for these two UAVs that is also subject to (3.76), i.e., for each UAV of the system a feasible reference trajectory is given satisfying

$$\dot{\rho}_{i,r} = R_{i,r} \nu_{i,r}, \quad (3.78a)$$

$$\dot{v}_{i,r} = -S(\omega_{i,r}) \nu_{i,r} + g R_{i,r}^\top e_3 - \frac{f_{i,r}}{m_i} e_3, \quad (3.78b)$$

$$\dot{R}_{i,r} = R_{i,r} S(\omega_{i,r}), \quad (3.78c)$$

$$J_i \dot{\omega}_{i,r} = S(J_i \omega_{i,r}) \omega_{i,r} + \tau_{i,r}, \quad (3.78d)$$

where $0 < f_{i,r}^{\min} \leq f_{i,r}(t)$ for $i \in \{1, 2\}$. Next, let a formation frame \mathcal{F} be located at a fixed, but free to choose virtual center of the formation, along the lines of [43]. Let $\rho_f \in \mathbb{R}^3$ denote the position of this frame relative to the NED inertial frame \mathcal{I} , and $R_f \in \text{SO}(3)$ the rotation matrix from the frame \mathcal{F} to \mathcal{I} and both are assumed to be twice continuously differentiable. With this, the reference position and velocity of each UAV can be, respectively, expressed in the formation frame \mathcal{F} [43] as

$$p_{i,r} = R_f^\top (\rho_{i,r} - \rho_f), \quad v_{i,r} = R_f^\top R_{i,r} \nu_{i,r}. \quad (3.79)$$

Similarly, the position p_i and velocity v_i of UAV i can be expressed in the formation frame as $p_i = R_f^\top (\rho_i - \rho_f)$ and $v_i = R_f^\top R_i \nu_i$, respectively. The relative position of UAV i with respect to j is then denoted in the formation frame as $p_{ij} = p_i - p_j = R_f^\top (\rho_i - \rho_j)$ and the relative distance is defined as $d_{ij} = \|p_{ij}\|$. Since only rotation matrices in $\text{SO}(3)$ are considered, one can write $d_{ij} = \|\rho_i - \rho_j\| = \|\rho_{ij}\| = \sqrt{\rho_{ij}^\top \rho_{ij}}$, and accordingly $d_{12,r} = \sqrt{\rho_{ij,r}^\top \rho_{ij,r}}$, where it should be noted that the relative distances are equal in every frame of reference. Furthermore, the relative velocity between UAV i and j expressed in the inertial frame is defined as $v_{ij} = (R_i \nu_i - R_j \nu_j)$ and with that, the relative speed is computed to be

$$\dot{d}_{ij} = \frac{v_{ij}^\top \rho_{ij}}{\sqrt{\rho_{ij}^\top \rho_{ij}}}, \quad (3.80)$$

for $\rho_{ij} \neq 0$, which likewise is equal in every frame of reference. Finally, this allows to express the individual position and velocity tracking errors in the mutually known formation frame as

$$p_{i,e} = p_{i,r} - p_i = R_f^\top (\rho_{i,r} - \rho_i), \quad (3.81a)$$

$$v_{i,e} = v_{i,r} - v_i = R_f^\top (R_{i,r} \nu_{i,r} - R_i \nu_i), \quad (3.81b)$$

which are to satisfy

$$\lim_{t \rightarrow \infty} p_{i,e} = 0, \quad \lim_{t \rightarrow \infty} v_{i,e} = 0, \quad (3.82)$$

in order for position tracking to be achieved. Since it is also desired to obtain tracking of the reference attitude, the attitude errors on $\text{SO}(3)$ expressed in the reference frame are defined as

$$R_{i,e} = R_i^\top R_{i,r}, \quad \omega_{i,e} = \omega_{i,r} - R_{i,e}^\top \omega_i, \quad (3.83)$$

which are required to satisfy

$$\lim_{t \rightarrow \infty} R_{i,e} = I_3, \quad \lim_{t \rightarrow \infty} \omega_{i,e} = 0, \quad (3.84)$$

for tracking to be achieved. The total corresponding error measure for agent i is denoted by

$$\varepsilon_i(p_{i,e}, v_{i,e}, R_{i,e}, \omega_{i,e}) = \|p_{i,e}\| + \|v_{i,e}\| + \log \|R_{i,e}\| + \|\omega_{i,e}\| \quad (3.85)$$

with which the tracking and collision avoiding control problem is stated as follows.

Problem 3.5. (cf. [25]) *Given a feasible reference trajectory $(\rho_{i,r}, \nu_{i,r}, R_{i,r}, \omega_{i,r}, f_{i,r}, \tau_{i,r})$ for UAV i , find control laws*

$$f_i = f_i(\rho_i, \nu_i, R_i, \omega_i, \rho_{i,r}, \nu_{i,r}, R_{i,r}, \omega_{i,r}), \quad (3.86a)$$

$$\tau_i = \tau_i(\rho_i, \nu_i, R_i, \omega_i, \rho_{i,r}, \nu_{i,r}, R_{i,r}, \omega_{i,r}), \quad (3.86b)$$

such that the resulting closed-loop (3.76), (3.78) and (3.86) yields

$$\lim_{t \rightarrow \infty} \varepsilon_i(p_{i,e}(t), v_{i,e}(t), R_{i,e}(t), \omega_{i,e}(t)) = 0 \quad \text{and} \quad d_{12}(t) \neq 0 \quad \forall t. \quad (3.87)$$

The position and attitude tracking part of Problem 3.5 are now analyzed separately in the following sections, before eventually considering the cascaded system.

3.4.1 Position tracking control with collision avoidance

Differentiating tracking errors (3.81) along (3.76) results in the position tracking dynamics as

$$\dot{p}_{i,e} = -S(\omega_f)p_{i,e} + v_{i,e}, \quad (3.88a)$$

$$\dot{v}_{i,e} = -S(\omega_f)v_{i,e} + u_{i,e}, \quad (3.88b)$$

where $u_{i,e}$ is considered a virtual input satisfying

$$u_{i,e} = R_f^\top \left(R_i \frac{f_i}{m_i} e_3 - R_{i,r} \frac{f_{i,r}}{m_i} e_3 \right), \quad (3.89)$$

to be achieved by the attitude tracking subsystem. Note that this virtual input couples the two tracking subsystems, indicating the cascaded structure. As stabilizing the system (3.88) accommodates a solution to Problem 3.5, consider the following proposition as a possible solution.

Proposition 3.4.1. *Consider the reference tracking dynamics (3.88) with $i \in \{1, 2\}$ and time-independent reference trajectories satisfying $\dot{p}_{i,r}(t) = 0$, $\dot{v}_{i,r}(t) = 0$, and $v_{1,r} = v_{2,r}$. Choosing the control law*

$$u_{i,e} = -k_{i+(i-1)}p_{i,e} - k_{2i}v_{i,e} - (-1)^i k_5 \frac{d_{12,r} - d_{12}}{d_{12,r}d_{12}^4} (p_{1,e} - p_{2,e} + p_{12,r}), \quad (3.90)$$

with $k_1, k_2, k_3, k_4, k_5 > 0$, control parameters, yields the time-invariant closed-loop system

$$\dot{p}_{1,e} = -S(\omega_f)p_{1,e} + v_{1,e}, \quad (3.91a)$$

$$\dot{v}_{1,e} = -S(\omega_f)v_{1,e} - k_1p_{1,e} - k_2v_{1,e} - k_5 \frac{d_{12,r} - d_{12}}{d_{12,r}d_{12}^4} p_{12}, \quad (3.91b)$$

$$\dot{p}_{2,e} = -S(\omega_f)p_{2,e} + v_{2,e}, \quad (3.91c)$$

$$\dot{v}_{2,e} = -S(\omega_f)v_{2,e} - k_3p_{2,e} - k_4v_{2,e} + k_5 \frac{d_{12,r} - d_{12}}{d_{12,r}d_{12}^4} p_{12}, \quad (3.91d)$$

of which the equilibria are asymptotically stable. Moreover, no collisions between agents occur in the system, i.e., for every solution to (3.91) with initial conditions satisfying $d_{12}(t_0) \neq 0$, there exists $\epsilon > 0$ such that $|d_{12}(t)| \geq \epsilon \quad \forall t$.

Proof. Consider the reference tracking dynamics (3.88). Subsequently, consider the candidate control Lyapunov function, based on (3.47), as

$$V = \frac{k_1}{2} p_{1,e}^\top p_{1,e} + \frac{1}{2} v_{1,e}^\top v_{1,e} + \frac{k_3}{2} p_{2,e}^\top p_{2,e} + \frac{1}{2} v_{2,e}^\top v_{2,e} + \frac{k_5}{2} \left(\frac{1}{d_{12}} - \frac{1}{d_{12,r}} \right)^2, \quad (3.92)$$

with $k_1, k_3, k_5 > 0$. Differentiating (3.92) along solutions yields

$$\dot{V} = k_1 v_{1,e}^\top p_{1,e} + v_{1,e}^\top u_{1,e} + k_3 v_{2,e}^\top p_{2,e} + v_{2,e}^\top u_{2,e} - k_5 \left(\frac{1}{d_{12}} - \frac{1}{d_{12,r}} \right) \frac{v_{12}^\top \rho_{12}}{d_{12}^3}, \quad (3.93)$$

where the property $b^\top S(a)b = 0$ of a skew-symmetric matrix is used and it is assumed that $\dot{d}_{12,r}(t) = 0$, implying $\dot{p}_{12,r}(t) = 0$. Next, the analysis is further restricted to time-independent reference trajectories satisfying $\dot{p}_{i,r}(t) = 0$, $\dot{v}_{i,r}(t) = 0$, and $v_{1,r} = v_{2,r}$, in order to have

$$v_{12}^\top = (v_{2,e}^\top - v_{1,e}^\top) R_f^\top + \nu_{1,r}^\top R_{1,r}^\top - \nu_{2,r}^\top R_{2,r}^\top = (v_{2,e}^\top - v_{1,e}^\top) R_f^\top. \quad (3.94)$$

Note that this definition allows nonzero ω_f in specific situations, as $\dot{p}_{i,r}(t) = 0$ allows constant $v_{i,r} = S(\omega_f) p_{i,r}$. With this restriction on the reference signal, (3.93) is written as

$$\dot{V} = v_{1,e}^\top \left[k_1 p_{1,e} + u_{1,e} + k_5 \frac{d_{12,r} - d_{12}}{d_{12}^4 d_{12,r}} p_{12} \right] + v_{2,e}^\top \left[k_3 p_{2,e} + u_{2,e} - k_5 \frac{d_{12,r} - d_{12}}{d_{12}^4 d_{12,r}} p_{12} \right], \quad (3.95)$$

and when the virtual control inputs $u_{1,e}$ and $u_{2,e}$ are now chosen as

$$u_{1,e} = -k_1 p_{1,e} - k_2 v_{1,e} - k_5 \frac{d_{12,r} - d_{12}}{d_{12,r} d_{12}^4} p_{12}, \quad (3.96a)$$

$$u_{2,e} = -k_3 p_{2,e} - k_4 v_{2,e} + k_5 \frac{d_{12,r} - d_{12}}{d_{12,r} d_{12}^4} p_{12}, \quad (3.96b)$$

it can be seen that

$$\dot{V} = -k_2 v_{1,e}^\top v_{1,e} - k_4 v_{2,e}^\top v_{2,e} \leq 0. \quad (3.97)$$

Since the closed-loop system (3.91) with the considered restrictions on the reference signals is time-invariant, LaSalle's invariance principle states that the system converges to the largest invariant subset, defined for the considered system as

$$v_{1,e} = 0, \quad v_{2,e} = 0, \quad k_1 p_{1,e} = k_5 \frac{d_{12,r} - d_{12}}{d_{12,r} d_{12}^4} p_{12} = -k_3 p_{2,e}, \quad (3.98)$$

similar to (3.70), and note that this set defines the equilibria of the closed loop system (3.91). Now, using $p_{12,r} = p_{12} + p_{1,e} - p_{2,e}$, one can write

$$p_{12,r} = p_{12} - p_{1,e} + p_{2,e} = \left[1 - \frac{(k_1 + k_3) k_5 (d_{12,r} - d_{12})}{k_1 k_3 d_{12,r} d_{12}^4} \right] p_{12}, \quad (3.99)$$

which is equal to (3.72), whereby it can be concluded that two suitable solutions for d_{12} in (3.99) are obtained, of which one is $d_{12} = d_{12,r}$ and the other can be swiftly found numerically by using, for example, bisection. With d_{12} known, the corresponding solutions, $p_{1,e}$ and $p_{2,e}$, to (3.98) are given as

$$p_{1,e} = \frac{k_3 k_5 (d_{12,r} - d_{12})}{k_1 k_3 d_{12,r} d_{12}^4 - (k_1 + k_3) k_5 (d_{12,r} - d_{12})} p_{12,r}, \quad (3.100a)$$

$$p_{2,e} = \frac{k_1 k_5 (d_{12} - d_{12,r})}{k_1 k_3 d_{12,r} d_{12}^4 - (k_1 + k_3) k_5 (d_{12,r} - d_{12})} p_{12,r}, \quad (3.100b)$$

which gives $p_{1,e} = p_{2,e} = 0$ for $d_{12} = d_{12,r}$, and in the particular case that $p_{1,e}$ and $p_{2,e}$ are on the line through $p_{1,r}$ and $p_{2,r}$, $p_{1,e}$ and $p_{2,e}$ relate according to $k_1 p_{1,e} = -k_3 p_{2,e}$ and can be defined by (3.100). Following Theorem 2.1, it can now be concluded that the equilibria of the closed-loop system (3.91) with the mentioned reference trajectories, are asymptotically stable. Moreover, according to Theorem 2.1, (3.97) indicates that $\frac{1}{d_{12}}$ is bounded, implicating that d_{12} is bounded away from zero and therefore, for every solution to (3.91) with initial conditions satisfying $d_{12}(t_0) \neq 0$, there exists $\epsilon > 0$ such that $|d_{12}(t)| \geq \epsilon \forall t$. \square

As Proposition 3.4.1 only shows that the closed-loop equilibria are asymptotically stable, and $p_{1,e}$ and $p_{2,e}$ are bounded for bounded $d_{12,r}$ according to (3.100), it is desired to expand the obtained local results to a global result. In order to do so it is desired to prove that the origin of the dynamics of the projection

$$z_1 = p_{1,e} + p_{2,e}, \quad (3.101a)$$

$$z_2 = v_{1,e} + v_{2,e}, \quad (3.101b)$$

given by

$$\dot{z}_1 = -S(\omega_f)z_1 + z_2, \quad (3.102a)$$

$$\dot{z}_2 = -S(\omega_f)z_2 + u_{1,e} + u_{2,e}, \quad (3.102b)$$

which is also time-invariant, is GAS and LES, and therefore prove the following theorem.

Proposition 3.4.2. *Consider the projected dynamics of (3.91), given by (3.102), with time-independent reference trajectories satisfying $\dot{p}_{i,r}(t) = 0$, $\dot{v}_{i,r}(t) = 0$, and $v_{1,r} = v_{2,r}$. Choosing the control law as in Proposition 3.4.1 yields the closed-loop system*

$$\dot{z}_1 = -S(\omega_f)z_1 + z_2, \quad (3.103a)$$

$$\begin{aligned} \dot{z}_2 &= -S(\omega_f)v_{1,e} - k_1 p_{1,e} - k_2 v_{1,e} - k_5 \frac{d_{12,r} - d_{12}}{d_{12,r} d_{12}^4} p_{12} \\ &\quad - S(\omega_f)v_{2,e} - k_1 p_{2,e} - k_2 v_{2,e} + k_5 \frac{d_{12,r} - d_{12}}{d_{12,r} d_{12}^4} p_{12}, \\ &= -S(\omega_f)z_2 - k_1 z_1 - k_2 z_2, \end{aligned} \quad (3.103b)$$

where the analysis is restricted to $k_3 = k_1$ and $k_4 = k_2$, and of which the origin is globally asymptotically stable (GAS) and locally exponentially stable (LES).

Proof. Consider the closed-loop projected dynamics (3.102) and consider the candidate Lyapunov function

$$V = \frac{k_1}{2} z_1^\top z_1 + \frac{1}{2} z_2^\top z_2, \quad (3.104)$$

and differentiating along solutions of (3.103) yields

$$\dot{V} = -k_2 z_2^\top z_2 \leq 0, \quad (3.105)$$

and it can be seen that $\dot{V} < 0 \forall z_2 \neq 0$. Next, LaSalle's invariance principle tells us that the solutions converge to the largest invariant subset, which in this case is given by

$$z_1 = 0, \quad z_2 = 0, \quad (3.106)$$

and the equilibrium $(z_1, z_2) = (0, 0)$ is found to be globally asymptotically stable (GAS). The found projected equilibrium is now expressed in the initial coordinates in order to express the found GAS equilibrium of (3.103) in the dynamics of the time-invariant system (3.91). This gives global asymptotic stability (GAS) of the equilibrium point satisfying $p_{1,e} = -p_{2,e}$ and

$v_{1,e} = -v_{2,e}$, for controller gains chosen as $k_3 = k_1$ and $k_4 = k_2$. Note that the equilibria found before satisfy these conditions.

Next, in order to analyze the local stability of the origin of (3.103), the Jacobian of (3.103) at the equilibrium point at the origin is computed to be

$$J = \begin{bmatrix} -S(\omega_f) & I_3 \\ -k_1 I_3 & -S(\omega_f) - k_2 I_3 \end{bmatrix}, \quad (3.107)$$

of which the eigenvalues are given according to

$$\lambda_{1,2} = \frac{-k_2 \pm \sqrt{k_2^2 - 4k_1}}{2}, \quad (3.108a)$$

$$\lambda_{3,4} = \frac{-k_2}{2} \pm \frac{1}{2} \sqrt{k_2^2 - 4 \left(\omega_f^\top \omega_f + \sqrt{(4k_1 - k_2^2) \omega_f^\top \omega_f + k_1} \right)}, \quad (3.108b)$$

$$\lambda_{5,6} = \frac{-k_2}{2} \pm \frac{1}{2} \sqrt{k_2^2 - 4 \left(\omega_f^\top \omega_f - \sqrt{(4k_1 - k_2^2) \omega_f^\top \omega_f + k_1} \right)}, \quad (3.108c)$$

which are all proven to have a strictly negative real part for $k_1, k_2 > 0$ and time-independent $\omega_f \in \mathbb{R}^3$ in Appendix B and by applying Proposition 2.2.3 it can be concluded that the origin of (3.103) is LES. \square

It should be noted that the presented proof of Proposition 3.4.1 only proves that the collision point, where the center of mass of both drones is located at the exact same point, will never be reached when the system is initialized elsewhere. In practice, naturally the drones have certain dimensions and as these are not taken into account in the analysis, it is not fully guaranteed that all collisions are avoided. However, the control action is repelling whenever $d_{12} < d_{12,r}$, as a result of the introduced APF in (3.92), and when this is combined with carefully selected initial conditions, it can be assumed that no collisions occur when the presented analysis is followed.

3.4.2 Attitude control

The proof of Proposition 3.4.2 shows global asymptotic stability (GAS) and local exponential stability (LES) of the origin of the time-invariant closed-loop projected reference tracking dynamics (3.103) when the designed virtual input $u_{i,e}$, as in (3.96), is achieved by control inputs f_i and τ_i according to (3.89), where R_i is controlled by τ_i . Thus, control laws need to be designed for f_i and τ_i such that $f_i R_{i,r}^\top R_i e_3$ converges to $f_{i,r} e_3 + m_i R_{i,r}^\top R_f u_{i,e}$, in order to achieve the virtual input with the actual control inputs. Using (3.89) gives

$$R_{i,r}^\top R_i f_i e_3 = f_{i,r} e_3 + m_i R_{i,r}^\top R_f u_{i,e}, \quad (3.109)$$

and using $R_{i,r}, R_i \in \text{SO}(3)$, the force magnitude is obtained as

$$f_i = \|f_{i,r} e_3 + m_i R_{i,r}^\top R_f u_{i,e}\|. \quad (3.110)$$

As one would actually want to guarantee a strictly positive total thrust, i.e., it is desired to have $0 < \epsilon_i \leq f_i(t)$, a convenient solution would be to set

$$\|u_{i,e}\| \leq \frac{f_{i,r}^{\min} - \epsilon_i}{m_i}, \quad (3.111)$$

as reference trajectories satisfying $0 < f_{i,r}^{\min} \leq f_{i,r}(t)$ are considered. Now using that (3.102) is LES, we can write $V(t) - V(t_0) \leq c_{i,1}(t_0)$ for V as in (3.104), where the initial conditions for $V(t_0)$ are chosen such that (3.111) is satisfied. Note however, that although this is a convenient solution to guarantee $0 < \epsilon_i \leq f_i(t)$, it is rather restrictive. Consider for example $R_{i,r}^\top R_f = I_3$,

$\omega_f = 0$ and assume that the reference positions are chosen in the same horizontal plane, and the initial conditions are also chosen in one horizontal plane. Then the x, y, z -directions of the system (3.103) are uncoupled and what remains is to guarantee that the $m_i(u_{i,e})_z > \epsilon_i - f_{i,r}^{\min}$, making restriction on the upper bound of $(u_{i,e})_z$ redundant, as well as restrictions on $u_{i,e}$ in x, y -direction. Although it would be favorable to account also for actuator saturation. Note however, that this second method is also quite restrictive.

With a properly defined f_i , the desired thrust direction can be defined as

$$R_{i,d}e_3 = \frac{f_{i,r}e_3 + m_i R_{i,r}^\top R_f u_{i,e}}{\|f_{i,r}e_3 + m_i R_{i,r}^\top R_f u_{i,e}\|} := f_{i,d} = \begin{bmatrix} f_{i1,d} \\ f_{i2,d} \\ f_{i3,d} \end{bmatrix}, \quad (3.112)$$

with

$$f_{i,d} = [f_{i1,d} \quad f_{i2,d} \quad f_{i3,d}]^\top, \quad (3.113)$$

and as a result it can be assumed that $f_{i3,d} > 0$. Note that (3.112) underlines the importance of having $0 < \epsilon_i \leq f_i(t)$, and it is actually desired to have a saturated f_i and therefore $u_{i,e}$, to justify the definition of $f_{i,d}$. Next, the rotation matrix $R_{i,d}$, that rotates the desired thrust vector to the thrust vector of the reference in the plane containing both vectors, consists of a rotation around an axis perpendicular to this plane, given by

$$n_i = \frac{f_{i,d} \times e_3}{\|f_{i,d} \times e_3\|}, \quad (3.114)$$

which is of unit length for all $f_{i,d} \times e_3 \neq 0$, and n_i is the zero vector otherwise. The rotation angle $\theta_{i,d}$ is now computed using the definition of the dot product as

$$\cos(\theta_{i,d}) = \frac{e_3 \cdot f_{i,d}}{\|f_{i,d}\| \|e_3\|} = f_{i3,d}, \quad (3.115)$$

and with Pythagoras in the unit disc and the property of rotation matrices that any column is of unit length, this also gives

$$\sin(\theta_{i,d}) = \sqrt{1 - \cos^2(\theta_{i,d})} = \sqrt{1 - f_{i3,d}^2}. \quad (3.116)$$

Now (3.114), (3.115), and (3.116) are combined in Rodrigues' rotation formula in order to obtain the rotation to the desired attitude as

$$R_{i,d} = I_3 + \sin(\theta_{i,d})S(n_i) + [1 - \cos(\theta_{i,d})]S(n_i)^2, \quad (3.117)$$

to finally define the desired rotation matrix as

$$R_{i,d} = \begin{bmatrix} 1 - \frac{f_{i1,d}^2}{1+f_{i3,d}} & -\frac{f_{i1,d}f_{i2,d}}{1+f_{i3,d}} & f_{i1,d} \\ -\frac{f_{i1,d}f_{i2,d}}{1+f_{i3,d}} & 1 - \frac{f_{i2,d}^2}{1+f_{i3,d}} & f_{i2,d} \\ -f_{i1,d} & -f_{i2,d} & f_{i3,d} \end{bmatrix} \in \text{SO}(3), \quad (3.118)$$

which, using $\dot{R}_{i,d} = R_{i,d}S(\omega_{i,d})$, gives

$$\omega_{i,d} = \begin{bmatrix} -\dot{f}_{i2,d} + \frac{f_{i2,d}\dot{f}_{i3,d}}{1+f_{i3,d}} \\ \dot{f}_{i1,d} - \frac{f_{i1,d}\dot{f}_{i3,d}}{1+f_{i3,d}} \\ \frac{f_{i2,d}\dot{f}_{i1,d} - f_{i1,d}\dot{f}_{i2,d}}{1+f_{i3,d}} \end{bmatrix}. \quad (3.119)$$

Combining (3.89), (3.110), and (3.118) one obtains

$$[f_{i,r}e_3 + m_i R_{i,r}^\top R_f u_{i,e}] = R_{i,d} f_i e_3, \quad (3.120)$$

and in order to have $R_{i,r}^\top R_i f_i e_3 = [f_{i,r}e_3 + m_i R_{i,r}^\top R_f u_{i,e}]$, an input τ_i needs to be found in order to let $R_{i,d} f_i e_3$ converge to $R_{i,r}^\top R_i f_i e_3$. In order to do so, the attitude and angular velocity errors expressed in the body-fixed frames \mathcal{B}_i are defined as

$$\tilde{R}_i = R_{i,d}^\top (R_{i,r}^\top R_i), \quad \tilde{\omega}_i = \omega_i - R_i^\top R_{i,r} \omega_{i,r} - \tilde{R}_i^\top \omega_{i,d}, \quad (3.121)$$

where it should be noted that expressing the attitude errors in the body-fixed frame \mathcal{B}_i of agent i introduces the control input τ_i plainly in the error dynamics, which are given by differentiating (3.121) along their solutions as

$$\dot{\tilde{R}}_i = \tilde{R}_i S(\tilde{\omega}_i), \quad (3.122a)$$

$$J_i \dot{\tilde{\omega}}_i = S(J_i \omega_i) \omega_i + \tau_i - J_i R_i^\top R_{i,r} \dot{\omega}_{i,r} + J_i S(\tilde{\omega}_i) [\omega_i - \tilde{\omega}_i] + J_i \tilde{R}_i^\top \left[S(\omega_{i,d}) R_{i,d}^\top \omega_{i,r} - \dot{\omega}_{i,d} \right], \quad (3.122b)$$

with which the attitude tracking control problem is stated as follows.

Problem 3.6. (cf. [25]) *Consider the attitude tracking dynamics (3.122) of which the desired equilibrium is given as $(I, 0) \in \text{SO}(3) \times \mathbb{R}^3$. Find an appropriate control law*

$$\tau_i = \tau_i(t, \tilde{R}, \tilde{\omega}_i), \quad (3.123)$$

such that the resulting closed-loop system yields

$$\lim_{t \rightarrow \infty} \tilde{R}_i = I_3, \quad \lim_{t \rightarrow \infty} \tilde{\omega}_i = 0. \quad (3.124)$$

Noting the similarities between the system (3.122) and the system considered in Proposition 2.2.5 a possible solution can be proposed along the lines of Proposition 2.2.5.

Proposition 3.4.3. (adopted from [14], cf. [40]) *Consider the attitude tracking dynamics (3.122). Choosing the control input τ_i as*

$$\begin{aligned} \tau_i = & -S(J_i \omega_i) \omega_i + J_i R_i^\top R_{i,r} \dot{\omega}_{i,r} - J_i S(\tilde{\omega}_i) [\omega_i - \tilde{\omega}_i] - J_i \tilde{R}_i^\top \left[S(\omega_{i,d}) R_{i,d}^\top \omega_{i,r} - \dot{\omega}_{i,d} \right] \dots \\ & - K_{\omega_i} \tilde{\omega}_i + K_{R_i} \sum_{j=1}^3 k_{ji} \left(e_j \times \tilde{R}_i^\top e_j \right), \end{aligned} \quad (3.125)$$

with $K_{\omega_i} = K_{\omega_i}^\top > 0$, $K_{R_i} = K_{R_i}^\top > 0$, and $k_{ji} > 0$ distinct, i.e., $k_{1i} \neq k_{2i} \neq k_{3i} \neq k_{1i}$, provides a closed-loop system that is equivalent [25] to

$$\dot{\tilde{R}}_i = \tilde{R}_i S(\tilde{\omega}_i), \quad (3.126a)$$

$$J_i \dot{\tilde{\omega}}_i = -K_{\omega_i} \tilde{\omega}_i + K_{R_i} \sum_{j=1}^3 k_{ji} \left(e_j \times \tilde{R}_i^\top e_j \right), \quad (3.126b)$$

for which the equilibrium $(I, 0)$ is uniformly locally exponentially stable (ULES) and uniformly almost globally asymptotically stable (UaGAS) (cf. Proposition 2.2.5, of which the proof is included [40]), under the assumption that $0 < \epsilon_i \leq f_i(t)$ in order to have $f_{i,d}$, and thus $\omega_{i,d}$ and $\dot{\omega}_{i,d}$ well defined. Note that this assumption can be satisfied by properly selecting initial conditions, when f_i is not saturated by the control input $u_{i,e}$.

Concluding remarks

The analysis of the position tracking subsystem with the considered group of reference trajectories and the designed virtual input, renders the equilibria of the resulting closed-loop system asymptotically stable. Moreover, with the designed virtual input, it is shown that no collisions occur in the system as long as the virtual input is attained by the attitude tracking dynamics. Additionally, it has been shown that the projection of the reference tracking subsystem yields a closed-loop system of which the origin is globally asymptotically stable (GAS) and locally exponentially stable (LES). The analysis of the attitude tracking subsystem renders the desired equilibrium uniformly locally exponentially stable (ULES) and uniformly almost globally asymptotically stable (UaGAS) under the assumptions on the total thrust. As the designed control law lacks a form of saturation, manually bounding the virtual input by selecting initial conditions close to the reference trajectories is necessary to have feasible f_i and $f_{i,d}$. This also strokes with the need to manually bound initial conditions in order to have collision avoidance in a network of drones with dimensions larger than a point mass. Lastly, it should be noted that when $v_{12}^\top = (v_{2,e}^\top - v_{1,e}^\top)R_f^\top$ and $d_{12} = \|p_{12}\|$ are combined with $p_{12} = p_{12,r} - p_{1,e} + p_{2,e}$, it can be seen from (3.96) that no attitude information of agent j is necessary to compute the input of agent i when reference trajectories of both drones are known to both agents. Additionally, the derivative of the virtual input of agent i , $\dot{u}_{i,e}$, necessary to compute $\omega_{i,d}$ among others, neither uses the orientation of agent j , as the necessary $\dot{p}_{j,e}$ can be computed by drone i using only $p_{j,e}$, $v_{j,e}$ and ω_f . This is convenient with respect to the necessary communication between two agents.

3.4.3 Cascaded system analysis

In preceding sections, a virtual control input $u_{i,e}$ is designed for the position tracking subsystem and a control law for f_i and τ_i is designed that asymptotically attains this virtual input. A final step in the analysis of a system of two quadcopter UAVs is to analyse stability of the cascaded system, consisting of the attitude controller and the desired position controller, similar to [14]. Now that the origin of (3.102) is proven to be GAS and LES, consider the dynamics (3.102) subject to reference trajectories (3.78), satisfying $\dot{p}_{i,r}(t) = 0$, $\dot{v}_{i,r}(t) = 0$, and $v_{1,r} = v_{2,r}$, with $i \in \{1, 2\}$, in closed-loop with control laws (3.96), (3.110) and (3.125) with controller gains $k_1 = k_3$, $k_2 = k_4$. The resulting closed-loop system expressed in (projected) error coordinates is denoted by

$$\dot{z}_1 = -S(\omega_f)z_1 + z_2, \quad (3.127a)$$

$$\dot{z}_2 = -S(\omega_f)z_2 - k_1 z_1 - k_2 z_2 + \frac{f_1}{m_1}(I_3 - \tilde{R}_1^\top)e_3 + \frac{f_2}{m_2}(I_3 - \tilde{R}_2^\top)e_3, \quad (3.127b)$$

$$\dot{\tilde{R}}_i = \tilde{R}_i S(\tilde{\omega}_i), \quad (3.127c)$$

$$J_i \dot{\tilde{\omega}}_i = -K_{\omega_i} \tilde{\omega}_i + K_{R_i} \sum_{j=1}^3 k_{ji} \left(e_j \times \tilde{R}_i^\top e_j \right), \quad (3.127d)$$

where the cascaded terms $\frac{f_i}{m_i}(I_3 - \tilde{R}_i^\top)e_3 = \frac{f_i}{m_i}(R_{i,r}^\top R_i - R_{i,d})e_3$ can be regarded a disturbance on the projected position tracking subsystem as a result of a not yet converged attitude error, i.e., virtual input $u_{i,e}$ is not yet fully achieved by f_i and τ_i . If it can now be guaranteed that

$$\lim_{t \rightarrow \infty} z_1 = 0, \quad \lim_{t \rightarrow \infty} z_2 = 0, \quad \lim_{t \rightarrow \infty} \tilde{R}_i = I_3, \quad \lim_{t \rightarrow \infty} \tilde{\omega}_i = 0, \quad \text{and} \quad d_{12}(t) \neq 0 \quad \forall t, \quad (3.128)$$

hold, the conditions of Problem 3.5 hold when solutions stay away from the situation where $p_{1,e}$ and $p_{2,e}$ are exactly on the line through $p_{1,r}$ and $p_{2,r}$, which forms a lower dimensional manifold when considering $p_{i,e}(t_0)$ and $v_{i,e}(t_0)$ to be well away from infinity. In order to do so, let us consider the following proposition.

Proposition 3.4.4. (cf. [25]) *Consider the closed-loop cascaded system (3.127). The origin of (3.127) with $i \in \{1, 2\}$ is uniformly almost globally asymptotically stable (UaGAS) and uniformly locally exponentially stable (ULES), i.e., for all $p_{i,e} \in \mathbb{R}^3$, $v_{i,e} \in \mathbb{R}^3$, and $(R_{i,e}, \omega_{i,e}) \in G$ with $G \subset SO(3) \times \mathbb{R}^3$ and $\mathcal{M} = (SO(3) \times \mathbb{R}^3) \setminus G$ a set with measure zero.*

Proof. Identify the cascaded nature of (3.127) as ((3.127a),(3.127b)) and ((3.127c),(3.127d)). Let G denote the almost global region of attraction of ((3.127c),(3.127d)), under the conditions mentioned in Section 3.4.2. Furthermore, (3.102) is GAS and LES, and combining both results provides the first two assumptions of Theorem 2.2. What remains to prove is that the cascaded term $\frac{f_i}{m_i}(I_3 - \tilde{R}_i^\top)e_3$ is bounded, providing that stability is maintained for the two subsystems in cascade. To prove that $\frac{f_i}{m_i}(I_3 - \tilde{R}_i^\top)e_3$ is bounded, similarly to [25], (3.104) is differentiated along solutions (3.127), yielding

$$\begin{aligned} \dot{V} &= -k_2 z_2^\top z_2 + z_2^\top \left(\frac{f_1}{m_1}(I_3 - \tilde{R}_1^\top)e_3 + \frac{f_2}{m_2}(I_3 - \tilde{R}_2^\top)e_3 \right) \\ &\leq z_2^\top \left(\frac{f_1}{m_1}(I_3 - \tilde{R}_1^\top)e_3 + \frac{f_2}{m_2}(I_3 - \tilde{R}_2^\top)e_3 \right) \leq c_1 \sqrt{V(z_1, z_2)} \left(\|I_3 - \tilde{R}_1^\top\| + \|I_3 - \tilde{R}_2^\top\| \right). \end{aligned} \quad (3.129)$$

Now, since ((3.127c),(3.127d)) is ULES, we have

$$\sqrt{V(z_1(t), z_2(t))} - \sqrt{V(z_1(t_0), z_2(t_0))} \leq c_2(t_0), \quad (3.130)$$

implying that $V(z_1, z_2)$ is bounded, and therefore solutions of ((3.127a),(3.127b)) are bounded, ensuring that the coupling term is bounded. Therefore, it can be concluded that the last assumption of Theorem 2.2 holds, and it is concluded that the cascaded system (3.127) is UGAS and ULES on $\mathbb{R}^{6n} \times G$ and UaGAS and ULES on $\mathbb{R}^{6n} \times SO(3)^{3n} \times \mathbb{R}^{3n}$, both under the assumptions stated in Section 3.4.2. \square

3.5 Expansion to network of arbitrary number of UAVs

Now that absence of collisions in a network of two quadcopter UAVs has been shown, and the origin of the closed loop cascaded system (3.127) is proven UaGAS and ULES, it is desired to expand the proof to a network of an arbitrary number of quadcopter UAVs. In order to do so, the position tracking dynamics expressed in the formation frame

$$\dot{p}_{i,e} = -S(\omega_f)p_{i,e} + v_{i,e}, \quad (3.131a)$$

$$\dot{v}_{i,e} = -S(\omega_f)v_{i,e} + u_{i,e}, \quad (3.131b)$$

is considered again, where now $i \in \{1, 2, \dots, n\}$, n an arbitrary number, and the same group of reference trajectories as before is considered. Subsequently, it is desired to prove the following proposition.

Proposition 3.5.1. *Consider the reference tracking dynamics (3.131) with $i \in \{1, 2, \dots, n\}$, n an arbitrary number, and time-independent reference trajectories satisfying $\dot{p}_{i,r}(t) = 0$, $\dot{v}_{i,r}(t) = 0$, and $v_{i,r} = v_{j,r}$. Choosing the control law*

$$u_{i,e} = -k_1 p_{i,e} - k_2 v_{i,e} - k_3 \sum_{j=1, j \neq i}^n \left[\frac{d_{ij,r} - d_{ij}}{d_{ij,r} d_{ij}^A} p_{ij} \right], \quad (3.132)$$

with $k_1, k_2, k_3 > 0$, control parameters, yields a time-invariant closed-loop system

$$\dot{p}_{i,e} = -S(\omega_f)p_{i,e} + v_{i,e}, \quad (3.133a)$$

$$\dot{v}_{i,e} = -S(\omega_f)v_{i,e} - k_1 p_{i,e} - k_2 v_{i,e} - k_3 \sum_{j=1, j \neq i}^n \left[\frac{d_{ij,r} - d_{ij}}{d_{ij,r} d_{ij}^A} p_{ij} \right], \quad (3.133b)$$

of which the equilibria are asymptotically stable. Moreover, no collisions between agents occur in the system, i.e., for every solution to (3.133) with initial conditions satisfying $d_{12}(t_0) \neq 0$, there exists $\epsilon > 0$ such that $|d_{12}(t)| \geq \epsilon \forall t$.

Proof. Consider the position tracking dynamics (3.131). Subsequently, consider the candidate control Lyapunov function, based on (3.92), as

$$V = \frac{1}{2} \sum_{i=1}^n \left(k_1 p_{i,e}^\top p_{i,e} + v_{i,e}^\top v_{i,e} + k_3 \sum_{j=i+1}^n \left[\left(\frac{1}{d_{ij}} - \frac{1}{d_{ij,r}} \right)^2 \right] \right), \quad (3.134)$$

with $k_1, k_3 > 0$. Differentiating (3.134) along solutions yields

$$\dot{V} = \sum_{i=1}^n \left(v_{i,e}^\top (k_1 p_{i,e} + u_{i,e}) - k_3 \sum_{j=i+1}^n \left[\frac{d_{ij,r} - d_{ij}}{d_{ij,r} d_{ij}^4} (v_{j,e}^\top - v_{i,e}^\top) p_{ij} \right] \right), \quad (3.135)$$

where the property $b^\top S(a)b = 0$ of a skew-symmetric matrix is used and it is assumed that $\dot{d}_{12,r}(t) = 0$, implying $\dot{p}_{12,r}(t) = 0$. Furthermore, to get (3.135) the analysis is further restricted to time-independent reference trajectories satisfying $\dot{p}_{i,r}(t) = 0$, $\dot{v}_{i,r}(t) = 0$, and $v_{i,r} = v_{j,r}$, in order to have

$$v_{ij}^\top = (v_{j,e}^\top - v_{i,e}^\top) R_f^\top + v_{i,r}^\top R_{i,r}^\top - v_{j,r}^\top R_{j,r}^\top = (v_{j,e}^\top - v_{i,e}^\top) R_f^\top, \quad (3.136)$$

and accordingly

$$\dot{d}_{ij} = \frac{(v_{j,e}^\top - v_{i,e}^\top) p_{ij}}{\sqrt{p_{ij}^\top p_{ij}}} = \frac{(v_{j,e}^\top - v_{i,e}^\top) p_{ij}}{d_{ij}}, \quad (3.137)$$

for $p_{ij}^\top p_{ij} \neq 0$. Note that this definition of constant reference trajectories allows nonzero ω_f in specific situations, as $\dot{p}_{i,r}(t) = 0$ allows constant $v_{i,r} = S(\omega_f) p_{i,r}$. When the virtual inputs $u_{i,e}$ are now chosen as

$$u_{i,e} = -k_1 p_{i,e} - k_2 v_{i,e} - k_3 \sum_{j=1, j \neq i}^n \left[\frac{d_{ij,r} - d_{ij}}{d_{ij,r} d_{ij}^4} p_{ij} \right], \quad (3.138)$$

with $k_2 > 0$, it can be seen that (3.135) becomes

$$\dot{V} = -k_2 \sum_{i=1}^n v_{i,e}^\top v_{i,e} \leq 0, \quad (3.139)$$

where $p_{ij} = -p_{ji}$, $p_{ij,r} = -p_{ji,r}$ is used, and as a result $d_{ij} = d_{ji}$ and $d_{ij,r} = d_{ji,r}$. Since the closed-loop system (3.133) with the considered restrictions on the reference signals is time-invariant, LaSalle's invariance principle tells us that the system converges to the largest invariant subset, defined for the considered system as

$$v_{i,e} = 0, \quad k_1 p_{i,e} = -k_3 \sum_{j=1, j \neq i}^n \left[\frac{d_{ij,r} - d_{ij}}{d_{ij,r} d_{ij}^4} p_{ij} \right], \quad (3.140)$$

for all i , and note that this set defines the equilibria of the closed loop system (3.133). Note that the trivial solution to (3.140) is easily distilled as $d_{ij} = d_{ij,r} \forall i, j \neq i \in \{1, 2, \dots, n\}$, giving $p_{i,e} = 0$. Following Theorem 2.1, it can now be concluded that the equilibria of the closed-loop system (3.133) with the mentioned reference trajectories, are asymptotically stable. Moreover, according to Theorem 2.1, (3.97) indicates that $\frac{1}{d_{ij}}$ is bounded, implying that d_{ij} is bounded away from zero and therefore, for every solution to (3.133) with initial conditions satisfying $d_{ij}(t_0) \neq 0$, there exists $\epsilon > 0$ such that $|d_{ij}(t)| \geq \epsilon \forall t$, for all $i, j \neq i \in \{1, 2, \dots, n\}$. \square

As Proposition 3.5.1 only shows that the closed-loop equilibria are asymptotically stable, it is desired to expand the obtained local results to a global result. In order to do so, it is desired to prove that the origin of the dynamics of the projection

$$z_1 = \sum_{i=1}^n p_{i,e}, \quad z_2 = \sum_{i=1}^n v_{i,e}, \quad (3.141)$$

given by

$$\dot{z}_1 = -S(\omega_f)z_1 + z_2, \quad (3.142a)$$

$$\dot{z}_2 = -S(\omega_f)z_2 + \sum_{i=1}^n u_{i,e} = -S(\omega_f)z_2 - k_1 z_1 - k_2 z_2, \quad (3.142b)$$

which is also time-invariant, is GAS and LES. By noting the similarity between (3.142) and (3.103), Proposition 3.4.2 can be immediately applied in order to obtain the contemplated results. Assuming that the initial conditions are chosen along the lines of Section 3.4.2 in order to guarantee $0 < \epsilon_i \leq f_i(t)$, what remains is to prove stability of the projected dynamics in cascade with the attitude tracking dynamics. The cascaded dynamics is now given along the lines of (3.127), but now with $i \in \{1, 2, \dots, n\}$ and n an arbitrary number, as

$$\dot{z}_1 = -S(\omega_f)z_1 + z_2, \quad (3.143a)$$

$$\dot{z}_2 = -S(\omega_f)z_2 - k_1 z_1 - k_2 z_2 + \sum_{i=1}^n \frac{f_i}{m_i} (I_3 - \tilde{R}_i^\top) e_3, \quad (3.143b)$$

$$\dot{\tilde{R}}_i = \tilde{R}_i S(\tilde{\omega}_i), \quad (3.143c)$$

$$J_i \dot{\tilde{\omega}}_i = -K_{\omega_i} \tilde{\omega}_i + K_{R_i} \sum_{j=1}^3 k_{ji} \left(e_j \times \tilde{R}_i^\top e_j \right), \quad (3.143d)$$

Noting the similarities between (3.143) and (3.127) it is now desired to prove the slightly adjusted Proposition 3.4.4, stated as follows.

Proposition 3.5.2. (cf. [25]) *Consider the closed-loop cascaded system (3.143). The origin of (3.143) is uniformly almost globally asymptotically stable (UaGAS) and uniformly locally exponentially stable (ULES), i.e., for all $p_{i,e} \in \mathbb{R}^3$, $v_{i,e} \in \mathbb{R}^3$, and $(R_{i,e}, \omega_{i,e}) \in G$ with $G \subset SO(3) \times \mathbb{R}^3$ and $\mathcal{M} = (SO(3) \times \mathbb{R}^3) \setminus G$ a set with measure zero.*

Proof. Identify the cascaded nature of (3.143) as ((3.143a),(3.143b)) and ((3.143c),(3.143d)). Let G denote the almost global region of attraction of ((3.143c),(3.143d)), under the conditions mentioned in Section 3.4.2. Furthermore, (3.142) is GAS and LES, and combining both results provides the first two assumptions of Theorem 2.2. What remains to prove is that the cascaded term $\sum_{i=1}^n \frac{f_i}{m_i} (I_3 - \tilde{R}_i^\top) e_3$ is bounded, providing that stability is maintained for the two subsystems in cascade. To prove that $\sum_{i=1}^n \frac{f_i}{m_i} (I_3 - \tilde{R}_i^\top) e_3$ is bounded, similarly to [25], (3.104) is differentiated along solutions (3.143), yielding

$$\begin{aligned} \dot{V} &= -k_2 z_2^\top z_2 + z_2^\top \sum_{i=1}^n \left(\frac{f_i}{m_i} (I_3 - \tilde{R}_i^\top) e_3 \right) \\ &\leq z_2^\top \sum_{i=1}^n \left(\frac{f_i}{m_i} (I_3 - \tilde{R}_i^\top) e_3 \right) \leq c_1 \sqrt{V(z_1, z_2)} \sum_{i=1}^n \|I_3 - \tilde{R}_i^\top\|. \end{aligned} \quad (3.144)$$

Now, since ((3.143c),(3.143d)) is ULES, we have

$$\sqrt{V(z_1(t), z_2(t))} - \sqrt{V(z_1(t_0), z_2(t_0))} \leq c_2(t_0), \quad (3.145)$$

implying that $V(z_1, z_2)$ is bounded, and therefore solutions of ((3.143a),(3.143b)) are bounded, ensuring that the coupling term is bounded. Therefore, it can be concluded that the last assumption of Theorem 2.2 holds, and it is concluded that the cascaded system (3.143) is UGAS and ULES on $\mathbb{R}^{6n} \times G$ and UaGAS and ULES on $\mathbb{R}^{6n} \times \text{SO}(3)^{3n} \times \mathbb{R}^{3n}$, both under the assumptions stated in Section 3.4.2. \square

Although the origin of (3.142), given by $\sum_{i=1}^n p_{i,e} = 0$ and $\sum_{i=1}^n v_{i,e} = 0$, is proven GAS and LES, it is not yet guaranteed that $p_{i,e}$ stays bounded. However, the conjecture is that the only stable equilibrium is $p_{i,e} = 0$, and that the remaining equilibria are saddle points.

3.6 Concluding remarks

This chapter considers two methods to achieve reference tracking, while collision avoidance is guaranteed for the controlled system. An initial method considers a kinematic model in 1D and exploits a control law resulting from an artificial potential field (APF) as based on [42], a projection of the reference tracking is considered, where the resulting equilibria are projected on the origin of the projected system. Using Lyapunov stability, the origin of the projected system is proven uniformly globally asymptotically stable (UGAS), while Chetaev's instability theorem is used to prove that the collision point is an unstable node. This method fails to scale conveniently to a network of double integrators, and applying converse Lyapunov theorem in Section 3.2 inspires the use of a control Lyapunov function incorporating an APF to achieve the control objectives of reference tracking and collision avoidance. A kinematic system in 1D is again considered in Section 3.3 to verify the effectiveness of the control Lyapunov function approach, under the restriction of only using constant reference signals in order to have a time-invariant closed-loop system. The equilibria of the resulting system are proven to be asymptotically stable and locally exponentially stable (LES), while collisions are successfully avoided again. This theoretical framework proves to scale conveniently to a network of double integrators in n D, and eventually to a network of quadcopter UAVs in 3D, both assuming appropriate definitions of constant reference signals. The analysis of a network of two quadcopter UAVs in 3D, as in Section 3.4, is split up in a position tracking subsystem and an attitude tracking subsystem which are analyzed separately. The position tracking dynamics is considered first and the origin of the projected z -dynamics is proven globally asymptotically stable (GAS) and LES, while collisions are successfully avoided under the stated restrictions on the reference trajectories. Although this analysis only proves that the centers of mass of two quadcopter UAVs will never coincide, a convenient base is provided to incorporate agent dimensions in future work. Subsequently, the attitude tracking dynamics is proven uniformly almost globally asymptotically stable (UaGAS) and uniformly locally exponentially stable (ULES). Finally, UaGAS and ULES of the total system is proven using cascaded system theory, and the combined results provide a solution to the stated control Problem 3.5, indicating successful reference tracking and collision avoidance in the network. Additionally, the results are expanded to a network with an arbitrary number of drones, in which UaGAS and ULES of the total cascaded system has also been proven.

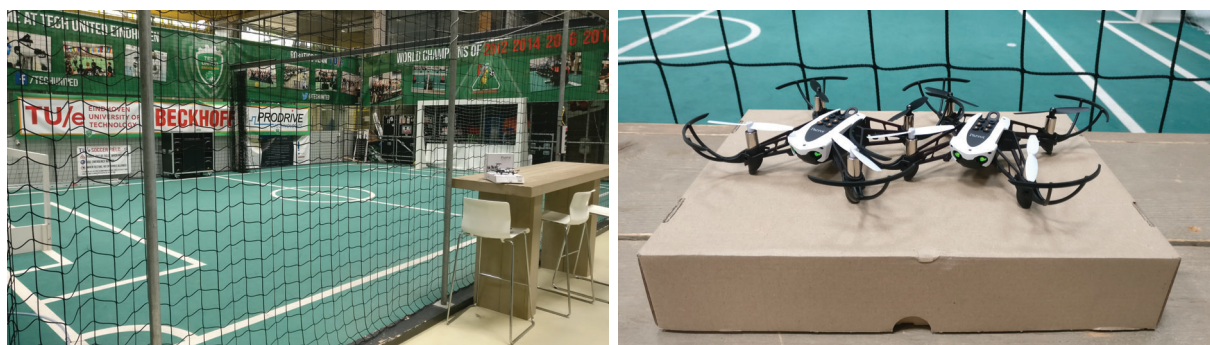
Chapter 4

Numerical and experimental validation

As theory and practice can be worlds apart, especially in the field of nonlinear control where accurate state information is often required, a numerical and experimental validation of the theoretical findings is aspired. The numerical simulation model considers the system dynamics for UAV i , with a specific group of reference trajectories, and the designed control laws as designed in Section 3.4. This section compares the numerical results with experiments. To this end, the experimental setup is introduced, the necessary preparations for experimental implementation are elucidated and the experimental results are presented and compared to numerical simulations throughout the upcoming pages.

4.1 Experimental setup

To test the theoretical results, the designed controller is implemented in an experimental setup and compared with a simulation model. The experimental setup consists of multiple Parrot Mambo Fly drones, a host computer running Matlab version R2019b with the provided Simulink Support Package for Parrot Minidrones for communication with the drones and execution of models on the drones, and the drone test area at the Mechanical Engineering department of the Eindhoven University of Technology. The drone test area can be found in Figure 4.1a and



(a) Drone test area at the TU/e.

(b) Parrot Mambo Fly on cardboard carrier.

Figure 4.1: The experimental setup.

is located at the Robocup soccer-field. The drone test area is actually just a large open space shielded with nets to prevent the drones from flying out. The Parrot Mambo Fly, see Figure 4.1b, and the supplementary Simulink support package are commercially available. Although Parrot has stopped production and recently removed the official support page for the Parrot Mambo Fly of their website. The Parrot Mambo Fly is a compact, lightweight minidrone with

dimensions about 0.18×0.18 meters, inertia given by $J_i = \text{diag}([0.069 \ 0.0775 \ 0.150]) \cdot 10^{-3}$ [26], and a mass of about $m_i = 0.068$ kilograms, including the weight of propeller bumpers to reduce impact upon crashing, resulting in a flight time of about ten minutes after a half hour charge. The Simulink support package of the host computer can communicate with the drone using its Bluetooth Low Energy adapter, combining large range and low energy usage. All the sensor data of the internal measurement unit (IMU), consisting of a three-axis accelerometer, three-axis gyroscope, air pressure sensor, ultrasonic distance sensor and downward facing camera with optical flow sensor, is accessible with the Simulink support package. The sensor data is combined in the model to internally determine the states of the drones using a state estimator developed in [26]. As the aim is autonomous operation of a network of drones, the usage of an external camera system, like OptiTrack [27], to determine positions or velocities is deemed superfluous as the state estimator is assumed to give sufficiently accurate state estimates. Before the experimental setup can be used to conduct the desired experiments, some modifications need to be made to the Simulink support package, including modifying the implemented controller to our needs and enabling connection of multiple drones.

4.2 Towards experimental validation

Now the experimental setup is introduced, the steps taken towards experimental validation are presented. A first step towards experimental validation of the controller designed in Chapter 3, is adjusting the Simulink support package. Initially, the support package only supports communication with a single Parrot Mambo Fly drone. In fact, it is found that using a Windows operating system it is not even possible to simply connect two drones to one host computer using the Network Access Point (NAP) connection that is required to connect with the drones. Therefore, the switch to an Ubuntu operating system is made, since an Ubuntu operating system can connect multiple NAP connections simultaneously. The Simulink support package is completely analyzed and the necessary adjustments to fly multiple drones are summarized in Appendix C. The current adjusted Simulink support package allows simultaneous flight of two drones, this number can be increased by following the steps mentioned also in Appendix C. Subsequently, the controller designed in Chapter 3 is converted to quaternions for computational efficiency. To reduce chance of collisions and therewith damaging the experimental setup, the overshoot of a step reference is analyzed, collision avoidance with a single real drone and a virtual drone is implemented and tested, and as a final step before implementation of the designed controller in the full experimental setup, a communication channel between drones is set up and analyzed.

4.2.1 Conversion of controller to quaternions

To implement the designed controller in the experimental setup, it is first converted to quaternions to attain the advantages stated in Section 2.1.2. Exploiting the characteristics of rotation quaternions, the dynamics of a quadcopter (3.76) is expressed using quaternions as

$$\dot{\rho}_i = q_i \odot \nu_i, \quad (4.1a)$$

$$\dot{\nu}_i = -S(\omega_i)\nu_i + g\bar{q}_i \odot e_3 - \frac{f_i}{m_i}e_3, \quad (4.1b)$$

$$\dot{q}_i = \frac{1}{2}q_i \otimes \begin{bmatrix} 0 \\ \omega_i \end{bmatrix} = \frac{1}{2}Q(q_i) \begin{bmatrix} 0 \\ \omega_i \end{bmatrix} \quad (4.1c)$$

$$J_i\dot{\omega}_i = S(J_i\omega_i)\omega_i + \tau_i, \quad (4.1d)$$

and the considered reference trajectory (3.78) is denoted along the same lines as

$$\dot{\rho}_{i,r} = q_{i,r} \odot \nu_{i,r}, \quad (4.2a)$$

$$\dot{\nu}_{i,r} = -S(\omega_{i,r})\nu_{i,r} + g\bar{q}_{i,r} \odot e_3 - \frac{f_{i,r}}{m_i}e_3, \quad (4.2b)$$

$$\dot{q}_{i,r} = \frac{1}{2}q_{i,r} \otimes \begin{bmatrix} 0 \\ \omega_{i,r} \end{bmatrix} = \frac{1}{2}Q(q_{i,r}) \begin{bmatrix} 0 \\ \omega_{i,r} \end{bmatrix} \quad (4.2c)$$

$$J_i \dot{\omega}_{i,r} = S(J_i \omega_{i,r})\omega_{i,r} + \tau_{i,r}, \quad (4.2d)$$

resulting in individual position and velocity tracking errors expressed in the formation frame \mathcal{F} as

$$p_{i,e} = p_{i,r} - p_i = \bar{q}_f \odot (\rho_{i,r} - \rho_i), \quad (4.3a)$$

$$v_{i,e} = \bar{q}_f \odot (q_{i,r} \odot \nu_{i,r} - q_i \odot \nu_i), \quad (4.3b)$$

which give the tracking error dynamics in the formation frame according to

$$\dot{p}_{i,e} = -S(\omega_f)p_{i,e} + v_{i,e}, \quad (4.4a)$$

$$\dot{v}_{i,e} = -S(\omega_f)v_{i,e} + u_{i,e}, \quad (4.4b)$$

where $u_{i,e}$ is considered the virtual input given as

$$u_{i,e} = -\bar{q}_f \odot \left(q_{i,r} \odot \frac{f_{i,r}}{m_i}e_3 - q_i \odot \frac{f_i}{m_i}e_3 \right), \quad (4.5)$$

to be achieved by the attitude tracking subsystem. The control inputs are selected as in (3.96) where $p_{12} = \bar{q}_f \odot \rho_{12}$ is used, and with which reference tracking and collision avoidance is achieved, see Section 3.4.1. Now the total force magnitude is represented using quaternions as

$$f_i = \|f_{i,r}e_3 + m_i\bar{q}_{i,r} \odot (q_f \odot u_{i,e})\|, \quad (4.6)$$

with which the desired force direction is given according

$$f_{i,d} = \frac{f_{i,r}e_3 + m_i(\bar{q}_{i,r} \otimes q_f) \odot u_{i,e}}{\|f_{i,r}e_3 + m_i(\bar{q}_{i,r} \otimes q_f) \odot u_{i,e}\|}. \quad (4.7)$$

According to [26, 35] the conversion of $R_{i,d}$ to a unit quaternion is given as

$$q_{i,d} = \frac{1}{2} \begin{bmatrix} 2 \cos(\frac{1}{2} \arccos(\frac{1}{2}(R_{i,d}[1,1] + R_{i,d}[2,2] + R_{i,d}[3,3] - 1))) \\ \text{sign}(R_{i,d}[3,2] - R_{i,d}[2,3])|\sqrt{1 + R_{i,d}[1,1] - R_{i,d}[2,2] - R_{i,d}[3,3]}| \\ \text{sign}(R_{i,d}[1,3] - R_{i,d}[3,1])|\sqrt{1 - R_{i,d}[1,1] + R_{i,d}[2,2] - R_{i,d}[3,3]}| \\ \text{sign}(R_{i,d}[2,1] - R_{i,d}[1,2])|\sqrt{1 - R_{i,d}[1,1] - R_{i,d}[2,2] + R_{i,d}[3,3]}| \end{bmatrix}, \quad (4.8)$$

where $R_{i,d}[j,k]$ represents the (j,k) th entry of matrix $R_{i,d}$. And after using $f_{i_1,d}^2 + f_{i_2,d}^2 + f_{i_3,d}^2 = 1$ (as $f_{i,d}$ is of unit length), and substituting the values for R_{ij} in (4.8), the resulting rotation quaternion is given as

$$q_{i,d} = \frac{1}{2} \begin{bmatrix} 2 \cos(\frac{1}{2} \arccos(f_{i_3,d})) \\ -f_{i_2,d} \sqrt{\frac{2}{1+f_{i_3,d}}} \\ f_{i_1,d} \sqrt{\frac{2}{1+f_{i_3,d}}} \\ 0 \end{bmatrix}, \quad (4.9)$$

which can be rewritten as

$$q_{i,d} = \begin{bmatrix} \frac{1}{2} \sqrt{2 + 2f_{i_3,d}} \\ \frac{f_{i_2,d}}{\sqrt{2+2f_{i_3,d}}} \\ \frac{f_{i_1,d}}{\sqrt{2+2f_{i_3,d}}} \\ 0 \end{bmatrix}. \quad (4.10)$$

Furthermore, the attitude and angular velocity errors are defined as

$$q_{i,e} = \bar{q}_{i,d} \otimes (\bar{q}_{i,r} \otimes q_i), \quad (4.11a)$$

$$\omega_{i,e} = \omega_i - (\bar{q}_i \otimes q_{i,r}) \odot \omega_{i,r} - \bar{q}_{i,e} \odot \omega_{i,d}, \quad (4.11b)$$

which define the attitude error dynamics as

$$\dot{q}_{i,e} = \frac{1}{2} q_{i,e} \otimes \begin{bmatrix} 0 \\ \omega_{i,e} \end{bmatrix}, \quad (4.12a)$$

$$J_i \dot{\omega}_{i,e} = S(J_i \omega_i) \omega_i + \tau_i - J_i (\bar{q}_i \otimes q_{i,r}) \odot \dot{\omega}_{i,r} \\ + J_i S(\omega_{i,e}) [\omega_i - \omega_{i,e}] + J_i (\bar{q}_{i,e} \odot [S(\omega_{i,d}) (\bar{q}_{i,d} \odot \omega_{i,r}) - \dot{\omega}_{i,d}]), \quad (4.12b)$$

and the selected input τ_i of (3.125) is written in quaternions as

$$\tau_i = -S(J_i \omega_i) \omega_i + J_i (\bar{q}_i \otimes q_{i,r}) \odot \dot{\omega}_{i,r} - J_i S(\omega_{i,e}) [\omega_i - \omega_{i,e}] \\ - J_i (\bar{q}_{i,e} \odot [S(\omega_{i,d}) (\bar{q}_{i,d} \odot \omega_{i,r}) - \dot{\omega}_{i,d}]) - K_{\omega_i} \omega_{i,e} + K_{R_i} \sum_{j=1}^3 k_{ji} (e_j \times (\bar{q}_{i,e} \odot e_j)), \quad (4.13)$$

with $K_{\omega_i} = K_{\omega_i}^\top > 0$, $K_{R_i} = K_{R_i}^\top > 0$, and $k_{ji} > 0$ distinct, i.e., $k_{1i} \neq k_{2i} \neq k_{3i} \neq k_{1i}$.

Concluding remarks

In this section, the system dynamics (3.76) and the designed controller (3.96) are rewritten using quaternions for computational and communication efficiency. With the control inputs defined by (4.5), (4.6) and (4.13), the designed controller is ready to be implemented in the experimental setup.

4.2.2 Performance of a single drone

Before immediately flying two drones simultaneously, it is desired to get an indication of how vigorous the drones move when tracking a constant reference, in order to avoid unnecessary damage to the setup. To this end, numerical simulations are conducted to evaluate the reference tracking performance of a single drone and the results are compared with the experimental situation. Subsequently, the obstacle avoidance capability of the controller is analyzed by introducing a virtual drone in both simulations and experiments. The control gains K_{ω_i} , K_{R_i} , and k_{ji} , for the control input τ_i of the attitude tracking subsystem, are chosen as

$$K_{\omega_i} = 30 \cdot J_i, \quad (4.14a)$$

$$K_{R_i} = 70 \cdot J_i, \quad (4.14b)$$

$$k_{1i} = 0.9, \quad (4.14c)$$

$$k_{2i} = 1.0, \quad (4.14d)$$

$$k_{3i} = 1.1, \quad (4.14e)$$

as this choice provides favorable tracking behavior [26]. The chosen control gains of the position tracking subsystem are varied and motivated with each executed experiment.

Reference tracking analysis

First, the overshoot of a single drone with a step reference is analyzed when using controller (3.96), (4.6) and (4.13) with $k_1 = 3k_2 = 3$, $k_3 = k_4 = k_5 = 0$ and reference position $\rho_{1,r} = [1 \ 0 \ 1.5]^\top$ of which the numeric result can be found in Figure 4.2, where a small offset in y -direction is introduced, as there will also be a disturbance present in the experimental setup up to a certain

level. As only a single drone is used in this experiment, the controller gains are selected as $k_3 = k_4 = k_5 = 0$. The remaining control parameters are chosen to prevent a steady state error in z -position that is observed in experiments, for example, when $k_1 = k_2 = 1$ is selected, while limiting the occurring overshoot. Note that the stability analysis indeed indicates stability of the system when the controller gains are chosen as in this situation. The corresponding experimental result can be found in Figure 4.3. When Figure 4.3 is compared with the simulated situation

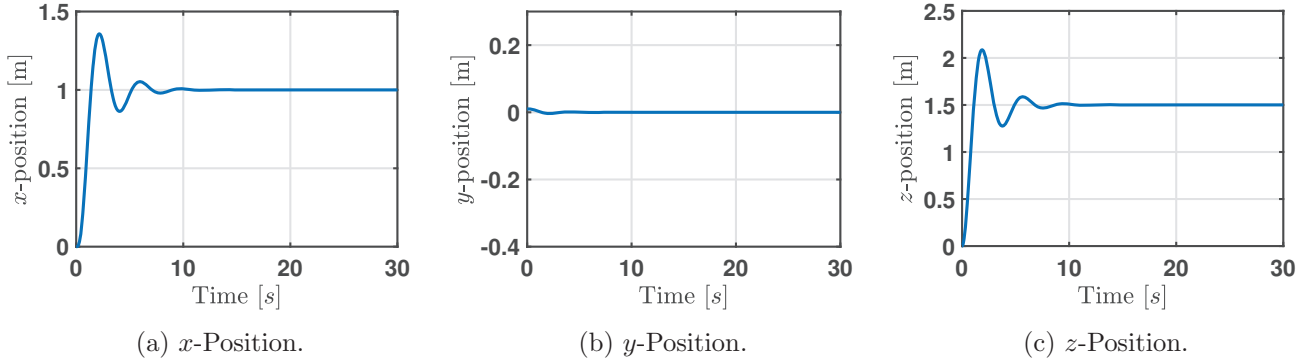


Figure 4.2: Overshoot in x , y , z -position of a step for a single drone in simulations.

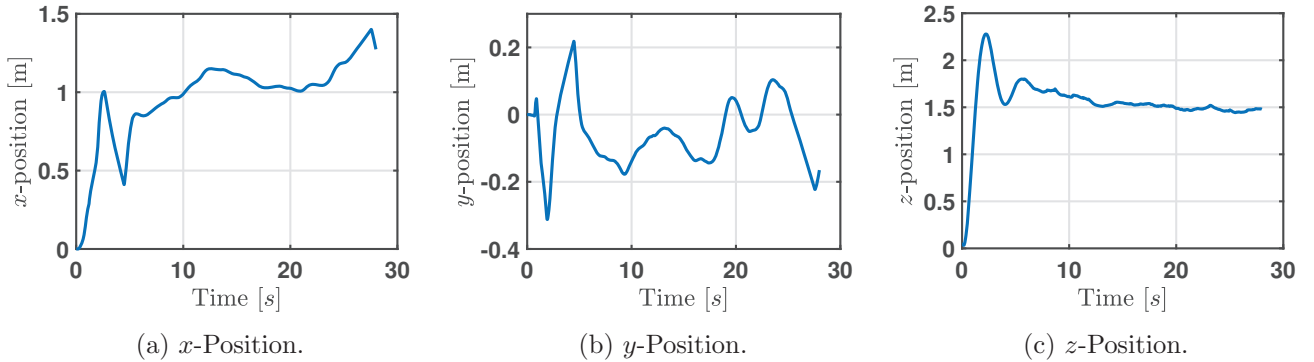


Figure 4.3: Estimated x , y , z -position a single drone subject to a step function in experiments.

of Figure 4.2, it seems that there is quite a disturbance present in the horizontal plane, while tracking of the z -position actually is comparable and quite smooth. To compare the performance of the position tracking of a single drone, the slightly modified root mean square (RMS) of the estimated $p_{i,e}$ in k -direction is computed according

$$p_{i,e,k}^{\text{RMS}} = \frac{1}{\Delta t} \sqrt{\left(p_{i,e,k}^2(1) + p_{i,e,k}^2(2) + \dots + p_{i,e,k}^2(n) \right)}, \quad (4.15)$$

where Δt represents the time duration of the experiment or simulation, and $n = 200\Delta t$ is the number of samples, and is presented for experiments and simulations in Table 4.1. From Table

Table 4.1: RMS value of estimated or simulated $p_{i,e}$ in x , y , z -direction as a result of a step function for a single drone.

	$p_{1,e,x}^{\text{RMS}}$	$p_{1,e,y}^{\text{RMS}}$	$p_{1,e,z}^{\text{RMS}}$	Δt
Position tracking simulation	0.5709	0.0057	0.7807	27.995
Position tracking experiment	0.7242	0.2962	0.7713	27.995

4.1 it can be seen that the RMS in z -direction is almost identical in simulations and experiments.

The observed disturbance present in the horizontal plane is also visible in the RMS values, where the disturbance in y -direction appears to be more influential than the disturbance in x -direction. The disturbance can be partly accounted for by the strong winds present at the drone test area caused by the air treatment system running at full power. Furthermore, it should also be noted that the behavior in the experiments is almost separated in a vertical tracking motion followed by a horizontal tracking motion, while in simulations vertical and horizontal tracking is executed simultaneously. This is underlined by analyzing the time it takes for the drone to first reach their referenced position in x , y and z position, respectively, see Table 4.2.

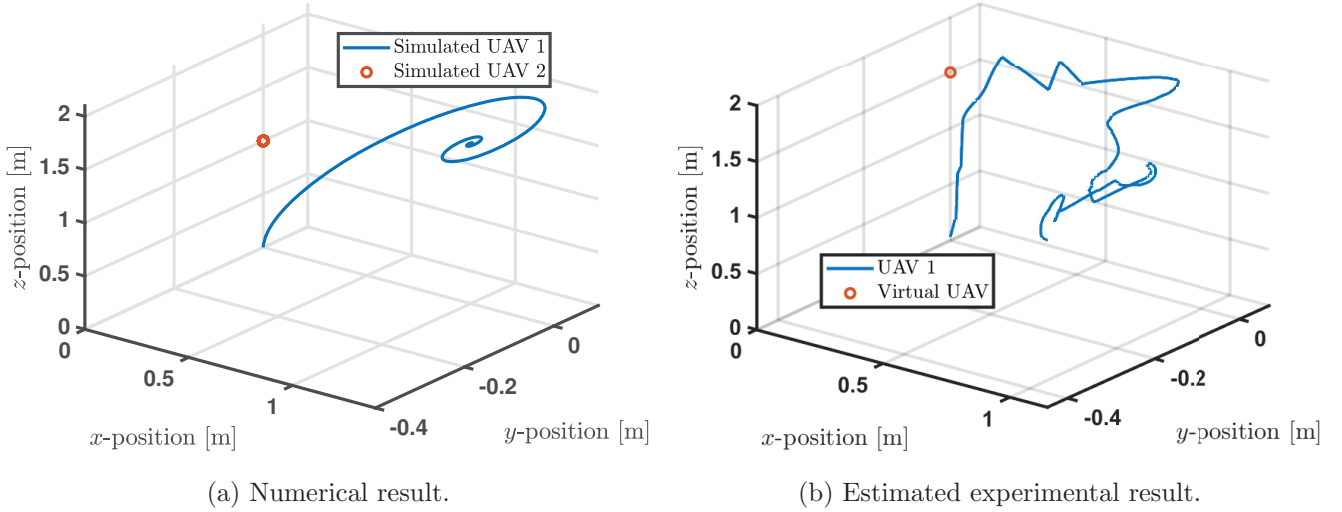
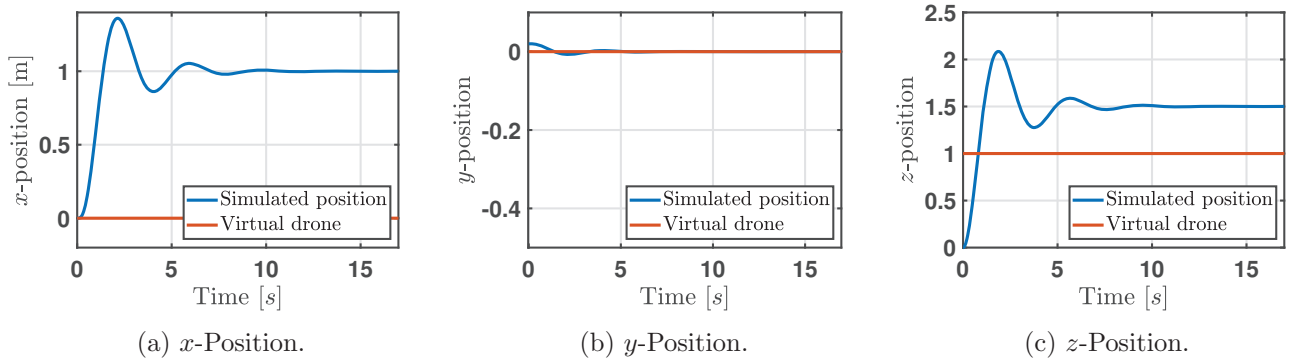
Table 4.2: Time it takes the drone to first reach the referenced value in seconds, in the considered directions in simulations and experiments.

	x -direction	y -direction	z -direction
Position tracking simulation	1.37	1.38	1.1
Position tracking experiment	2.52	0	1.26
Virtual drone with $k_5 = 0$ simulation	1.37	1.38	1.1
Virtual drone with $k_5 = 0$ experiment	3.16	0	0.77
Virtual drone with $k_5 = 1$ simulation	1.07	2.31	1.59
Virtual drone with $k_5 = 1$ experiment	1.5	0	2.27

From Table 4.2 it can be seen that, while the time it takes to reach the referenced z -position for the first time is comparable in simulations and experiments, the time it takes to reach the referenced x -position for the first time differs considerably more. Note also that it takes quite long for the simulated drone to reach the referenced y -position for the first time, it even takes longer than reaching the referenced x -position for the first time, although that can be explained by the fact that the (1,1) and (2,2) elements of J_i are not equal. Altogether, the position tracking performance is deemed to be in line with the simulations, although naturally some differences exist.

Obstacle avoidance with virtual drone

Now that the overshoot of a single, reference tracking, drone is deemed to be within acceptable bounds, a virtual drone is introduced to test the collision avoidance behavior with low risk of damaging the setup. To this end, a virtual drone is placed at its reference position exactly above the initial position of the real drone at $\rho_v = [0 \ 0 \ 1.5]^\top$ and the reference position for the real drone is set to $\rho_{1,r} = [1 \ 0 \ 1.5]^\top$. In the simulated situation, the drone is placed at $\rho_v = [0 \ 0 \ 1]^\top$ since the takeoff behavior is observed to differ from experiments in the simulated situation, and with $\rho_v = [0 \ 0 \ 1]^\top$ the situations are found to be more similar. Now the controller gains are selected as $k_1 = 3k_2 = k_3 = 3k_4 = 3$, as this choice seemed to provide good position tracking behavior, and in order to have a reference situation $k_5 = 0$ is first selected. The resulting behavior can be found in Figure 4.4, with the corresponding action sequence depicted in Figure 4.10a, and it is observed that the centers of mass of the virtual drone and the real drone pass each-other closely in both simulation and experiments. In the simulated situation it is computed that $\min(d_{12}) = 0.3360$ which in experiments is only $\min(d_{12}) = 0.13$, see Figure 4.5 and 4.6. This difference is explained by the fact that takeoff behavior between simulations and experiments is not corresponding, and in experiments. The considered situation would have definitely resulted in a collision since the drones are some nine centimeters in radius around their center of mass. The time it takes the drone to first reach its referenced positions can also be found in Table 4.2, which underlines the difference in take-off behavior. Additionally, the RMS values of the resulting behavior in x , y , z -direction are again computed and can be found in Table 4.3, from which it can be seen that the RMS values correspond quite well, apart from a large disturbance in y -direction. In fact, in the x and z -direction, the experimental data even seems to outperform the simulation data with respect to tracking behavior.

Figure 4.4: Collision avoidance with a virtual drone and $k_5 = 0$.Figure 4.5: Behavior of a single drone and a virtual drone with $k_5 = 0$ in a simulated environment.

Next, we slightly deviate from the analysis as presented in Section 3.4 by setting $k_5 = 1$, while keeping the virtual drone fixed in space, implying $k_5 = 0$ in the control law of the virtual drone, i.e., $k_5 = 1$ is used in (3.91b) and $k_5 = 0$ is used in (3.91d). Although we deviate from the analysis as in Section 3.4, this experiment can still give valuable insights as it allows to test the collision avoidance capabilities of a single drone without risk of damaging the experimental setup. Furthermore, setting $k_5 = 1$ activates the collision avoidance strategy of the control law, and ensures a balance between the amount of collision avoidance and the vehemence of the resulting behavior.

With k_5 now set as $k_5 = 1$, it can be seen in Figure 4.7b, that the virtual drone is avoided nicely, with $\min(d_{12}) = 0.4629$ in simulations and $\min(d_{12}) = 0.28$ in experiments, and no collision would have occurred, see Figures 4.8 and 4.9. The corresponding action sequence is depicted in Figure 4.10b. And it should be noted that an increase in $\min(d_{12})$ is observed in both simulations and experiments as a consequence of activating the collision avoidance strategy. From the experiment it is observed that the evasion maneuver is rather aggressive while the drone still manages to end up close to its reference position. This also implies that the situation for which $\min(d_{12}) = 0.28$ is only of very short duration, indicating that the collision avoidance strategy is rather fast, see Figure 4.9. Furthermore, the evasive maneuver is rather aggressive and the drone rotates up to about 90 degrees around its y -axis in the experimental situation. This could explain why the position estimation seems rather noisy, especially in y -direction. This is underlined by the fact that state estimation largely depends on optical flow and sonar

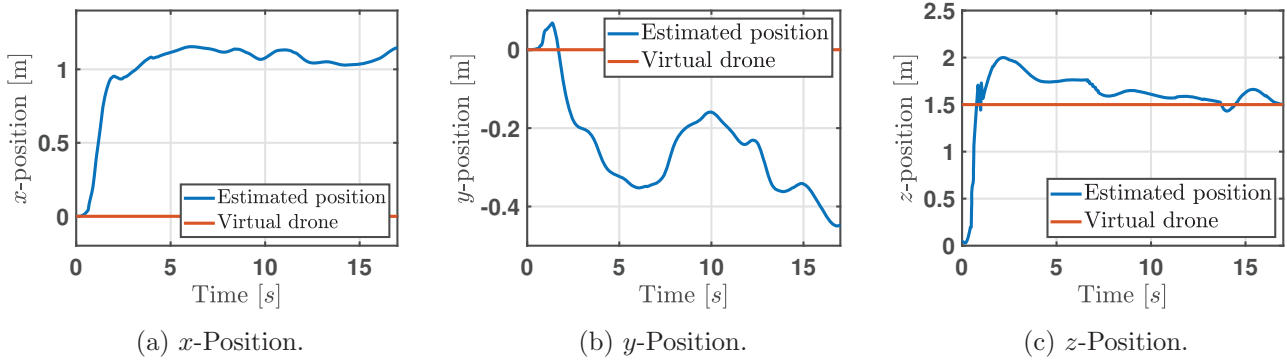


Figure 4.6: Estimated behavior of a single drone and a virtual drone with $k_5 = 0$ in experiments.

Table 4.3: RMS value of estimated or simulated $p_{i,e}$ in x, y, z -direction as a result of a step function for a single drone and a virtual drone.

	$p_{1,e,x}^{\text{RMS}}$	$p_{1,e,y}^{\text{RMS}}$	$p_{1,e,z}^{\text{RMS}}$	Δt
Virtual drone with $k_5 = 0$ simulation	0.9371	0.0093	1.2815	17.055
Virtual drone with $k_5 = 0$ experiment	0.8813	0.9497	1.1280	17.055
Virtual drone with $k_5 = 1$ simulation	0.8321	0.0119	1.0315	22.73
Virtual drone with $k_5 = 1$ experiment	2.7898	0.9202	1.4056	22.73

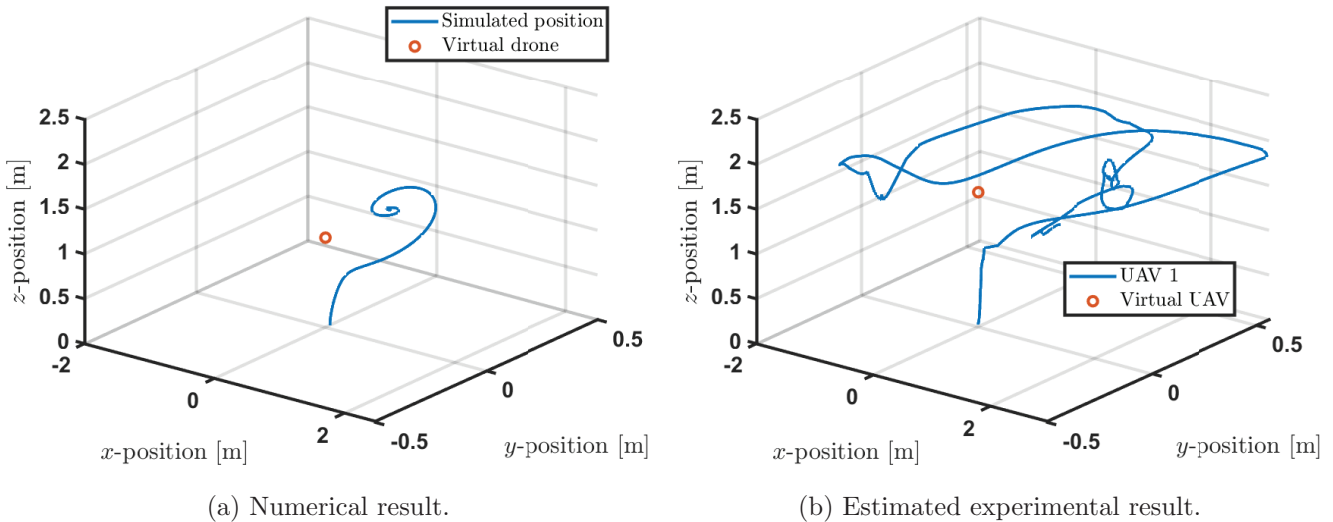
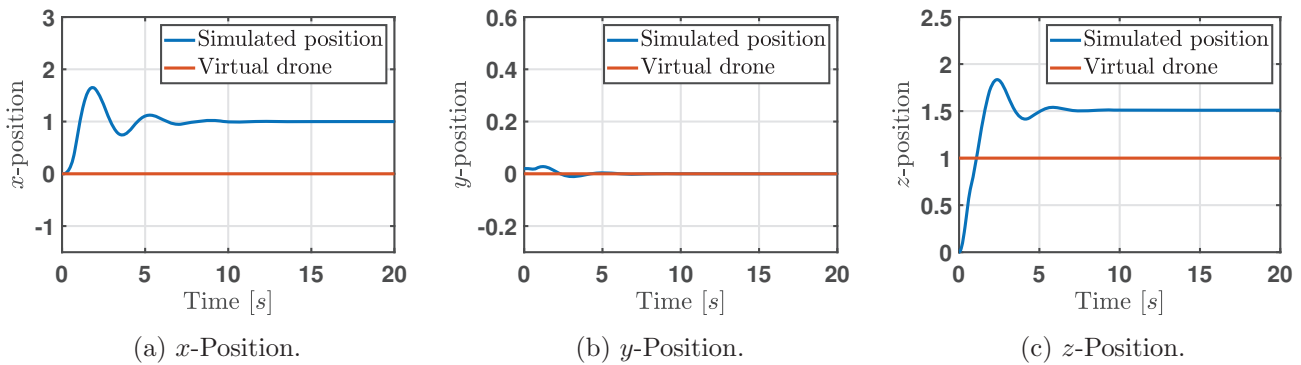
data, which both become unreliable when the bottom of the drone is perpendicular with the horizontal plane [26]. This can also be seen from the computed RMS values $p_{1,e,k}^{\text{RMS}}$ in Table 4.3, where especially the difference in x -direction stands out, which is in line with the observed fierce rotation around the drones y -axis.

Concluding remarks

The reference tracking and collision avoidance capabilities of a single drone are tested, where first simulations and experiments show favorable position tracking behavior. A subsequent experiment introducing obstacle avoidance with a virtual drone shows that introducing a collision avoidance strategy ($k_5 = 1$) successfully avoids collisions, unlike a control law that does not include a collision avoidance strategy ($k_5 = 0$), in both simulation and experiment, as demonstrated in Figures 4.4 and 4.7. A side note should be made here that we slightly deviated from the approach as in Section 3.4, as the virtual drone is kept fixed in space. Furthermore, it is observed that influential disturbances are present at the drone test area caused by the air treatment system, which become obvious when the simulations are compared with experiments. Additionally, a difference in take-off behavior is observed. Nevertheless, the controller is deemed ready for implementation in a system of two drones with active collision avoidance and reference tracking.

4.2.3 Setting up the communication channel

As the Simulink support package is not created to control multiple Parrot minidrones simultaneously, a means to implement a form of communication also has to be introduced. Luckily, the support package contains blocks to communicate with the host computer [44] and example models exist to control the motor speed of a minidrone using the host computer [45]. This is exploited by connecting to the NAP of multiple drones and bridging the connected interfaces on the host computer, implying that the signals from one drone to another, all pass by the host computer. The support package comes with two types of communication blocks, one exploits the TCP/IP protocol and the other makes use of the UDP protocol. The most significant difference between these two well known communication protocols is that one incorporates an acknowledge message when a message is received (TCP/IP), and the other does not (UDP). Therefore, the

Figure 4.7: Collision avoidance with a virtual drone and $k_5 = 1$.Figure 4.8: Behavior of a single drone and a virtual drone with $k_5 = 1$ in a simulated environment.

UDP protocol is most used in real-time applications where connection speed is preferred over data accuracy, like phone or video calls, while the TCP/IP protocol is preferred when a reliable data stream is required, for example for email or file transfer [46]. Along these lines, experiments are first conducted using the UDP communication protocol.

Communication with UDP protocol

To test the quality of the communication channel, two drones are placed on a cardboard carrier, see Figure 4.1b, and the UDP Send and UDP Receive blocks are incorporated in the Simulink project to send the z -direction of the accelerometer data over the communication channel. When the carrier is now moved up and down, a pattern will appear in the accelerometer data, introducing a means of indicating time delay over the communication channel. The resulting sent and received data is found in Figure 4.11 from which it becomes immediately clear that the obtained data is rather poor. It is observed that the shape of the received data is similar to the shape of the sent data but the data seems to be stretched over a significantly longer time period, which would indicate a time-varying time delay.

Communication with TCP/IP protocol

As the data stream communicated using a UDP communication protocol seems rather poor, experiments are conducted using the TCP/IP protocol in the quest to improve data quality.

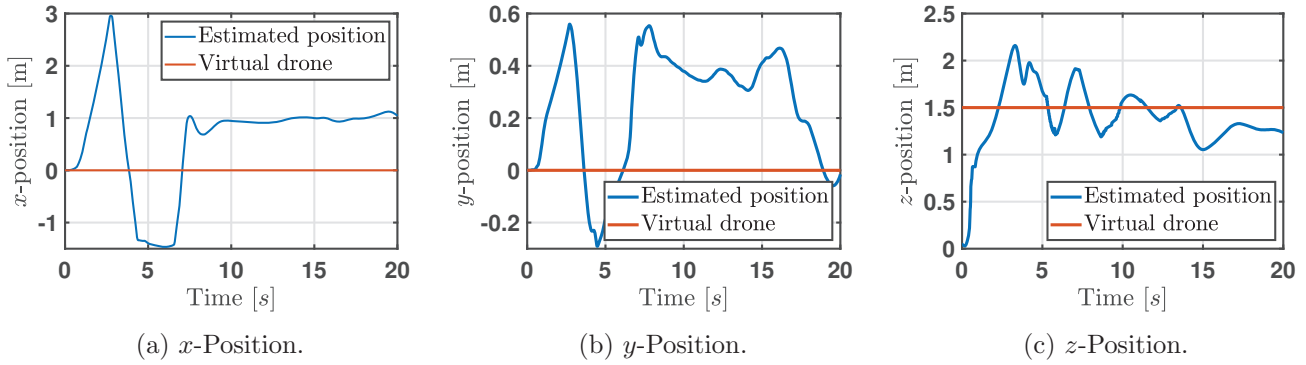


Figure 4.9: Estimated behavior of a single drone and a virtual drone with $k_5 = 1$ in experiments.

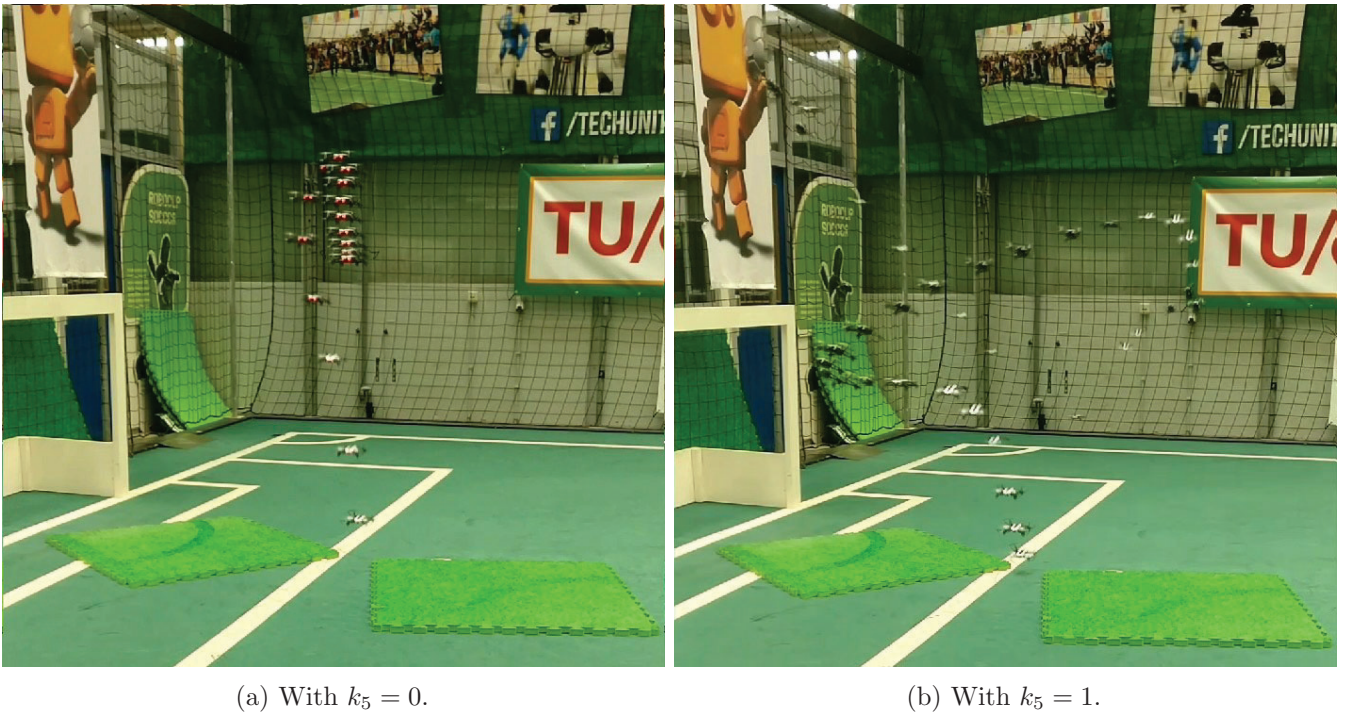
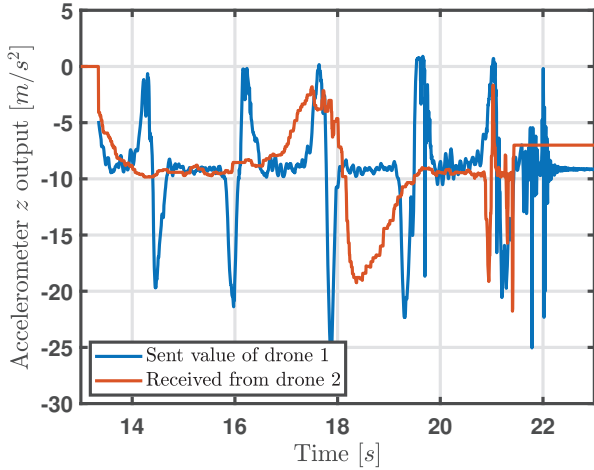


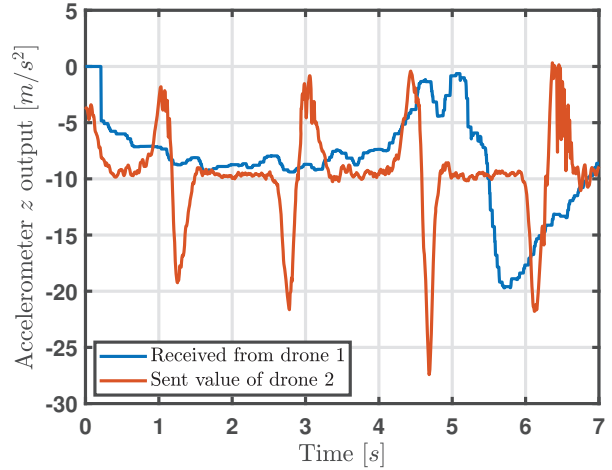
Figure 4.10: Action sequence of a collision avoidance experiment with a virtual drone.

The drones are again placed on a cardboard carrier and moved up and down while sending accelerometer data back and forth. The results of the initial experiment can be found in Figure 4.12. From this figure, it is observed that the communication delay of the sent signal by drone two is an acceptable 0.2 – 0.3 seconds, while the delay of the sent signal by drone one is about ten times as large; two full seconds. An explanation for this probably lies in the fact that the Simulink support package initially only supports a single drone, because of which they cannot start simultaneously. The hypothesis is that this causes information packets to queue up while waiting for a connection to be established with the second drone, which takes approximately ten seconds. Now, when a connection is finally set up with the second drone, it will start processing the oldest packets first, resulting in a major delay. It is noted however, that the drones are capable of processing packages sent with the TCP/IP protocol at the same rate as the processor frequency, at 200Hz.

To reduce the delay of the signal sent by drone one, the TCP/IP send block of drone one is placed inside a so called ‘Enabled Subsystem’ which is enabled only after receiving a first status message of the second drone. An example of this can be found in Figure 4.13. The Enabled

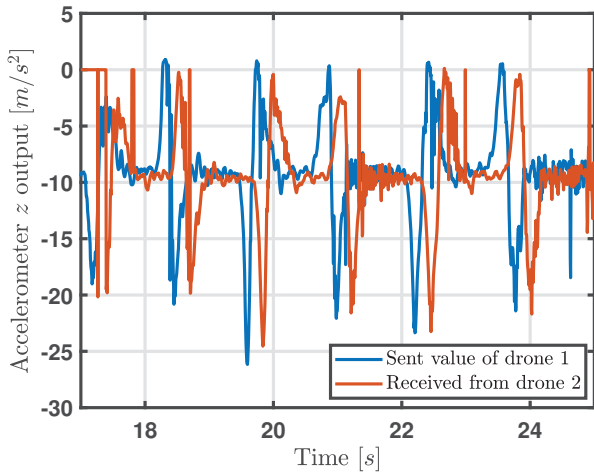


(a) Perspective drone 1.

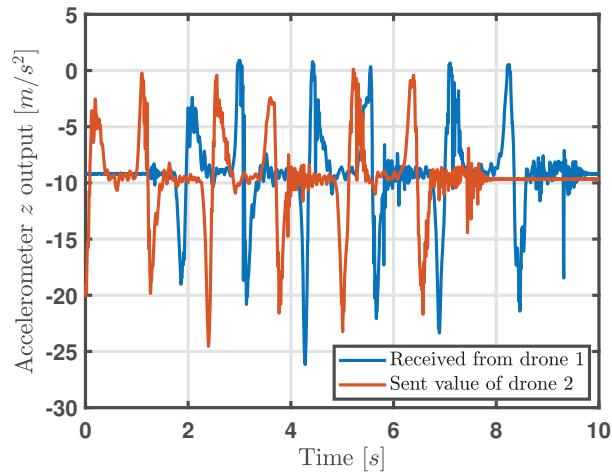


(b) Perspective drone 2.

Figure 4.11: Communication test with UDP communication protocol.



(a) Perspective drone 1.



(b) Perspective drone 2.

Figure 4.12: Communication test with TCP/IP communication protocol.

Subsystem, containing only a TCP/IP send block sending $p_{1,e}$ and $v_{1,e}$, is now enabled when the value entering the so called ‘Enable Port’ is larger than one. Note that this also enables simultaneous takeoff while the drones are initiated non-synchronously. For simultaneous takeoff it is found that the performance of the state estimator significantly increases when also placed in an enabled subsystem, instead of using the status signal of the connection as a gain of the actuator inputs. The resulting communication signal is found in Figure 4.14, where the sent signal is of the `int16` data type, instead of the `double` data type, to save even more bandwidth. Figure 4.14 shows that the delay of the signal sent to drone two is reduced with a factor ten, to about 200 milliseconds. This is reckoned to be satisfactory as a simple ping signal from the host computer to a drone usually takes about 50 milliseconds, with outliers just above 200 milliseconds. And the time delay of 200 milliseconds even incorporates the fact that the connected drones communicate through the host computer’s interfaces. To even further decrease the communication delay, one could change the nature of the Bluetooth communication network in such a way that the drones could directly communicate with each-other, rather than utilizing the bridged interfaces of the host computer. Notice that for some time instants, the connection

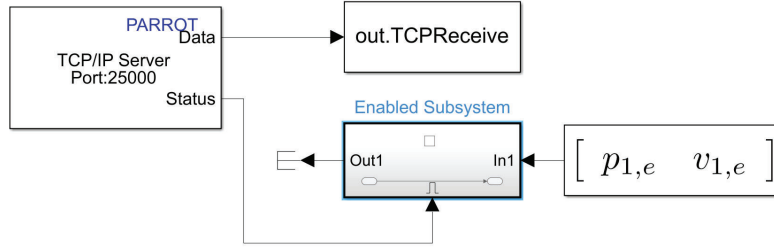


Figure 4.13: Implementation of TCP/IP send block in enabled subsystem

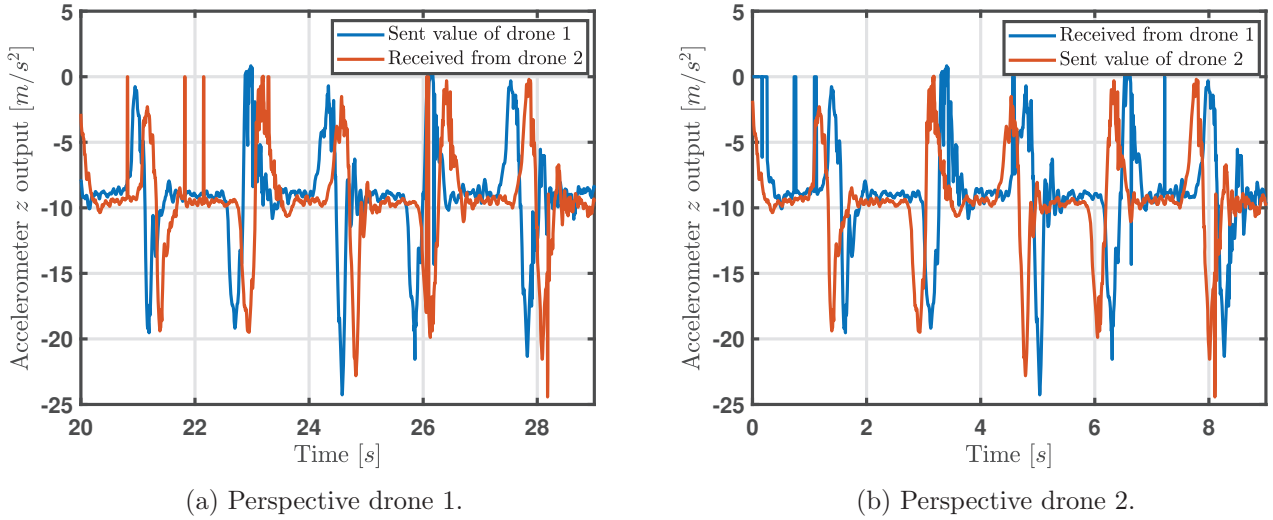


Figure 4.14: Communication test with TCP/IP communication protocol.

is poor or lost, resulting in a received value equal to zero, for example around $t = 22$ in the signal received by drone one from drone two in Figure 4.14a. It is also observed that the stability of the connection can be poor when just initiated, an example of which can be found in Figure 4.15. From this figure it can be seen that the connection is extremely poor when just initiated, however, the stability of the signal seems to vary with each experiment and this figure is chosen as it illustrates the phenomenon quite well. The poor connection during the initial moments of an experiment becomes especially problematic when the drones are initiated in such a way that an evasion maneuver is to be executed in these initial moments in order to avoid a collision. Since the values of $p_{i,e}$ and $v_{i,e}$ are to be communicated, a failure in communication will signify that the receiving drone observes the sending drone in its respective reference position $p_{i,e} = 0$, $v_{i,e} = 0$, most probably being further away from the receiving drone than the sending drone actually is.

Concluding remarks

A final comparison is made to evaluate the quality of the signal, to be found in Figure 4.16. To get this result, both drones are again placed on the cardboard carrier and moved up and down. This time, estimated z -positions are sent back and forth rather than accelerometer data and drone 1 receives the estimated z -position of drone two using the TCP/IP protocol, while sending its estimated z -position to drone two using the UDP protocol. From Figure 4.16 it becomes clear that the time delay, while using the UDP protocol, is not constant. Moreover, it is observed that the received signal also differs in shape with respect to the corresponding sent signal. Therefore, the choice for using the TCP/IP protocol seems a trivial one as the time delay is constant and

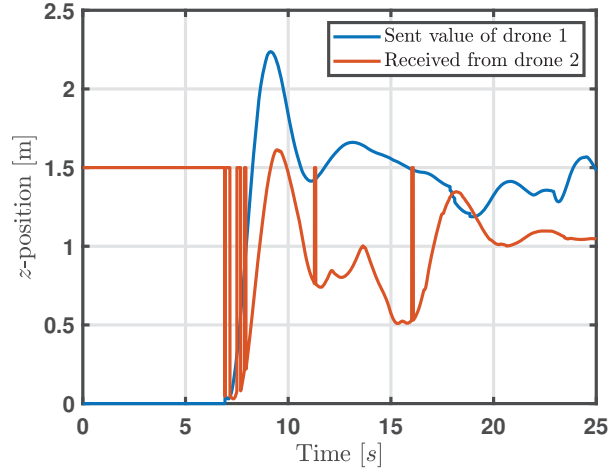


Figure 4.15: Estimated z -position of drone one and two as observed by drone one to illustrate stability of connection when just established.

small, and the received signal fully corresponds to the sent signal, apart for some time instants where the connection is flawed or lost. However, it should be noted that the UDP protocol should be faster in theory, and investigating implementation of a communication channel using the UDP protocol in the current experimental setup could be interesting to further reduce the communication delay for future research.

4.3 Results

After analyzing the tracking behavior and setting up and testing the communication channel, the final controller can be implemented in a system of two drones with collision avoidance. For this, the formation frame is positioned 1.5 meters above the origin, $\rho_f = [0 \ 0 \ 1.5]^\top$, and the reference positions of the drones expressed in the formation frame are $p_{1,r} = -p_{2,r} = [-0.5 \ 0 \ 0]^\top$. The drones are initiated at $\rho_1(t_0) = -\rho_2(t_0) = [0.1375 \ 0 \ 0]^\top$, and the controller gains are first chosen as $k_1 = 3k_2 = k_3 = 3k_4 = 3$ with $k_5 = 0$, to see whether indeed a collision occurs when the obstacle avoidance strategy is inactive. A small disturbance in initial y -position is introduced in the simulated situation to resemble the experimental situation: $\rho_1(t_0) = -\rho_2(t_0) = [0.1375 \ -0.01 \ 0]^\top$. The resulting simulated situation is found in Figure 4.17a and the minimal inter-agent distance is computed to be $\min(d_{12}) = 0.0156$, clearly resulting in a collision when implemented in experiments. To increase quality and reliability of the final experiments, the air treatment system is turned off and the results of the controller with inactive collision avoidance strategy can be found in Figure 4.17b, where the straight lines represent a short instability of the connection. The estimated positions look rather unexpected but this is because the two drones indeed fly into each-other and crash, losing their connection. The minimal inter-agent distance that occurred during this experiment is $\min(d_{12}) = 0.240$ which seems pretty large, but appears to be sufficiently small to make the two drones crash. The estimated position is not compensated for the present time delay so the real $\min(d_{12})$ is most likely smaller than the estimated $\min(d_{12})$. Now that a reference situation is obtained, the collision avoidance strategy is now activated by setting $k_5 = 0.5$. Setting $k_5 = 0.5$ activates the collision avoidance strategy of the control law, and ensures a balance between the amount of collision avoidance and the vehemence of the resulting behavior, as it is found that ferocious evasion maneuvers degrade estimator performance, and thus tracking capability. When the reference positions and initial conditions are chosen identical to the experiment depicted in Figure 4.17, with as only difference choosing $k_5 = 0.5$ instead of $k_5 = 0$, the minimal inter-agent distance is obtained to be $\min(d_{12}) = 0.2757$ and

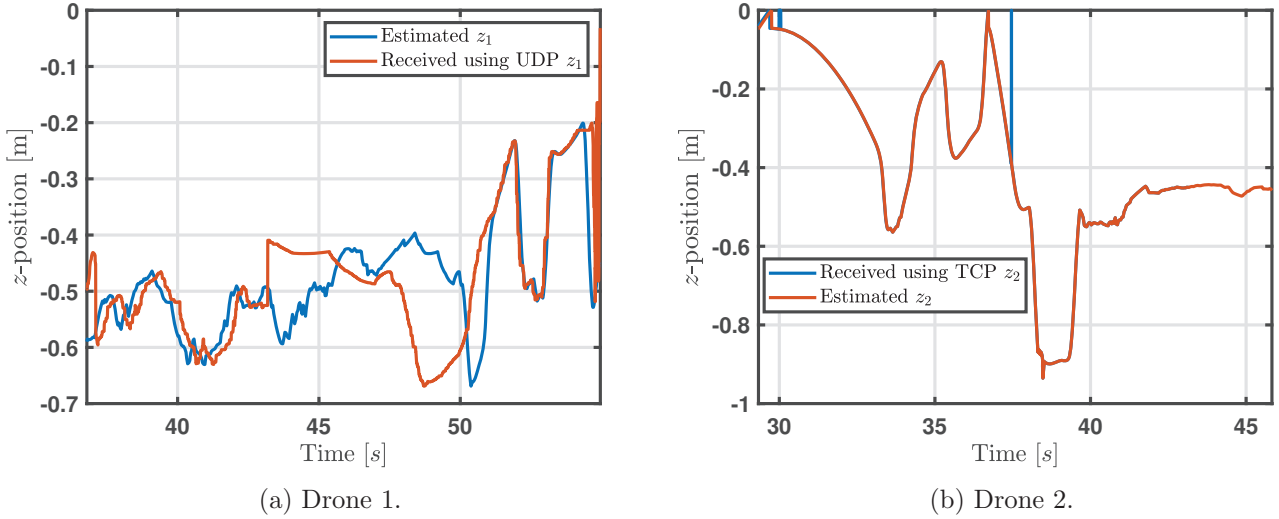


Figure 4.16: Communication test comparing UDP and TCP/IP communication protocols where the sent and received values are superimposed and for the UDP protocol the peaks at about $t = 52$ are used for superimposing.

$\min(d_{12}) = 0.275$ for, respectively, the simulated and experimental situation. Note that both these values of $\min(d_{12})$ are equal to $d_{12}(t_0)$ and the corresponding behavior is found in Figure 4.18a and 4.18b for, respectively, the simulated and experimental situation, and the experimental action sequence is found in Figure 4.19. Furthermore, it should be noted that an interesting difference in behavior is observed when the two drones are just initiated. Where the quadcopters immediately create more inter-agent distance in the simulated situation, the drones almost seem to move closer during the initial moments of the experiment. This difference can be accounted for by the fact that the communication channel is not yet stable at these initial moments, causing agent i to think that agent j is already at its reference position as it receives $p_{j,e} = v_{j,e} = 0$ over the communication channel. However, the observed behavior indicates the overall ability of the drones to avoid collisions with evasion maneuvers resulting from the collision avoidance strategy, even under challenging circumstances where the drones already are very close together, and while the connection is most unstable when just initiated. Note that the tracking behavior is not perfect, see Table 4.4, as the drones converge respectively to about $\rho_1(t_{\text{end}}) = [-1 \ 0.4 \ 1.5]^\top$ and $\rho_2(t_{\text{end}}) = [0.9 \ -0.4 \ 1.5]^\top$, however, the offset seems to be constant and in opposite direction for the drones, which is probably related to the ferociousness of the maneuver as mentioned before. Note also that the RMS values of the position estimates of drone 1, in all directions, is closer to simulations than that of drone 2. Although the observed difference between in position between drone 1 and 2 in experiments seems to be less than the estimated difference, as can be seen in Figure 4.19. Furthermore, as also mentioned in [26], the estimated state becomes less reliable when movement in the horizontal and vertical plane simultaneously is required, which also partly accounts for degradation of the performance. To eliminate this degradation, it would be desired to have $\rho_1(t_0) = [a \ b \ 1.5]^\top$, $\rho_2(t_0) = [c \ d \ 1.5]^\top$, with arbitrary constants $a, b, c, d \in \mathbb{R}$, and the respective reference positions in the horizontal plane containing a, b, c, d . This would also be favorable with respect to the stability of the connection that can be poor when just initiated, as mentioned before. Since the communication would in this case be well established after takeoff already, before the maneuvering in the horizontal plane will occur. However, as it is not possible to synchronize two drones' internal clocks, and thereby their reference signals, in the current setup, the mismatched $d_{12,r}$ results in asynchronous behavior and faulty $p_{i,e}$ and $v_{i,e}$ values being communicated, which eventually could lead to collisions.

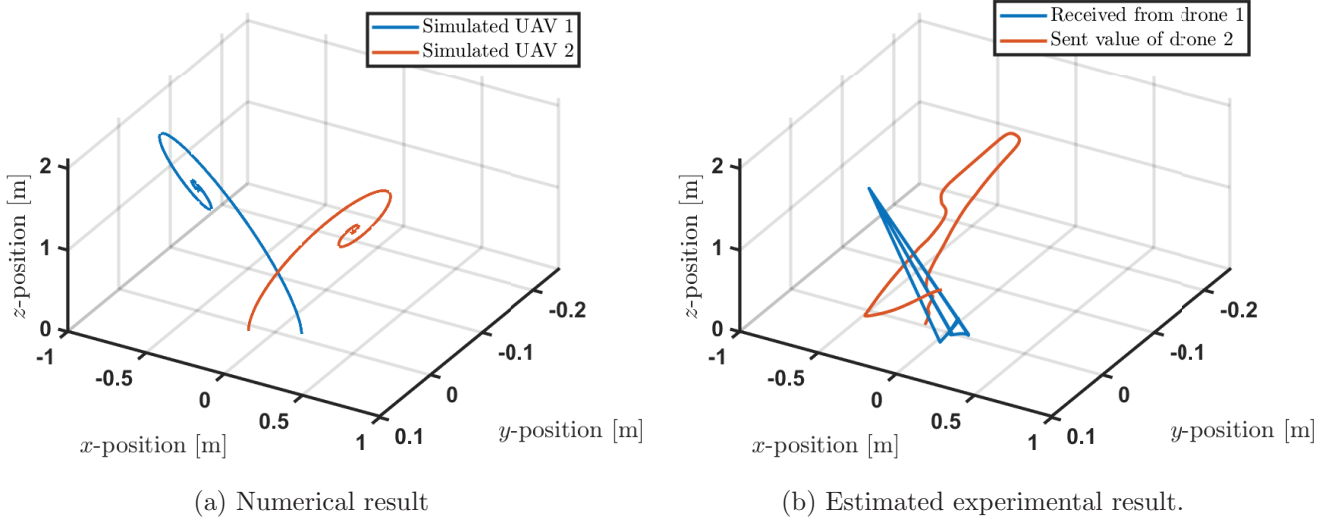


Figure 4.17: Test with position tracking active but collision avoidance inactive, i.e., $k_5 = 0$.

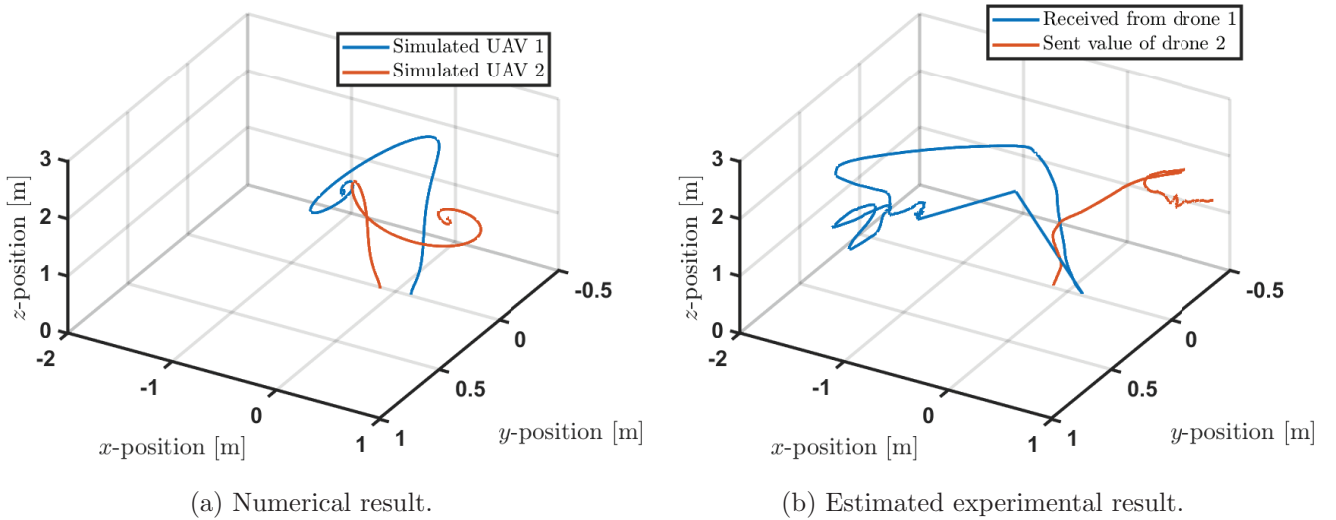


Figure 4.18: Test with position tracking active but collision avoidance inactive, i.e., $k_5 = 0.5$.

4.4 Concluding remarks

After introducing the experimental setup, a first step towards experimental validation is adjusting the available Simulink support package in such a way that the software supports multiple drones instead of a single one. Next, the considered system and the corresponding control inputs are converted to quaternions enabling computationally efficient experimental implementation. Thereafter, performance of a single drone is analyzed in both simulations and experiments, before introducing a communication channel in the experimental setup. Despite the general use of the UDP protocol in real-time applications, it is found that the TCP/IP communication protocol functions significantly better, both in terms of time delay and signal quality. Finally, a reduced time delay of only 200 milliseconds is effectuated, equal even to some of the slower ping signals from the host computer to the drone. Before finally implementing the designed controller in the experimental setup, the collision avoidance is successfully tested by introducing a virtual drone to be avoided. Although differences are found between simulation and experiments, experimental results seem to be in line with simulations. Finally, the designed controller is tested and it is

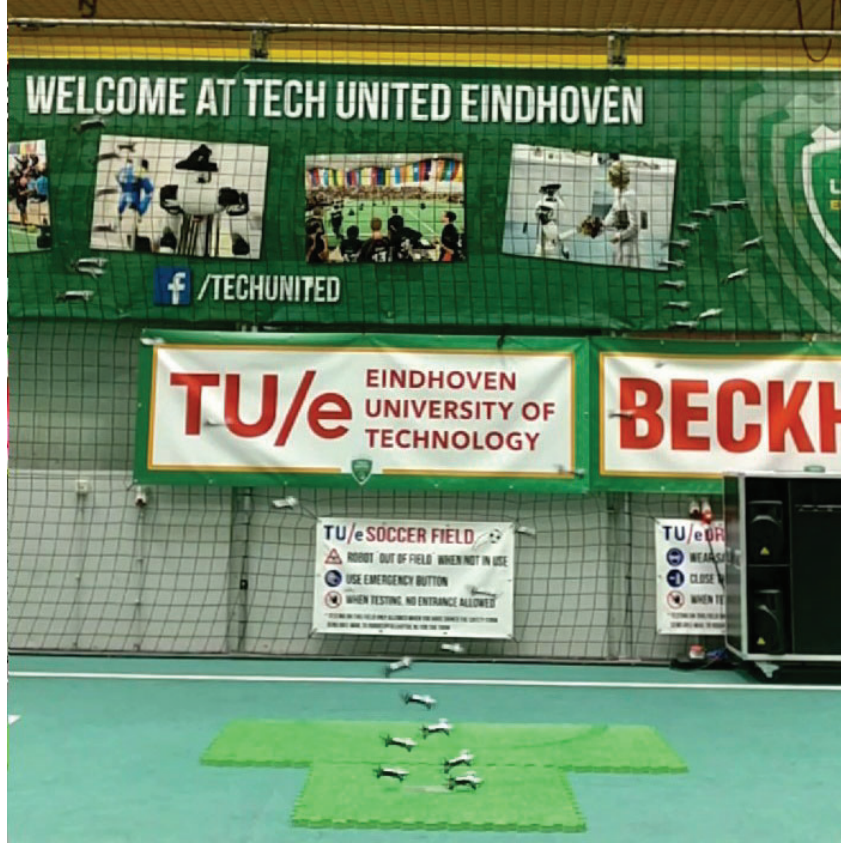


Figure 4.19: Action sequence of a collision avoidance experiment with two drones and $k_5 = 0.5$.

Table 4.4: RMS value of estimated or simulated $p_{i,e}$ in x, y, z -direction in a network of two drones with obstacle avoidance and position tracking.

	$p_{i,e,x}^{\text{RMS}}$	$p_{i,e,y}^{\text{RMS}}$	$p_{i,e,z}^{\text{RMS}}$	Δt
Final controller simulated $p_{1,e,k}$	0.6540	0.2413	0.8788	23.82
Final controller simulated $p_{2,e,k}$	0.5881	0.2170	0.7902	26.49
Final controller experiment $p_{1,e,k}$	1.7374	1.2310	0.9700	23.82
Final controller experiment $p_{2,e,k}$	0.9278	0.7301	0.8016	26.49

found that collisions are indeed avoided when the collision avoidance strategy is online, while collisions are not avoided in the same situation with the collision avoidance strategy offline. Even in challenging situations, like closely initialized agents, and under disturbances in the form of an unstable connection, the collision avoidance strategy shows to be capable of avoiding collisions. In the final experiments, external disturbances are accounted for as much as possible by turning off all air treatment systems and closing all doors of the drone test area. To even further decrease the time delay the network structure could be altered by making the drones able to connect with each-other directly instead of through the host computer, this could even enable omitting the host computer completely in the future.

Chapter 5

Conclusions and recommendations

As existing control strategies fail to prove the avoidance of collisions and mostly provide only an optimal strategy, this thesis aims to deliver a theoretical framework that can actually prove avoidance of collisions in a network. The main results from theory and validation are highlighted after which the report is concluded with encountered limitations, promises and future work.

5.1 Conclusions

This section first presents a reflection on the used theoretical methods to prove that no collisions occur in the system. Subsequently, the conclusions on the theoretical results obtained in the different considered systems are presented. And finally, the experimental setup and the obtained experimental and numerical results are contemplated and concluded upon.

Proof of collision avoidance

Initially, a kinematic model of point masses with time-varying reference signals is considered in 1D, which could be considered as an autonomously driving platoon on a single lane in which it is desired to implement collision avoidance. This situation provides useful information in the process of finding a control law that simultaneously achieves position tracking and collision avoidance in the network. The initial approach exploits the usage of a collision avoidance strategy based on an artificial potential field (APF) found in literature and proves to be successful in the considered system. The origin of a projection of the resulting closed-loop reference tracking dynamics is proven uniformly globally asymptotically stable (UGAS), while absence of collisions in the system is proven by showing instability of the collision point.

The initially used approach in a system of single integrators in 1D fails to conveniently scale to a network of double integrators. As the contemplated results regarding stability and collision avoidance stayed off, converse Lyapunov theory is used on the system to numerically determine a Lyapunov function. Examining the resulting numerical Lyapunov function sparked the idea to use a control Lyapunov function which tends to infinity when approaching the collision point. This approach constructs a Lyapunov function jointly with a control law to simultaneously prove stability of the reference tracking dynamics, and absence of collisions.

The resulting theory turned out to supply a convenient framework to prove stability in networks of cooperating single integrator systems, cooperating double integrator systems and even networks of cooperating quadcopters. In the approach to apply the developed theoretical framework, a step back is taken and a system of single integrators in 1D is considered again in order to compare with the previously obtained results. Where it should be noted that the considered reference signals are now restricted in such a way that only time-invariant closed-loop systems result. With this restriction taken into account, a Lyapunov function is constructed incorporating an APF, which induces the collision avoidance strategy in the jointly designed control law. With

this approach it has been shown that the equilibria of the resulting closed-loop system are locally exponentially stable (LES), and in a network of double integrators in arbitrary dimension it has been proven that both resulting equilibria are asymptotically stable. Moreover, it has been proven that no collisions occur in both considered systems.

As no saturation is present in the designed control law, one further assumption is made in order to have the resulting analysis feasible when considering a system of cooperating quadcopter UAVs in 3D. The total thrust magnitude control input has to be larger than zero, as a negative thrust cannot be achieved because of actuator limitations, and a total thrust magnitude equal to zero would result in an undefined desired thrust vector. Under the assumption that initial conditions are chosen relatively close to the reference trajectory, the total thrust magnitude is manually bounded, and the remainder of the analysis is deemed feasible. The designed control law proves, under the mentioned assumptions, the origin of a projection of the position tracking dynamics to be globally asymptotically stable (GAS) and locally exponentially stable (LES), the desired equilibrium point of the attitude tracking subsystem to be uniformly locally exponentially stable (ULES) and uniformly almost globally asymptotically stable (UaGAS), and proves the avoidance of collisions in the system. Finally, by using cascaded theory, the total cascaded system is proven UaGAS and ULES. Additionally, the results obtained in a network of two quadcopter UAVs is extended to a network of an arbitrary number of UAVs and the origin of the resulting system is again proven UaGAS and ULES.

Validation of collision avoidance strategy

The designed control law implementing a collision avoidance strategy is validated using both a simulation model and an experimental setup. Before the experimental setup could be used, the provided Simulink support package is adjusted so that it supports multiple drones. To this end, the complete support package is analyzed and adjusted such that it now supports two drones. If desired, the support package can be extended fairly easily by following the steps attached in Appendix C. With the improved setup prepared for implementation, the control law is expressed using quaternions to represent rotations for computational efficiency.

To prevent unnecessary damage to the experimental setup, a simulation study is used to indicate the behavior to expect. To further decrease the chances of damaging the experimental setup, the reference tracking and collision avoidance capabilities of a single drone are tested before flying two quadcopters simultaneously. Reference tracking turned out to be along the lines of simulations, except for the drift in y -direction which is partly explained by the strong gusts of wind present at the drone test area as a result of the air treatment system being operated at full power. A subsequent experiment introduced obstacle avoidance with a virtual drone and showed that introducing a collision avoidance strategy successfully avoids collisions. The experimental results of the same situation even outperformed the simulation results as the takeoff behavior in experiments is observed to somewhat differ from the takeoff behavior in simulations.

As the performance of a single drone is deemed favorable, both in reference tracking and collision avoidance capabilities, a communication channel is constructed to enable implementation of the designed controller in a system of two quadcopters. Surprisingly, the TCP/IP communication protocol outperformed the UDP communication protocol in both communication speed and data quality, and it is decided to construct the communication channel using the TCP/IP communication protocol. The initial experienced time delay over the communication channel, which could take as long as two full seconds, is reduced to only a tenth of that. The residual time delay over the communication channel of about 200 milliseconds is deemed sufficient as it even approaches the time delay corresponding to a ping signal from the host computer to the drone. The instability of the connection when the communication is just initiated is the main remaining inconvenience, but this problem is overcome for now by repeatedly executing experiments as the instability varies with every experiment.

Finally, the designed controller is successfully implemented in the full experimental setup.

Challenging initial conditions are selected and it is shown that a collision is indeed avoided with active collision avoidance strategy, while the collision is not avoided when the strategy is inactive. The occurrence of a collision when no collision avoidance strategy is present, is especially well illustrated in simulations. From simulations it is observed that the drones' center of masses would pass each-other with a minimum distance of about 1.5 centimeters, clearly resulting in a collision when implemented in the experimental setup. The performance of the collision avoidance strategy is best illustrated by the achieved minimal inter-agent distances, and as the minimal inter-agent distances never drop below the initial inter-agent distance when collision avoidance is active, it is concluded that the initial inter-agent distance is indeed challenging. Overall it can be concluded that the designed control strategy, including collision avoidance, performs quite well. Even though assumptions are made with respect to saturation, it is shown that the designed controller satisfies hopes and expectations in both a simulated environment, and in an experimental setup. Successful implementation in the experimental setup also indicates robustness of the designed control law as the nonlinear control law requires precise state estimates, particularly for the attitude tracking controller and the collision avoidance part.

5.2 Recommendations

Although the main objective of the research is generally achieved, improvements can still be made to both theory and numerical or experimental implementation. Regarding theory, a main improvement would be to incorporate saturation in the designed control law. Without saturation of the control law, it cannot be guaranteed that total thrust magnitude, desired thrust vector, and desired attitude are well defined without introducing assumptions on initial conditions and reference trajectories. When considering only constant reference trajectories, a guarantee that the control law is well defined can be given up to a certain extend. However, considering only constant reference trajectories is rather restrictive and it would be desirable to extend the presented proofs to systems that allow for time-varying reference trajectories. After all, most applications presented in the introduction utilize time varying trajectories. Also, the analysis presented in this research considers a network of only two quadcopters and an extension of the analysis to allow expanding the network to make the number of drones in the network i arbitrary large is desirable. A final improvement regarding the performed theoretical analysis, would be to incorporate social distancing and give the agents some personal space to account for dimensions of the drone, as the presented theory only proves that the centers of mass of two quadcopters will never coincide. Although the APF incorporated in the designed control law is repelling whenever the two drones are closer together than their reference relative distance, no drones exist with the dimensions of a point mass, and thus collisions can still occur in practice.

Although the designed control law with collision avoidance proves to be robust, as implementation in experiments is quite successful, it is always desirable to have more accurate tracking and behavior. Therefore, future research could focus on improving the internal state estimator even further. As the aim is autonomous flight, this research has chosen to only make use of this internal state estimator and not use an external localization technique. This choice prevents additional communication delays with an external localization system, but comes at the cost of lower quality state estimates.

Lastly, improvements to the experimental setup can be made. The air treatment system was only turned off during final experiments, as it turned out to be rather difficult to have the air treatment turned off. A major shortcoming of the current setup is that it is not possible to initiate two drones simultaneously. Although placing state estimator and communication blocks inside Enabled Subsystems enables simultaneous takeoff, time dependent reference trajectories will be asynchronous as it is not yet achieved to synchronize internal clocks. This could be overcome by communicating also reference trajectory information but this would come at the cost of communication bandwidth and would also be subject to time delays.

Appendix A

Local stability analysis of equilibrium of 1D kinematic model

Consider the closed-loop reference tracking system of two single integrators in 1D

$$\dot{\tilde{x}}_1 = -k_1 \tilde{x}_1 + k_3 \left(\frac{1}{d_{12}} - \frac{1}{d_{12,r}} \right) \left(\frac{1}{d_{12}^2} \right), \quad (\text{A.1a})$$

$$\dot{\tilde{x}}_2 = -k_2 \tilde{x}_2 - k_3 \left(\frac{1}{d_{12}} - \frac{1}{d_{12,r}} \right) \left(\frac{1}{d_{12}^2} \right), \quad (\text{A.1b})$$

where \tilde{x}_i represents the position error, $d_{12} = \tilde{x}_1 - \tilde{x}_2 + d_{12,r}$ the inter-agent distance, $d_{12,r}$ the referenced inter-agent distance, and with control parameters $k_1, k_2, k_3 > 0$, of which the Jacobian is computed to be

$$J(\tilde{x}_1, \tilde{x}_2) = \begin{bmatrix} -k_1 + B(\tilde{x}_1, \tilde{x}_2) & -B(\tilde{x}_1, \tilde{x}_2) \\ -B(\tilde{x}_1, \tilde{x}_2) & -k_2 + B(\tilde{x}_1, \tilde{x}_2) \end{bmatrix}, \quad (\text{A.2})$$

with

$$B(\tilde{x}_1, \tilde{x}_2) = k_3 \frac{2(\tilde{x}_1 - \tilde{x}_2) - d_{12,r}}{(\tilde{x}_1 - \tilde{x}_2 + d_{12,r})^4 d_{12,r}}. \quad (\text{A.3})$$

Evaluating J on the equilibria

$$\tilde{x}_1 = \left(\sqrt[3]{\frac{-k_3}{k_1 d_{12,r}} \left(1 + \frac{k_1}{k_2} \right) - d_{12,r}} \right) \left(1 + \frac{k_1}{k_2} \right)^{-1}, \quad (\text{A.4a})$$

$$\tilde{x}_2 = -\frac{k_1}{k_2} \left(\sqrt[3]{\frac{-k_3}{k_1 d_{12,r}} \left(1 + \frac{k_1}{k_2} \right) - d_{12,r}} \right) \left(1 + \frac{k_1}{k_2} \right)^{-1}, \quad (\text{A.4b})$$

gives

$$B(\tilde{x}_1, \tilde{x}_2) = \frac{2 \sqrt[3]{\frac{-k_3}{k_1 d_{12,r}} \left(1 + \frac{k_1}{k_2} \right) - 3d_{12,r}}}{\left(\sqrt[3]{\frac{-k_3}{k_1 d_{12,r}} \left(1 + \frac{k_1}{k_2} \right)} \right)^4 d_{12,r}}, \quad (\text{A.5})$$

with which the eigenvalues of the corresponding $J(\tilde{x}_1, \tilde{x}_2)$ are computed as

$$\lambda_{J(\tilde{x}_1, \tilde{x}_2)} = \frac{-(c_3 + c_4 + c_5 + c_6 + c_7 + c_8 + c_9 \pm \sqrt{c_2})}{c_1}, \quad (\text{A.6})$$

with the constants $c_1, c_2, c_3, c_4, c_5, c_6, c_7, c_8, c_9$ given according to

$$c_1 = 2(k_1 + k_2)^{\frac{7}{3}} k_3^{\frac{1}{3}} \sqrt{d_{12,r}}, \quad (\text{A.7a})$$

$$\begin{aligned} c_2 = & k_1^4 k_3^{\frac{2}{3}} (k_1 + k_2)^{\frac{8}{3}} d_{12,r} + 72 k_1^{\frac{11}{3}} k_2^{\frac{11}{3}} d_{12,r}^{\frac{11}{3}} + 36 k_1^{\frac{14}{3}} k_2^{\frac{8}{3}} d_{12,r}^{\frac{11}{3}} \dots \\ & + 36 k_1^{\frac{8}{3}} k_2^{\frac{14}{3}} d_{12,r}^{\frac{11}{3}} + k_2^4 k_3^{\frac{2}{3}} (k_1 + k_2)^{\frac{8}{3}} d_{12,r} + 14 k_1^2 k_2^2 k_3^{\frac{2}{3}} (k_1 + k_2)^{\frac{8}{3}} d_{12,r} \dots \\ & + 48 k_1^{\frac{7}{3}} k_2^{\frac{13}{3}} k_3^{\frac{1}{3}} (k_1 + k_2)^{\frac{1}{3}} d_{12,r}^{\frac{7}{3}} + 96 k_1^{\frac{10}{3}} k_2^{\frac{10}{3}} k_3^{\frac{1}{3}} (k_1 + k_2)^{\frac{1}{3}} d_{12,r}^{\frac{7}{3}} \dots \\ & + 48 k_1^{\frac{13}{3}} k_2^{\frac{7}{3}} k_3^{\frac{1}{3}} (k_1 + k_2)^{\frac{1}{3}} d_{12,r}^{\frac{7}{3}}, \end{aligned} \quad (\text{A.7b})$$

$$c_3 = 6 k_1^{\frac{7}{3}} k_2^{\frac{4}{3}} d_{12,r}^{\frac{11}{6}}, \quad (\text{A.7c})$$

$$c_4 = 6 k_1^{\frac{4}{3}} k_2^{\frac{7}{3}} d_{12,r}^{\frac{11}{6}}, \quad (\text{A.7d})$$

$$c_5 = 4(k_1 + k_2)^{\frac{1}{3}} k_1^2 k_2 k_3^{\frac{1}{3}} \sqrt{d_{12,r}}, \quad (\text{A.7e})$$

$$c_6 = 4(k_1 + k_2)^{\frac{1}{3}} k_1 k_2^2 k_3^{\frac{1}{3}} \sqrt{d_{12,r}}, \quad (\text{A.7f})$$

$$c_7 = 2(k_1 + k_2)^{\frac{4}{3}} k_1 k_2 k_3^{\frac{1}{3}} \sqrt{d_{12,r}}, \quad (\text{A.7g})$$

$$c_8 = (k_1 + k_2)^{\frac{4}{3}} k_2^2 k_3^{\frac{1}{3}} \sqrt{d_{12,r}}, \quad (\text{A.7h})$$

$$c_9 = (k_1 + k_2)^{\frac{4}{3}} k_1^2 k_3^{\frac{1}{3}} \sqrt{d_{12,r}}, \quad (\text{A.7i})$$

where it is noted that $c_1, c_2, c_3, c_4, c_5, c_6, c_7, c_8, c_9 > 0$. Now, after some elaborate computations and simplifications, it is found that the inequality

$$c_3 + c_4 + c_5 + c_6 + c_7 + c_8 + c_9 > \sqrt{c_2} \quad (\text{A.8})$$

holds for $k_1, k_2, k_3, d_{12,r} > 0$, and thus, both eigenvalues given in (A.6) are strictly negative.

Appendix B

Local stability analysis in projected position tracking dynamics in 3D

Consider the closed-loop (z_1, z_2) dynamics in 3D

$$\dot{z}_1 = -S(\omega_f)z_1 + z_2, \quad (\text{B.1a})$$

$$\dot{z}_2 = -S(\omega_f)z_2 - k_1z_1 - k_2z_2, \quad (\text{B.1b})$$

with $k_1, k_2 > 0$ and time-independent $\omega_f \in \mathbb{R}^3$, of which the Jacobian is computed to be

$$J = \begin{bmatrix} -S(\omega_f) & I_3 \\ -k_1I_3 & -S(\omega_f) - k_2I_3 \end{bmatrix} \quad (\text{B.2})$$

with eigenvalues

$$\lambda_{1,2} = \frac{-k_2 \pm \sqrt{k_2^2 - 4k_1}}{2}, \quad (\text{B.3a})$$

$$\lambda_{3,4} = \frac{-k_2}{2} \pm \frac{1}{2} \sqrt{k_2^2 - 4 \left(\omega_f^\top \omega_f + \sqrt{(4k_1 - k_2^2) \omega_f^\top \omega_f + k_1} \right)}, \quad (\text{B.3b})$$

$$\lambda_{5,6} = \frac{-k_2}{2} \pm \frac{1}{2} \sqrt{k_2^2 - 4 \left(\omega_f^\top \omega_f - \sqrt{(4k_1 - k_2^2) \omega_f^\top \omega_f + k_1} \right)}. \quad (\text{B.3c})$$

First we set $k_2^2 - 4k_1 \leq 0$ and evaluate the real part of the eigenvalues of (B.3). For $\lambda_{1,2}$ this gives

$$\lambda_{1,2} = \frac{-k_2 \pm \sqrt{4k_1 - k_2^2}i}{2}, \quad (\text{B.4})$$

where i is the imaginary number satisfying $i^2 = -1$, with which it becomes obvious that $\text{Re}(\lambda_{1,2}) > 0$ for $k_2^2 - 4k_1 \leq 0$. Next, for $k_2^2 - 4k_1 < 0$ we can have

$$k_2^2 - 4 \left(\omega_f^\top \omega_f + \sqrt{(4k_1 - k_2^2) \omega_f^\top \omega_f + k_1} \right) \leq 0, \quad (\text{B.5a})$$

$$k_2^2 - 4 \left(\omega_f^\top \omega_f - \sqrt{(4k_1 - k_2^2) \omega_f^\top \omega_f + k_1} \right) \leq 0, \quad (\text{B.5b})$$

resulting in $\text{Re}(\lambda_{3,4}) = \text{Re}(\lambda_{5,6}) = -\frac{1}{2}k_2 < 0$, or

$$k_2^2 - 4 \left(\omega_f^\top \omega_f + \sqrt{(4k_1 - k_2^2) \omega_f^\top \omega_f + k_1} \right) > 0, \quad (\text{B.6a})$$

$$k_2^2 - 4 \left(\omega_f^\top \omega_f - \sqrt{(4k_1 - k_2^2) \omega_f^\top \omega_f + k_1} \right) > 0, \quad (\text{B.6b})$$

in which case we obtain

$$\lambda_3 = \frac{-k_2}{2} - \frac{1}{2} \sqrt{k_2^2 - 4 \left(\omega_f^\top \omega_f + \sqrt{(4k_1 - k_2^2) \omega_f^\top \omega_f + k_1} \right)} < 0, \quad (\text{B.7a})$$

$$\lambda_5 = \frac{-k_2}{2} - \frac{1}{2} \sqrt{k_2^2 - 4 \left(\omega_f^\top \omega_f - \sqrt{(4k_1 - k_2^2) \omega_f^\top \omega_f + k_1} \right)} < 0. \quad (\text{B.7b})$$

Which leaves us to prove

$$\lambda_4 = \frac{-k_2}{2} + \frac{1}{2} \sqrt{k_2^2 - 4 \left(\omega_f^\top \omega_f + \sqrt{(4k_1 - k_2^2) \omega_f^\top \omega_f + k_1} \right)} < 0, \quad (\text{B.8a})$$

$$\lambda_6 = \frac{-k_2}{2} + \frac{1}{2} \sqrt{k_2^2 - 4 \left(\omega_f^\top \omega_f - \sqrt{(4k_1 - k_2^2) \omega_f^\top \omega_f + k_1} \right)} < 0. \quad (\text{B.8b})$$

To show that (B.8a) holds we can write

$$k_2^2 - 4 \left(\omega_f^\top \omega_f + \sqrt{(4k_1 - k_2^2) \omega_f^\top \omega_f + k_1} \right) < k_2^2, \quad (\text{B.9a})$$

$$- \left(\omega_f^\top \omega_f + \sqrt{(4k_1 - k_2^2) \omega_f^\top \omega_f + k_1} \right) < 0, \quad (\text{B.9b})$$

and by combining $k_1, k_2 > 0$ and $\omega_f \in \mathbb{R}^3$ with the fact it is assumed that $4k_1 - k_2^2 \geq 0$, $\lambda_4 < 0$ is obtained in the considered case. To finally prove that (B.8b) holds, we write

$$k_2^2 - 4 \left(\omega_f^\top \omega_f - \sqrt{(4k_1 - k_2^2) \omega_f^\top \omega_f + k_1} \right) < k_2^2, \quad (\text{B.10a})$$

$$- \left(\omega_f^\top \omega_f - \sqrt{(4k_1 - k_2^2) \omega_f^\top \omega_f + k_1} \right) < 0, \quad (\text{B.10b})$$

$$- \omega_f^\top \omega_f + \sqrt{(4k_1 - k_2^2) \omega_f^\top \omega_f + k_1} < 0, \quad (\text{B.10c})$$

where a quadratic function in $\sqrt{\omega_f^\top \omega_f}$ is recognized in (B.10c). Note that the vertex of a quadratic function in x as $ax^2 + bx + c$ is given according

$$\frac{-(b^2 - 4ac)}{4a}, \quad (\text{B.11})$$

and by noting that the parabola of (B.10c) is opening to the bottom, and substituting $a = -1$, $b = \sqrt{4k_1 - k_2^2}$ and $c = -k_1$, we obtain

$$\max(-\omega_f^\top \omega_f + \sqrt{(4k_1 - k_2^2) \omega_f^\top \omega_f + k_1}) = -\frac{1}{4} k_2^2, \quad (\text{B.12})$$

and using again $k_1, k_2 > 0$ and $\omega_f \in \mathbb{R}^3$, $\lambda_6 < 0$ is obtained.

As it has been shown that the real part of all eigenvalues is strictly negative for all time-independent $\omega_f \in \mathbb{R}^3$, and k_1, k_2 satisfying $k_2^2 - 4k_1 \leq 0$, the sign of the real part of the eigenvalues when $k_2^2 - 4k_1 > 0$ is now investigated. Now, in the case that $k_2^2 - 4k_1 > 0$, $\lambda_1 = -\frac{1}{2}(k_2 + \sqrt{k_2^2 - 4k_1}) < 0$ is obtained from (B.3a), and by stating $\lambda_2 = -\frac{1}{2}(k_2 - \sqrt{k_2^2 - 4k_1}) < 0$ we can write

$$\sqrt{k_2^2 - 4k_1} < k_2, \quad (\text{B.13a})$$

$$k_2^2 - 4k_1 < k_2^2, \quad (\text{B.13b})$$

$$-4k_1 < 0, \quad (\text{B.13c})$$

now noting $k_1, k_2 > 0$, we can conclude that indeed $\lambda_2 < 0$ for $k_2^2 > 4k_1$. Next, using $k_2^2 - 4k_1 > 0$ in (B.3b) and (B.3c), we can write

$$\lambda_{3,4} = \frac{-k_2}{2} \pm \frac{1}{2} \sqrt{(k_2^2 - 4k_1) - 4\omega_f^\top \omega_f - 4i \sqrt{(k_2^2 - 4k_1)\omega_f^\top \omega_f}}, \quad (\text{B.14a})$$

$$\lambda_{5,6} = \frac{-k_2}{2} \pm \frac{1}{2} \sqrt{(k_2^2 - 4k_1) - 4\omega_f^\top \omega_f + 4i \sqrt{(k_2^2 - 4k_1)\omega_f^\top \omega_f}}, \quad (\text{B.14b})$$

where i is again the imaginary number satisfying $i^2 = -1$. Note that a square root of a complex number can be written as

$$\sqrt{a + bi} = x + yi, \quad (\text{B.15})$$

with $a, b, x, y \in \mathbb{R}$, where the real part x and the imaginary part y are computed according to

$$x = \pm \sqrt{\frac{a + \sqrt{a^2 + b^2}}{2}}, \quad y = \pm \sqrt{\frac{-a + \sqrt{a^2 + b^2}}{2}}, \quad (\text{B.16})$$

with the signs of x and y determined according

$$\text{sign}(x) = \text{sign}(y), \quad \text{for } b < 0, \quad (\text{B.17a})$$

$$\text{sign}(x) = -\text{sign}(y), \quad \text{for } b > 0, \quad (\text{B.17b})$$

$$\text{sign}(x) = 0 \vee \text{sign}(y) = 0, \quad \text{for } b = 0. \quad (\text{B.17c})$$

When we now set $a = (k_2^2 - 4k_1) - 4\omega_f^\top \omega_f$ and $b = \pm 4\sqrt{(k_2^2 - 4k_1)\omega_f^\top \omega_f}$, we can compute the real part x , of the complex square roots as in (B.14) as

$$x = \pm \sqrt{\frac{a + \sqrt{a^2 + b^2}}{2}} = \pm \sqrt{k_2^2 - 4k_1}, \quad (\text{B.18})$$

indicating that $\text{Re}(\lambda_{3,5}) = -\frac{1}{2}(\sqrt{k_2^2 - 4k_1} + k_2) < 0$ and using the result of (B.13) we can conclude that $\text{Re}(\lambda_{4,6}) = \frac{1}{2}(\sqrt{k_2^2 - 4k_1} - k_2) < 0$. And thus, all eigenvalues of (B.3) of the Jacobian (B.2) are proven strictly negative for all $k_1, k_2 > 0$ and time-independent $\omega_f \in \mathbb{R}^3$, and thus the origin of (B.1) is locally exponentially stable (LES).

Appendix C

Modification of Simulink Support Package for Parrot Minidrones

Before implementing the control law designed in Section 3.4 in the experimental setup as described in Section 4.1, the Simulink Support Package for Parrot Minidrones needs some adjustments, as it is not suitable to communicate with two drones simultaneously in the form in which it is provided by Parrot. The used software version of the Simulink Support Package for Parrot Minidrones is 19.2.0, which is run on an Ubuntu 18.04.3 LTS operated PC with MATLAB 9.7 (released under the name R2019b) installed. The files of this support package version that need adjustment are stated below and are located in the folder `/root/Documents/MATLAB/SupportPackages/R2019b/toolbox/target/supportpackages/parrot`. For most `.m` files, there exists a `.p` file with the same name which should be deleted.

`/parrot`

- `/+codertarget/+parrot/+internal`
 - `/@parrotio/parrotio.m`
 - `loadAndRun.m`
 - `onAfterCodeGenHook.m`
 - `ParrotConstants.m`
 - `PostFlightAnalysis.m`
 - `Utility.m`
- `/+parrot/+util`
 - `ConnectDroneToBlueTooth.m`
- `/registry`
 - `/attributes/parrotMambo2_AttributeInfo.xml`
 - `/parameters/parrotMambo2_ParameterInfo.xml`
 - `/targethardware/parrotMambo2_TargetHardwareInfo.xml`

Then, in the file `/usr/local/MATLAB/R2019b/rtw/c/ert/ert.tlc`, the last three lines should be commented out. And in order to regenerate or recompile certain parts of the code, the target hardware selected in the Simulink project should be changed once before selecting the desired target hardware. This is in order to reload the file `ert.tlc`.

When all adjustments are made, the following approach should be taken in order to successfully communicate with multiple drones simultaneously.

Connect the first drone and set up a telnet connection with it using the terminal command `telnet 192.168.2.1` when the drone is connected using USB, or `telnet 192.168.3.1` when the drone is only connected over Bluetooth (in the last case the telnet connection will be lost since the IP address is changed). When a telnet connection with the drone is established and access to the drone is acquired, the command `ifconfig bnep 192.168.3.X up` is executed to change the Bluetooth IP address of the drone to the desired value `X`. The whole process can now be repeated for every additional drone, attention is required to ensure that every drone has its own IP address assigned to it correctly. Note that the adjustments made to the support package for the experiments executed for this report use the IP addresses `192.168.3.91` and `192.168.3.91` for the 'Mambo' and 'Mambo 2' target hardware board.

Next, the Bluetooth interfaces of the Ground Station (GS) which are connected to the drones need to be bridged. Make sure that both drones are connected using the same Bluetooth adapter, a choice should be made between an external Bluetooth dongle or the built-in Bluetooth adapter. A bridge `br0` is then created by using the command `sudo brctl addbr br0` and the adapters can be added to it using the command `sudo brctl addif br0 bnepX`, where `X` represents the respective adapter numbers starting at zero. When all adapters are added to the the bridge, it can be initiated by using the command `sudo ifconfig br0 192.168.3.2 up`. Now all connected drones can be pinged and when a telnet connection with a drone is established it can also ping the other drones. Note that pinging the drones is a good measure to check whether the bridging of the two adapters is executed correctly.

Now, a Matlab client should be opened from its own terminal for every drone. In the file `Utility.m` lines 31 and 33 need to be adjusted with the desired IP address (as '`192.168.3.X`') and name (as '`Mambo`' or '`Mambo X`'), respectively, every time a drone is going to be used to build and deploy a model on. When the Flight Interface appears, the next model can be built and deployed on the subsequent drone. When all models are built and deployed, the models can be initiated by pressing the start button in the flight control interface. Make sure that whenever a communication with the drone is required, e.g. to build and deploy a model, to download the MAT-file or to start a built model on the drone, the `Utility.m` file should be adjusted to communicate with the corresponding drone. Note that the package is now able to support a maximum of two drones, if this number is to be increased, all files stated above should be adjusted accordingly.

Bibliography

- [1] Wing Medium. Wing delivers library books to students in Virginia. <https://medium.com/wing-aviation/wing-delivers-library-books-to-students-in-virginia-b2cd0ad86551>, 2020.
- [2] K. van Eijk, Haarlems Dagblad. Primeur in Nederland: Politie gaat met drone strandgangers waarschuwen. https://www.haarlemsdagblad.nl/cnt/dmf20200327_85340545/primeur-in-nederland-politie-gaat-met-drone-strandgangers-waarschuwen-video?utm_source=google&utm_medium=organic, 2020.
- [3] M. Hochstenbach, C. Notteboom, B. Theys, and J. De Schutter. Design and control of an unmanned aerial vehicle for autonomous parcel delivery with transition from vertical take-off to forward flight - VertiKUL, a quadcopter tailsitter. *International Journal of Micro Air Vehicles*, 7(4):395–405, 2015.
- [4] G. Cai, J. Dias, and L. Seneviratne. A Survey of Small-Scale Unmanned Aerial Vehicles: Recent Advances and Future Development Trends. *Unmanned Systems*, 2(2):175–199, 2014.
- [5] F. G. Costa, J. Ueyama, T. Braun, G. Pessin, F. S. Osorio, and P. A. Vargas. The use of unmanned aerial vehicles and wireless sensor network in agricultural applications. In *International Geoscience and Remote Sensing Symposium (IGARSS)*, pages 5045–5048, 2012.
- [6] B. R. Sharma, K. S. V. Narasimha, S. Ramakrishnan, and M. Kumar. Distributed cyclic motion control of multiple UAVs for wildfire monitoring. In *ASME 2010 Dynamic Systems and Control Conference, DSCC2010*, volume 2, pages 401–407, 2010.
- [7] K. N. McGuire, C. de Wagter, K. Tuyls, H. J. Kappen, and G. C. H. E. de Croon. Minimal navigation solution for a swarm of tiny flying robots to explore an unknown environment. *Science Robotics*, 9710, 2019.
- [8] Blue Jay Eindhoven. Blue Jay drone lends a helping hand during fire. <https://www.bluejayeindhoven.nl/category/blog/>, 2020.
- [9] DARPA. Teams test swarm autonomy in second major offset field experiment. <https://www.darpa.mil/news-events/2019-08-07>, 2019.
- [10] I. H. B. Pizetta, A. S. Brandao, and M. Sarcinelli-Filho. Cooperative quadrotors carrying a suspended load. *2016 International Conference on Unmanned Aircraft Systems, ICUAS 2016*, pages 1049–1055, 2016.
- [11] Amazon. Amazon prime air. <https://www.amazon.com/Amazon-Prime-Air/b?ie=UTF8&node=8037720011>, 2016.
- [12] Intel. Intel drone light show breaks guinness world records title at olympic winter games pyeongchang 2018. <https://newsroom.intel.com/news-releases/>

- intel-drone-light-show-breaks-guinness-world-records-title-olympic-winter-games-pyeong
#gs.fxp3d, 2018.
- [13] E. Lefeber, S. J. A. M. van den Eijnden, and H. Nijmeijer. Almost global tracking control of a quadrotor UAV on $SE(3)$. *2017 IEEE 56th Annual Conference on Decision and Control, CDC 2017*, 56:1175–1180, 2018.
- [14] E. Lefeber, M. F. A. Van De Westerlo, and H. Nijmeijer. Almost global decentralised formation tracking for multiple distinct UAVs. *Joint 8th IFAC Symposium on Mechatronic Systems and 11th IFAC Symposium on Nonlinear Control Systems*, 52(16):186–191, 2019.
- [15] P. Stone and M. Veloso. Multiagent systems: a survey from a machine learning perspective. *Autonomous Robots*, 8(3):345–383, 2000.
- [16] H. Gutiérrez, A. Morales, and H. Nijmeijer. Synchronization Control for a Swarm of Unicycle Robots: Analysis of Different Controller Topologies. *Asian Journal of Control*, 19(5):1822–1833, 2017.
- [17] T. Balch and R. C. Arkin. Behavior-based formation control for multirobot teams. *IEEE Transactions on Robotics and Automation*, 14(6):926–939, 1998.
- [18] C. Jewison, R. S. Erwin, and A. Saenz-Otero. Model Predictive Control with ellipsoid obstacle constraints for spacecraft rendezvous. *IFAC-PapersOnLine*, 28(9):257–262, 2015.
- [19] A. Eskandarpour and V. J. Majd. Cooperative formation control of quadrotors with obstacle avoidance and self collisions based on a hierarchical MPC approach. *2014 2nd RSI/ISM International Conference on Robotics and Mechatronics, ICRoM 2014*, pages 351–356, 2014.
- [20] J. Jin and N. Gans. Collision-free formation and heading consensus of nonholonomic robots as a pose regulation problem. *Robotics and Autonomous Systems*, 95:25–36, 2017.
- [21] D. Zhou and M. Schwager. Virtual Rigid Bodies for coordinated agile maneuvering of teams of micro aerial vehicles. *Proceedings - IEEE International Conference on Robotics and Automation*, 2015-June(June):1737–1742, 2015.
- [22] J. Gonzalez-Sierra, J. Santiaguillo-Salinas, and E. Aranda-Bricaire. Reciprocal collision avoidance for a group of second order agents. In *18th Congreso Mexicano de Robotica, COMRob 2016*, 2017.
- [23] H. Su, X. Wang, and Z. Lin. Synchronization of coupled harmonic oscillators in a dynamic proximity network. *Proceedings of the IEEE Conference on Decision and Control*, 45(10):4985–4990, 2009.
- [24] S. J. A. M. van den Eijnden. Cascade Based Tracking Control of Quadrotors. Technical report, MSc Thesis, Eindhoven University of Technology, Department of Mechanical Engineering, Dynamics and Control Group, 2017.
- [25] M. F. A. Westerlo. Formation tracking with multiple mutually coupled quadrotor UAVs on $SE(3)$. Technical report, MSc Thesis, Eindhoven University of Technology, Department of Mechanical Engineering, Dynamics and Control Group, Eindhoven, 2019.
- [26] G. H. Brekelmans. Extended quadrotor dynamics: from simulations to experiments. Technical report, MSc Thesis, Eindhoven University of Technology, Department of Mechanical Engineering, Dynamics and Control Group, Eindhoven, 2019.
- [27] OptiTrack. Motion capture system. <https://optitrack.com/>.

- [28] W. Ren. On consensus algorithms for double-integrator dynamics. *IEEE Transactions on Automatic Control*, 53(6):1503–1509, 2008.
- [29] D. Eberly. Rotation representations and performance issues. *Geometric Tools. Inc*, pages 1–13, 2002.
- [30] M.W. Spong, S. Hutchinson, and M. Vidyasagar. *Robot Modeling and Control*. Wiley, 2005.
- [31] B. Siciliano, L. Sciavicco, L. Villani, and G. Oriolo. *Robotics: Modelling, Planning and Control*. Advanced Textbooks in Control and Signal Processing. Springer London, 2010.
- [32] N. van de Wouw. Multibody and nonlinear dynamics: Multibody dynamics. *Eindhoven University of Technology*, 2016. Lecture notes, Course ID: 4DM10.
- [33] G. Cai, B. M. Chen, and T. H. Lee. *Unmanned Rotorcraft Systems*. Advances in Industrial Control. Springer London, 2011.
- [34] E. Eade. Lie Groups for 2D and 3D Transformations. <http://ethaneade.com/lie.pdf>, 2017.
- [35] J. Diebel. Representing Attitude: Euler Angles, Unit Quaternions, and Rotation Vectors. Technical report, Stanford University, 2006.
- [36] W. R. Hamilton. On the quaternions; or on a new system of imaginaries in algebra. *The London, Edinburgh, and Dublin Philosophical Magazine and Journal of Science*, 36(243):305–306, 1850.
- [37] J. Cariño, H. Abaunza, and P. Castillo. Quadrotor quaternion control. *2015 International Conference on Unmanned Aircraft Systems, ICUAS 2015*, 06 2015(1):825–831, 2015.
- [38] D. M. Henderson. Euler Angles, Quaternions and Transformation Matrices. Technical report, National Aeronautics and Space Administration, Houston, Texas, 1977.
- [39] H.K. Khalil. *Nonlinear Systems: Pearson New International Edition*. Always Learning. Pearson Education Limited, 2013.
- [40] A. K. Sanyal and N. A. Chaturvedi. Almost global robust attitude tracking control of spacecraft in gravity. In *AIAA Guidance, Navigation and Control Conference and Exhibit*, pages 1–10, 2008.
- [41] E. Panteley and A. Loría. On global uniform asymptotic stability of nonlinear time-varying systems in cascade. *Systems and Control Letters*, 33(2):131–138, 1998.
- [42] H. Zhou, W. Zhou, and W. Zeng. Flocking Control of Multiple Mobile Agents with the Rules of Avoiding Collision. *Mathematical Problems in Engineering*, 2015, 2015.
- [43] A. Sadowska, T. van den Broek, H. Huijberts, N. van de Wouw, D. Kostić, and H. Nijmeijer. A virtual structure approach to formation control of unicycle mobile robots using mutual coupling. *International Journal of Control*, 84(11):1886–1902, 2011.
- [44] The MathWorks, Inc. Simulink Support Package for Parrot Minidrones — Blocks. https://nl.mathworks.com/help/supportpkg/parrot/referencelist.html?type=block&s_tid=CRUX_gn_block, 2020.
- [45] The MathWorks, Inc. Communicating with a Parrot Minidrone Using TCP/IP and UDP. <https://nl.mathworks.com/help/supportpkg/parrot/ref/communicating-with-parrot-minidrone-using-tcpip-and-udp.html>, 2020.

- [46] D. Comer and D. L. Stevens. *Internetworking with TCP/IP: Principles, protocols, and architecture*. Internetworking with TCP/IP. Pearson Prentice Hall, 2006.